REPORT NO. DOT-TSC-OST-77-56

RATE OF HEAT RELEASE IN DIESEL ENGINES

David Anderton

University of Southampton
Institute of Sound and Vibration Research
Southampton England

OCTOBER 1977

FINAL REPORT

DOCUMENT IS AVAILABLE TO THE U.S. PUBLIC THROUGH THE NATIONAL TECHNICAL INFORMATION SERVICE, SPRINGFIELD, VIRGINIA 22161

Prepared for

U.S. DEPARTMENT OF TRANSPORTATION
OFFICE OF THE SECRETARY
Office of the Assistant Secretary for Systems Development and Technology
Office of Noise Abatement
Washington DC 20590

NOTICE

This document is disseminated under the sponsorship of the Department of Transportation in the interest of information exchange. The United States Government assumes no liability for its contents or use thereof.

NOTICE

The United States Government does not endorse products or manufacturers. Trade or manufacturers' names appear herein solely because they are considered essential to the object of this report.

Technical Report Documentation Page

1. Report No.	2. Government Accession No.	3. Recipient's Catalog No.
DOT-TSC-OST-77-56		

4. Title and Subtitle	5. Report Date
RATE OF HEAT RELEASE IN DIESEL ENGINES	October 1977
	6. Performing Organization Code
7. Author(s)	8. Performing Organization Report No.
David Anderton	DOT-TSC-OST-77-56
9. Performing Organization Name and Address	10. Work Unit No. (TRAIS)
University of Southampton* Institute of Sound and Vibration Research Southampton England	OS707/R8509
	11. Contract or Grant No. DOT-TSC-1101
12 Sponsoring Agency Name and Address	13. Type of Report and Period Covered
U.S. Department of Transportation Office of the Secretary Office of the Assistant Secretary for Systems Development and Technology Office of Noise Abatement Washington DC 20590	FINAL REPORT May-October 1976
	14. Sponsoring Agency Code

15. Supplementary Notes

* Under contract to: U.S. Department of Transportation
Transportation Systems Center
Kendall Square
Cambridge MA 02142

16. Abstract

In this report, the concept of heat release in diesel engines is compared with reaction rates in petrol engines as a means of describing combustion. The intimate relationships between heat release, cylinder pressure development and cylinder pressure spectra are illustrated. A combustion model for the prediction of heat release and combustion noise, based primarily on physical aspects of diesel combustion system design, is put forward. This model indicates that fuel droplet size and the temperature of the cylinder contents are of prime importance in determining cylinder pressure noise excitation. The relationship between cylinder pressure spectra and combustion induced engine noise is described and used to show how the combustion model can predict combustion induced noise at the design stage. A simplified procedure based on the results of this modelling is put forward to predict combustion induced noise as a function of rate of pressure rise, speed and bore and applied to a Standard Engine Structure. As an approximation the prediction formulae are also given in terms of initial peak rate of heat release, engine speed and bore. Mechanical noise aspects of diesel engines, although important, are excluded from the work.

17. Key Words	18. Distribution Statement
Heat release, diesel engine, combustion noise	DOCUMENT IS AVAILABLE TO THE U.S. PUBLIC THROUGH THE NATIONAL TECHNICAL INFORMATION SERVICE, SPRINGFIELD, VIRGINIA 22161

19. Security Classif. (of this report)	20. Security Classif. (of this page)	21. No. of Pages	22. Price
Unclassified	Unclassified	146	

Form DOT F 1700.7 (8-72) Reproduction of completed page authorized

PREFACE

This report was performed under contract to the U.S. Department of Transportation, Transportation Systems Center, Cambridge MA, by the Institute of Sound and Vibration Research of the University of Southampton at Southampton, England. It is part of an on-going project on diesel engine noise reduction sponsored by the U.S. Department of Transportation, Office of the Secretary, Office of Noise Abatement. The subject covered is the rate of heat release in diesel engines and its relationship to combustion noise.

METRIC CONVERSION FACTORS

Approximate Conversions to Metric Measures

Symbol	When You Know	Multiply by	To Find	Symbol
	LENGTH			
in	inches	2.5	centimeters	cm
ft	feet	30	centimeters	cm
yd	yards	0.9	meters	m
mi	miles	1.6	kilometers	km
	AREA			
in^2	square inches	6.5	square centimeters	cm^2
ft^2	square feet	0.09	square meters	m^2
yd^2	square yards	0.8	square meters	m^2
mi^2	square miles	2.6	square kilometers	km^2
	acres	0.4	hectares	ha
	MASS (weight)			
oz	ounces	28	grams	g
lb	pounds	0.45	kilograms	kg
	short tons (2000 lb)	0.9	tonnes	t
	VOLUME			
tsp	teaspoons	5	milliliters	ml
Tbsp	tablespoons	15	milliliters	ml
fl oz	fluid ounces	30	milliliters	ml
c	cups	0.24	liters	l
pt	pints	0.47	liters	l
qt	quarts	0.95	liters	l
gal	gallons	3.8	liters	l
ft^3	cubic feet	0.03	cubic meters	m^3
yd^3	cubic yards	0.76	cubic meters	m^3
	TEMPERATURE (exact)			
°F	Fahrenheit temperature	5/9 (after subtracting 32)	Celsius temperature	°C

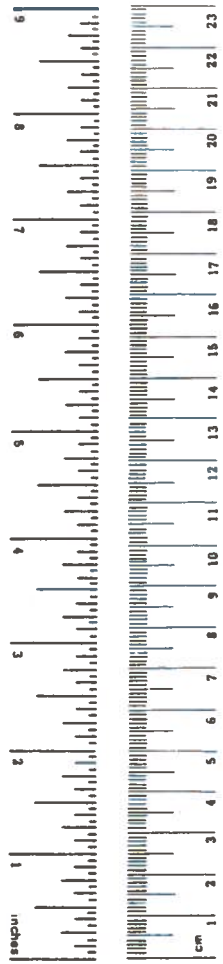

Approximate Conversions from Metric Measures

Symbol	When You Know	Multiply by	To Find	Symbol
	LENGTH			
mm	millimeters	0.04	inches	in
cm	centimeters	0.4	inches	in
m	meters	3.3	feet	ft
m	meters	1.1	yards	yd
km	kilometers	0.6	miles	mi
	AREA			
cm^2	square centimeters	0.16	square inches	in^2
m^2	square meters	1.2	square yards	yd^2
km^2	square kilometers	0.4	square miles	mi^2
ha	hectares (10,000 m^2)	2.5	acres	
	MASS (weight)			
g	grams	0.035	ounces	oz
kg	kilograms	2.2	pounds	lb
t	tonnes (1000 kg)	1.1	short tons	
	VOLUME			
ml	milliliters	0.03	fluid ounces	fl oz
l	liters	2.1	pints	pt
l	liters	1.06	quarts	qt
l	liters	0.26	gallons	gal
m^3	cubic meters	35	cubic feet	ft^3
m^3	cubic meters	1.3	cubic yards	yd^3
	TEMPERATURE (exact)			
°C	Celsius temperature	9/5 (then add 32)	Fahrenheit temperature	°F

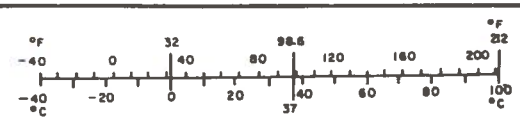

TABLE OF CONTENTS

TABLE OF CONTENTS (CONT.)

LIST OF ILLUSTRATIONS

LIST OF ILLUSTRATIONS (Cont.)

LIST OF ILLUSTRATIONS (Cont.)

1. INTRODUCTION

In gasoline engines the combustion process can be visualised as the burning of a homogeneous mixture, burning being initiated at a single point in the mixture by a spark. The amount of energy released (as heat initially) is controlled by the rate of burning of the mixture which will vary according to the fuel and overall air to fuel ratio employed. To model this process it is necessary to know the reaction rates of the combustible materials and how much of the heat produced is lost to the engine parts. This knowledge is available and the gasoline combustion process can be analysed. Partly as a result of this type of analysis, performed to predict gaseous emissions behaviour rather than performance, a greater control over the combustion process has been found necessary and the stratified charge engine represents one approach to combustion control. In this type of engine variations in the homogeneity of the combustible mixture are deliberately introduced and therefore, in order to model the process of combustion the local air to fuel ratio distributions as a function of engine crankangle must be taken into account. This introduces considerable complexity into the combustion model and much current work on gasoline engine combustion is concerned with obtaining satisfactory stratified charge models.

Combustion in the diesel engine can be visualised as a more complex version of the stratified charge gasoline engine in which the local air to fuel ratio distribution with crankangle varies more and in which the burning rates are far from uniform and controlled by physical (air and fuel mixing) processes rather than chemical reactions. The modelling of the diesel combustion therefore requires a much deeper understanding of the details of the fuel and air mixing process than is required even for stratified charge gasoline engines.

The power developed in an I.C. engine depends upon the cylinder pressure time history. The cylinder pressure time history upon the engine geometry; the amount of fuel and its distribution, the heat loss to the engine parts and the burning rates of the local fuel distributions. For diesel combustion there are no appropriate burning rates because of the non-uniform nature of the combustible mixture. However the concept of an overall 'heat release rate' is appropriate to the diesel combustion and can be loosely equated to the 'burning rate' of gasoline combustion.

2. DIESEL ENGINE HEAT RELEASE RATE

The object of modelling combustion is to enable the prediction of cylinder pressure and temperature, for performance and noise, and also the end products of combustion when gaseous and particulate emissions are concerned. A convenient analysis for determining the requirements for such models is to turn the process back to front and to study the energy flows which would be required to produce a measured cylinder pressure diagram, knowing only the geometry of the actual engine, and the trapped mass of air and fuel. With this information the state of the cylinder contents at any instant is uniquely defined.

Starting from the non-flow energy equation :

$$Q - W = U \tag{1}$$

with $$W = \int pdV \tag{2}$$

the differential form becomes

$$dQ - pdV = mdu \tag{3}$$

Now $$mdu = m\ Cv\ dT \tag{4}$$

and $$pV = m\ RT \tag{5}$$

So that if a semi-perfect gas is assumed,

i.e. $U = f(T) \times$ const. only

then $C_v = f(T) \times$ const. only and

Differentiating (5) gives

$$pdV + Vdp = m\ R\ dT \tag{6}$$

and so $$m\ dT = \frac{1}{R}\ (pdV - Vdp)$$

thus $$dQ = \frac{Cv}{R}\ pdV + \frac{Cv}{R}\ Vdp + pdV \tag{7}$$

Now $Cp - Cv = R$ and $Cp/Cv = \gamma$

and so, assuming the number of moles of reactants equals the number of moles of products, i.e.

R = Constant

then $$\frac{dQ}{d\theta} = \frac{1}{\gamma - 1}\ \left(\gamma p \frac{dV}{d\theta} + V\frac{dP}{d\theta}\right) \tag{8}$$

dQ is the heat transfer to the cylinder contents, and $\frac{dQ}{d\theta}$ is generally called the rate of heat release. The total heat input to the engine dQ_{in} is related by

$$dQ_{in} = dQ + dQ_W \qquad (9)$$

or

total heat input = heat input to cylinder contents + heat transferred to engine parts

and so the total rate of heat release to the cylinder contents and engine parts is given by :

$$\frac{dQin}{d\theta} = \frac{1}{\gamma-1}\left(P\frac{dV}{d\theta} + V\frac{dP}{d\theta}\right) + \frac{dQ_W}{d\theta} \qquad (10)$$

Since the pressure P and volume V are known as a function of θ and γ can be estimated then the rate of heat release can be calculated. If additionally the heat lost to the engine parts can also be estimated then the rate of heat rleeased by the fuel in the cylinder can also be calculated.

3. RELATION BETWEEN DIESEL ENGINE HEAT RELEASE, CYLINDER PRESSURE DEVELOPMENT AND CYLINDER PRESSURE SPECTRUM

Figure 1 shows typical measured characteristics of diesel combustion for a direct injection automotive engine. The heat rate of injection (assuming instantaneous burning on entry to the combustion chamber) is shown together with the cylinder pressure development and rate of heat release to the cylinder contents (net heat release). This heat release rate curve is typical in that, until initiation of combustion, its value is low and negative whilst during the initial rapid burning of the premixed fuel and air accumulated during the delay period there its value is large and positive. This phase generally lasts until around top dead centre when it is generally acknowledged that a mixing process then controls the rate of combustion (diffusion burning) and a second but usually lower, peak in the heat release curve occurs with a gradual reduction of heat release for the rest of the cycle. Equation (8) in Section 2 shows that rate of heat release is related to the cylinder pressure development, engine geometry and properties of the cylinder contents. Figure 2 (reproduced from reference 1) shows the effect of various simple representations of the rate of heat release curve and the resulting cylinder pressure developments. In general the more abrupt the initial

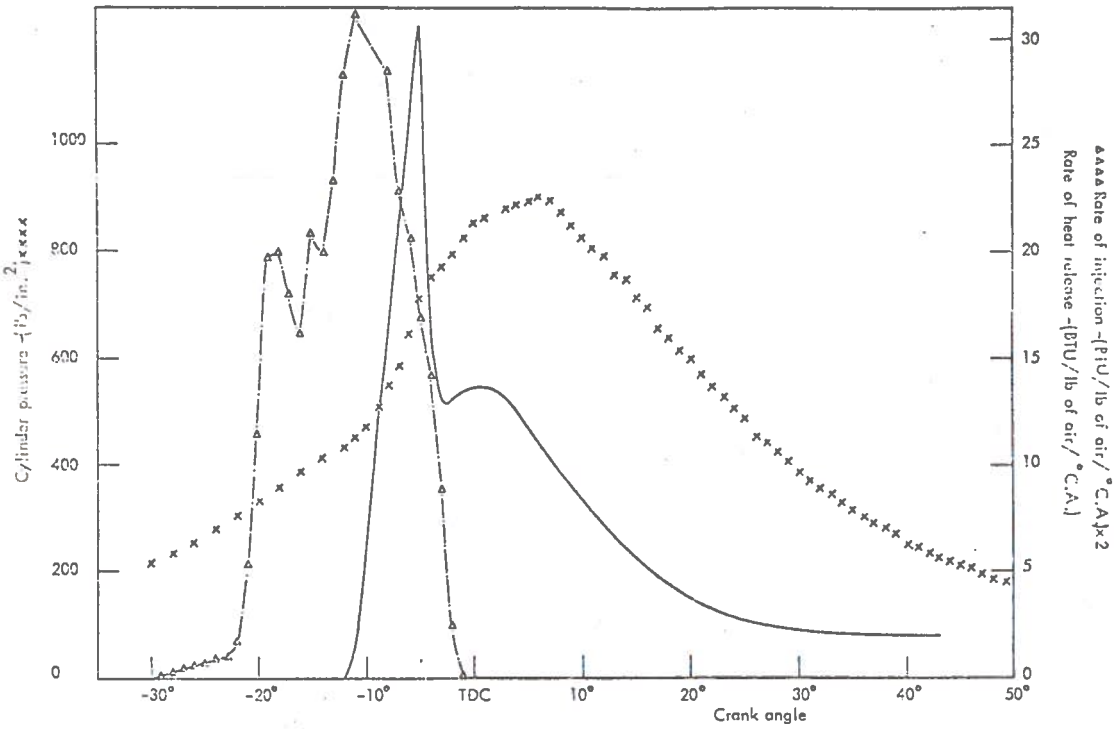

FIGURE 1. TYPICAL CYLINDER PRESSURE, FUEL INJECTION AND HEAT RELEASE DIAGRAMS FOR DIRECT INJECTION ENGINE - 1800 rev/min FULL LOAD

Heat release diagram	20:1 COMPRESSION RATIO		
	$\frac{dP}{dt}$ max	P max	Efficiency %
(a)	75	1140	52.5
(b)	25	770	49.3
(c)	25	770	45.4
(d)	45	910	49.1

(Fixed injection timing and burn of 40^0 C.A.)

(a) Tabulated Pressure Diagram Data Produced by Lyn's Combustion Model

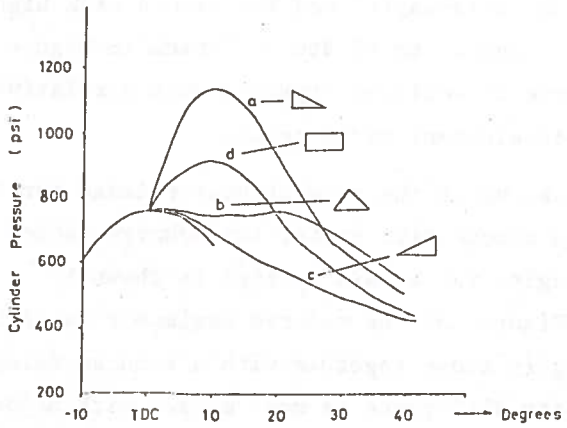

(b) Cylinder Pressure Diagrams

FIGURE 2. EFFECT OF SHAPE OF RATE OF HEAT RELEASE CURVE ON THE RESULTING CYLINDER PRESSURE DIAGRAM

rate of heat release the more abrupt is the cylinder pressure development after initiation of combustion. In the practical case the variations in shape of the rate of heat release curve will result from the differences in engine geometry, combustion chamber shape, type of cycle etc. For the direct injection engine some typical results over the speed range are presented in Figure 3. Here the second peak in the heat release curve is absent and it can be seen that the initial peak of heat release varies both in magnitude and position (crankangle) over the speed range and this considerably influences the shape of the cylinder pressure diagram between 15^{o} b.t.d.c. and t.d.c. These differences also show in the cumulative heat release. However, the difference in cylinder pressure development after 10^{o} a.t.d.c. are small and show that the cycle power stroke is not much affected.

The measured rate of heat release curve for the 'M' system of combustion where, in a high swirl direct injection engine, the fuel is sprayed onto the wall of the chamber is shown in Figure 4. The initial peak of heat release is low, 28 Btu/lb/^{o}crankangle as compared to a normal D.I. engine (80 - 90 Btu/lb/^{o}crankangle) and the second peak high (20 Btu/lb/^{o}crankangle as compared to 13 Btu/lb/^{o}crank in Figure 1). From this heat release curve it would be expected that a relatively smooth cylinder pressure development would result.

The effect of turbocharging on the rate of heat release for the same engine geometry (i.e. same compression ratio, turbocharger added to N/A engine and turbocharged engine run at N/A rating) is shown in Figure 5. At part load (Figure 5a) the reduced maximum rate of heat release with turbocharging is shown together with a reduced delay period. At full load (Figure 5b) the difference is most marked with major premixed burning evident on the normally aspirated engine. It is clear that an exceptionally smooth pressure development could result at full load from turbocharging but this would not be so at part load. At full load the maximum rate of heat release is reduced from 65 Btu/lb/^{o}crankangle to 21 Btu/lb/^{o}crankangle.

The examples so far given illustrate that the shape and magnitude of the heat release diagram can be used to estimate the characteristics of the resulting cylinder pressure development and in particular there appears to be a marked correlation between the initial peak of the rate

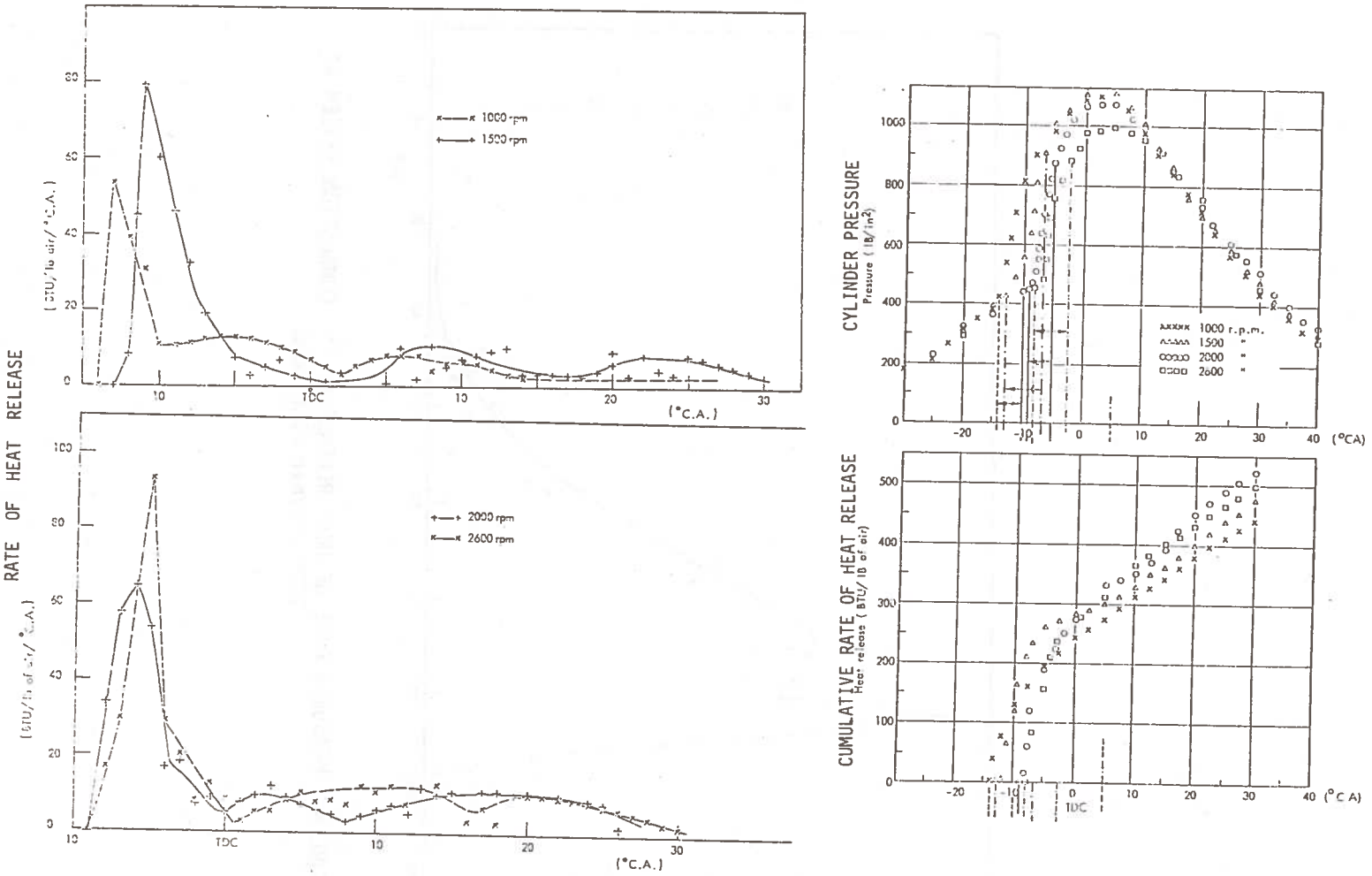

FIGURE 3. EFFECT OF ENGINE SPEED ON RATE OF HEAT RELEASE, CYLINDER PRESSURE DEVELOPMENT AND CUMULATIVE HEAT RELEASE

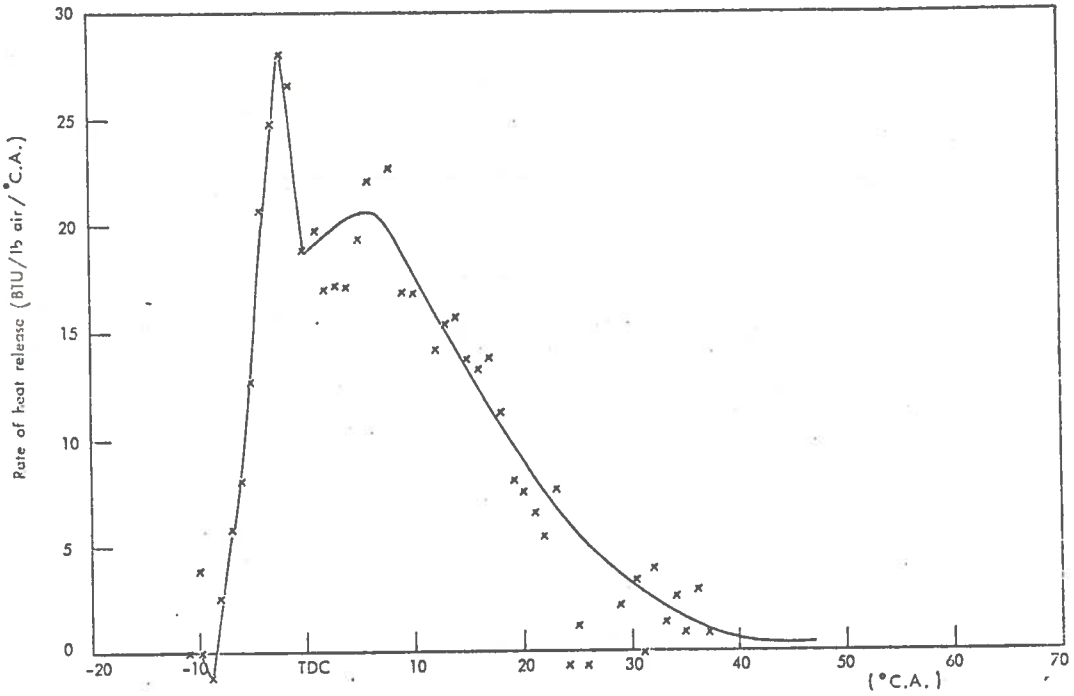

FIGURE 4. MEASURED RATE OF HEAT RELEASE OF 'M' COMBUSTION SYSTEM AT 1000 rev/min FULL LOAD

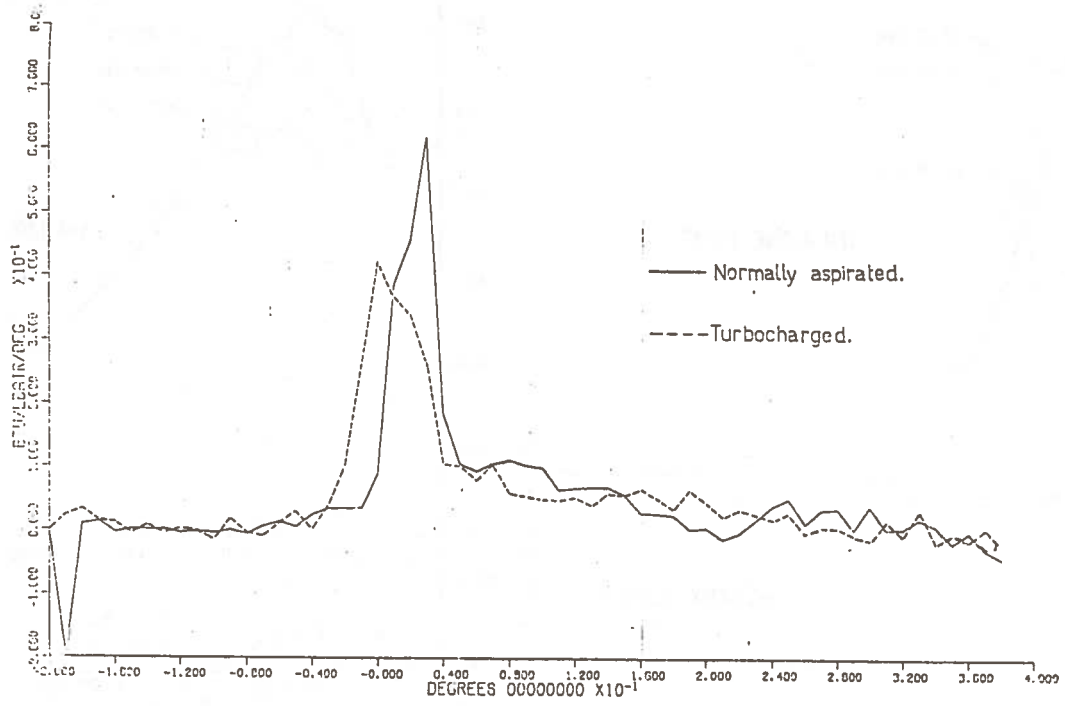

(a) Half Load

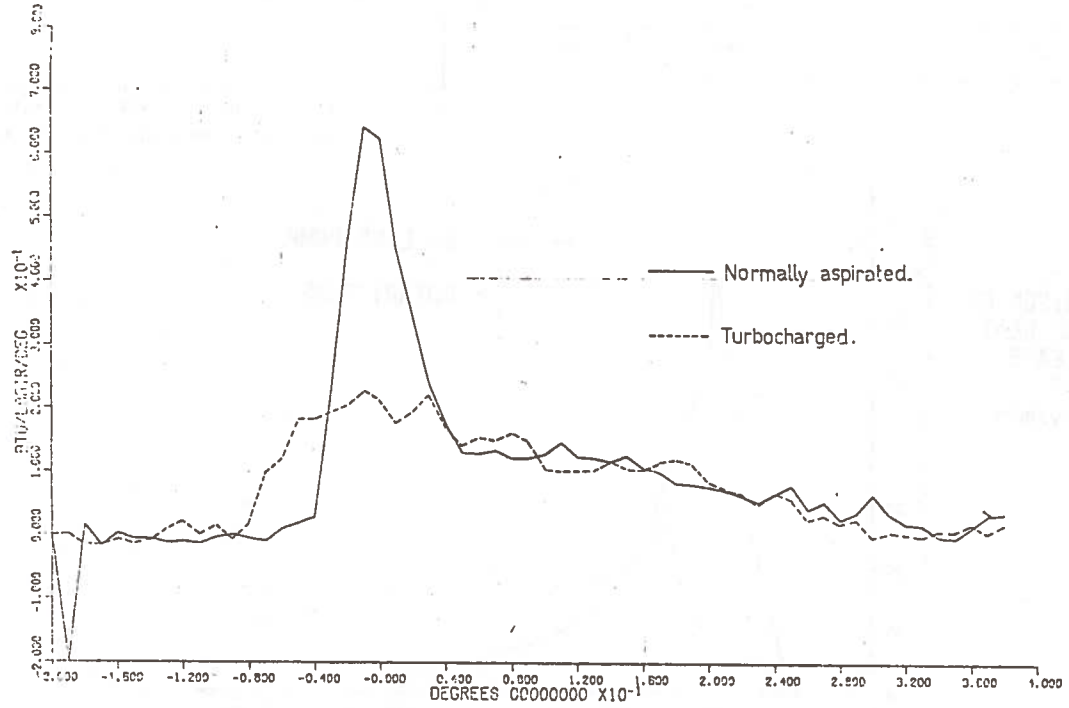

(b) Full Load

FIGURE 5. EFFECT OF TURBOCHARGING ON RATE OF HEAT RELEASE IN D.I. ENGINE AT 2600 rev/min

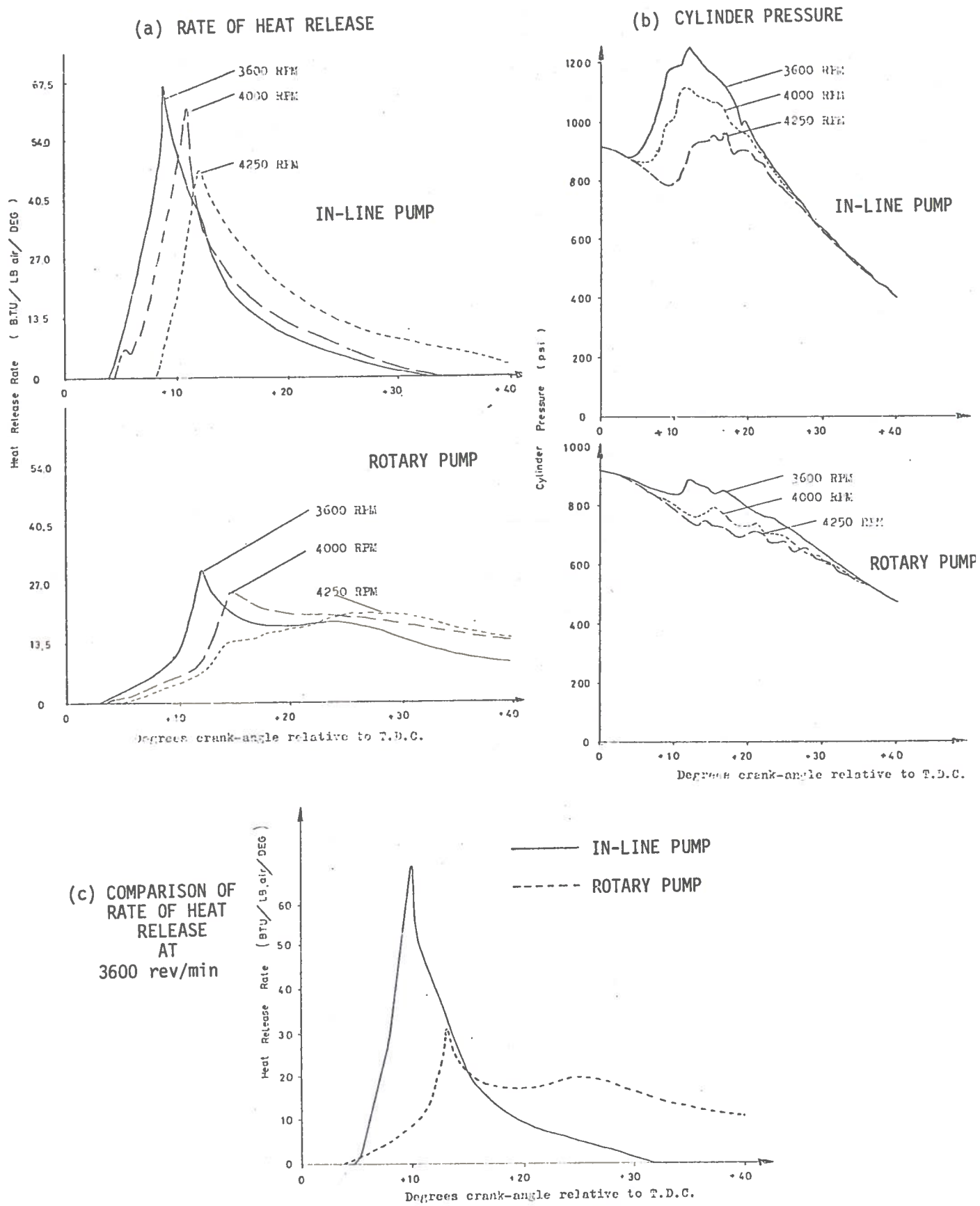

FIGURE 6. EFFECT OF FUEL INJECTION TYPE ON RATE OF HEAT RELEASE AND CYLINDER PRESSURE DEVELOPMENT IN HIGH SPEED I.D.I. DIESEL

of heat release and the severity of the maximum cylinder pressure rise rate. This is illustrated in Figure 7 where the effect of varying the number of nozzle holes on the heat release and cylinder pressure spectra was assessed. As the number of nozzle holes was increased so the magnitude and severity of the initial rate of pressure rise was increased. The corresponding rates of heat release show that as this magnitude and severity increased so did the initial peak rate of heat release. Measurements of the cylinder pressure spectra showed that as the initial peak of the rate of heat release curve became more pronounced the level of the spectra, in the critical frequency range from about 500 Hz increased markedly. Thus it can be concluded that the combustion induced noise of diesel engines is closely associated with the initial peak in the rate of heat release diagram.

Examination of equation (8) indicates that for the rate of pressure rise to be related directly to the rate of heat release then

$$\gamma\, p\frac{dv}{d\theta} \leqslant V\frac{dp}{d\theta} \qquad (11)$$

or work done/^{o}C.A. $\leqslant$ Internal energy change/^{o}C.A.

For a typical 4½ inch bore normally aspirated direct injection engine the ratio of rate of work done to rate of change of internal energy is plotted, as a function of crankangle, in Figure 8. As combustion is initiated and until shortly after top dead centre there is a dramatic increase in internal energy associated with the premixed burning stage representing a condition where the condition (11) is satisfied. Over this portion of the cycle the rate of heat release is given approximately by :

$$\frac{dQ}{d\theta} \simeq \frac{1}{m(\gamma-1)}\left(V_f\,\frac{d\rho}{d\theta}\right) \qquad (12)$$

For a normally aspirated engine at full load the ratio $V_{f/m}$ is generally smoke limited and therefore the rate of heat release becomes dependent not only on the actual mass of the cylinder contents, m, but also on the cylinder volume at the point of initiation of combustion. Figure 9 shows the measured data from a number of diesel engines (primarily normally aspirated D.I.) superimposed on which is the predicted relationship according to equation (12) for normally aspirated D.I. engines with combustion initiation between 16^{o} b.t.d.c. and t.d.c. It is clear that there is a strong relationship between rate of pressure

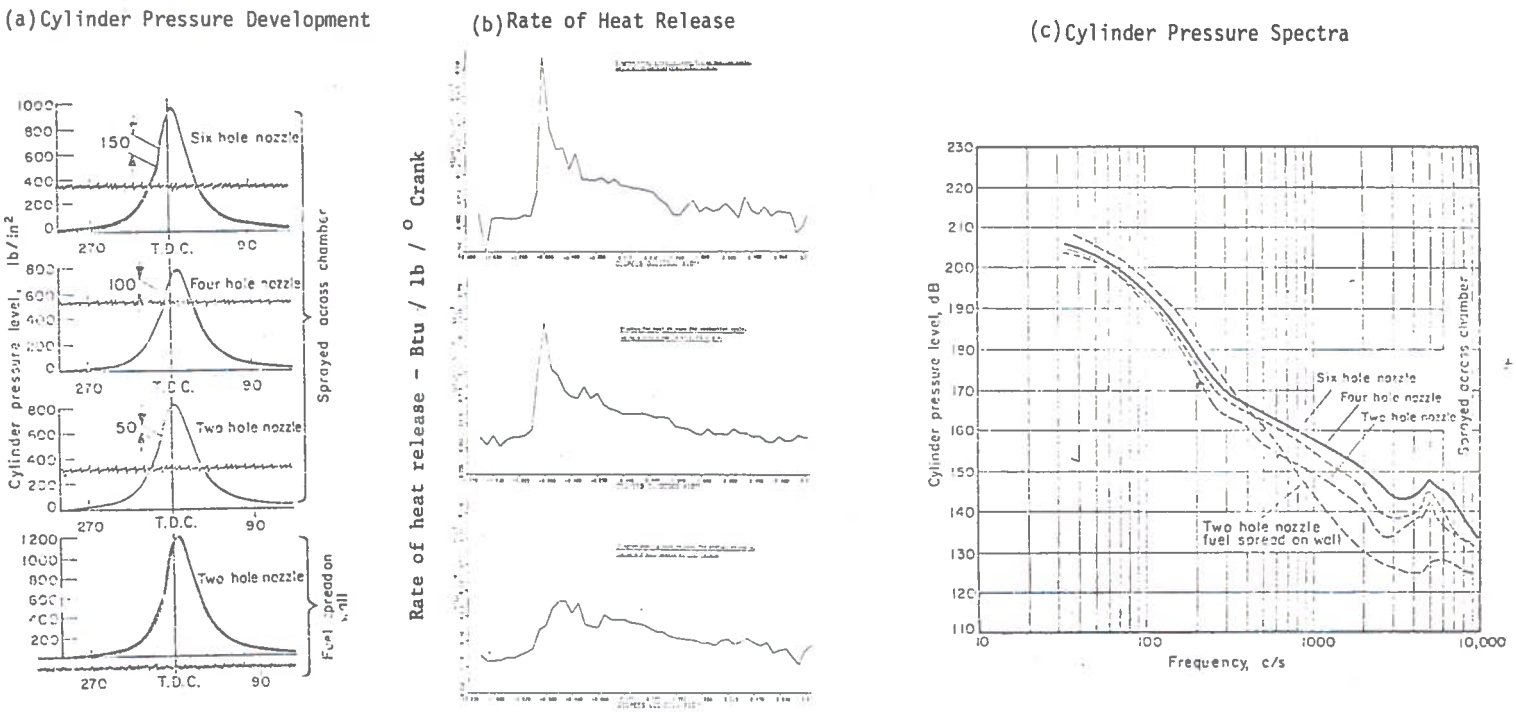

FIGURE 7. RELATION BETWEEN RATE OF HEAT RELEASE, CYLINDER PRESSURE DEVELOPMENT AND SPECTRA

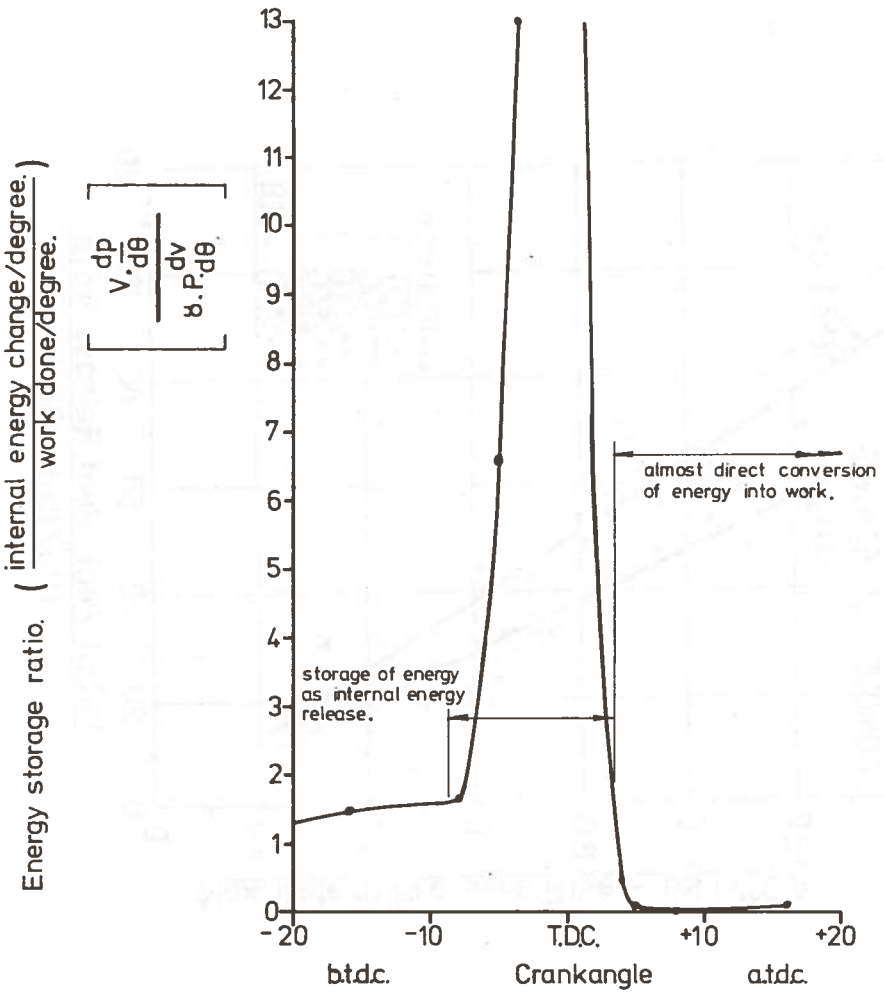

FIGURE 8. ENERGY STORAGE RATIO AS A FUNCTION OF CRANKANGLE FOR A K.I. DIESEL ENGINE

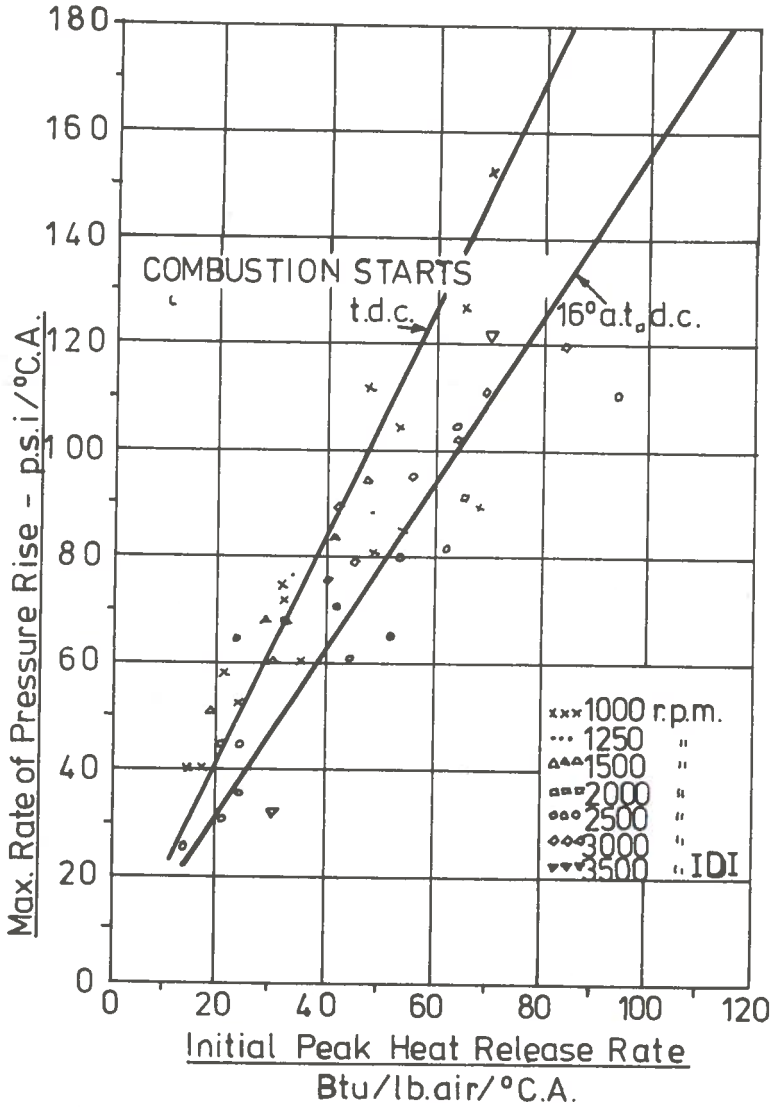

FIGURE 9. RELATIONSHIP BETWEEN RATE OF PRESSURE RISE AND INITIAL PEAK HEAT RELEASE RATE

rise and initial peak of heat release rate. Therefore there will be a strong relationship between combustion induced noise and the initial peak of heat release rate.

Since the rate of heat release curve together with the rate of heat lost to the engine parts in communication with the engine geometry specifies the cylinder pressure development then the task for combustion modelling is to predict these two characteristics. In general the rate of heat loss to the engine parts is small compared to the total rate of heat input and thus effort is concentrated on the prediction of the heat release from fuel injection, air motion etc characteristics. (references 2, 3, 4, 5, 6, 7, 8, 9). This basic approach was initiated by Wiebe and, except for some emissions models, primarily aimed at the prediction of performance. In this way detailed investigations of the premixed phase have not in the past been considered important. However, as has been shown, when the object of a combustion model is to predict engine combustion induced noise characteristics the premixed burning phase becomes of prime importance. The following description of a model for the prediction of combustion induced noise is based on the work of Ogegbo carried out at Southampton University.

4. A THEORETICAL SIMULATION OF DIESEL ENGINE COMBUSTION - THE I.S.V.R. COMBUSTION MODEL

4.1. General

Simulation of a diesel engine combustion is an extremely complex problem and involves an almost infinite number of processes. Since most of the processes involved are only partially understood, a sophisticated simulation containing all the relevant processes is unlikely to be achieved at the present level of knowledge or even economically feasible. The problem thus becomes one of a careful selection of the appropriate processes which can yield an approximation to the actual combustion and provide some reasonable results to guide a practical engineer in his design and performance calculations.

Before going into the details of the simulation, it is worthwhile to state the fundamental assumptions made and to give a brief indication of a theoretical and empirical treatment of each of the processes considered in the simulation.

It is assumed that the processes which control a diesel engine combustion are more physical in nature than chemical. This means that the chief factors considered to affect the diesel combustion are the cylinder temperature, pressure, the oxygen supply, air swirl and the rate of preparation (i.e. the rate of vaporisation and the mixing of fuel/vapour and cylinder charge air). The basic processes considered in this simulation are as follows :

4.1.1. The Fuel Spray Atomisation (i.e. Jet Break-up and Droplet Size Distribution) In a diesel engine, the fuel issues from the injector into a combustion chamber as a liquid stream. The surface of the stream comes into contact with the cylinder charge air, and the friction between the two results in the formation of sheets or ligaments that ultimately break up into spray of different droplet sizes and velocities. Since the surface/volume ratio does not become appreciable for sheets and ligaments, vaporisation is usually assumed negligible until the break-up has occurred.

The mechanism of atomisation is very complex and complicated. It depends on fuel properties, the atomising device and conditions such as nozzle pressures (velocities) and the density of the charge air into which fuel is being injected (Figures 10, 11). For simplicity, the atomisation process may be summarized as follows:

(a) The spreading of the fuel stream into sheets, threads or ligaments by virtue of its own velocity.

(b) The breaking of ligaments or thin sheets into various droplet sizes as a result of a relative motion between the cylinder air and liquid stream on one hand, and surface tension forces on the other.

(c) Owing to a reduction in the droplet relative velocity (generally towards the end of injection), instability and adherence of droplets, as a result of collision with large droplets, may continue to exist.

Moreover, the degree of atomisation is usually expressed in terms of the smallness of the size of the droplets in the spray and also by the smallness of the variation in size of droplets. The most significant parameters which affect the degree of atomisation are the initial fuel velocity and the diameter of the injector orifice. The former depends primarily upon the injection pressure, being a function of the square root of the difference between the injection and chamber pressure. With the smallest orifice, largest percentages of the smaller sizes of fuel droplets are generated; however, the effect of cylinder air density upon the degree of atomisation is somehow uncertain yet (10).

Successful analyses of experimental and photographic studies of a series of different atomisation system by Tanasawa and others (11,12) have provided expressions for calculating the droplet mean diameter (sometimes known as Sauter Mean Diameter, SMD). The following empirical equations proposed by Tanasawa et al and Knight (13) respectively, have been used extensively and they are :

$$SMD = 70.5 \frac{D_{sh}}{U_{orel}} \left(\frac{Surten}{D_{eng}}\right)^{0.25} \sqrt{g} \left(1 + \frac{3.31\ Vislf\ \sqrt{g}}{(surten \times Denlf \times D_{sh})}\right) \quad (13)$$

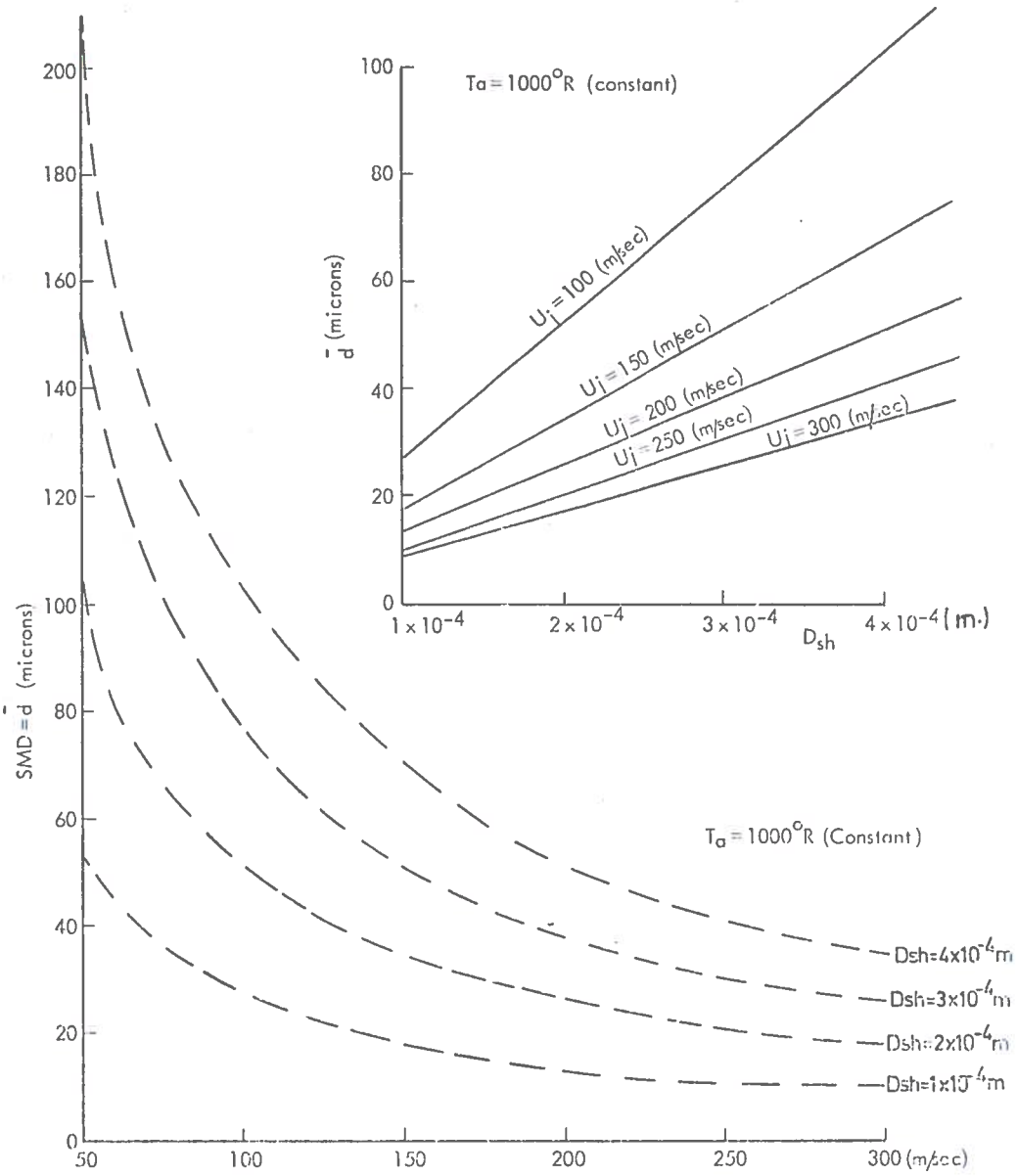

FIGURE 10. EFFECT OF INJECTOR NOZZLE HOLE AND VELOCITY ON DROPLET MEAN DIAMETER

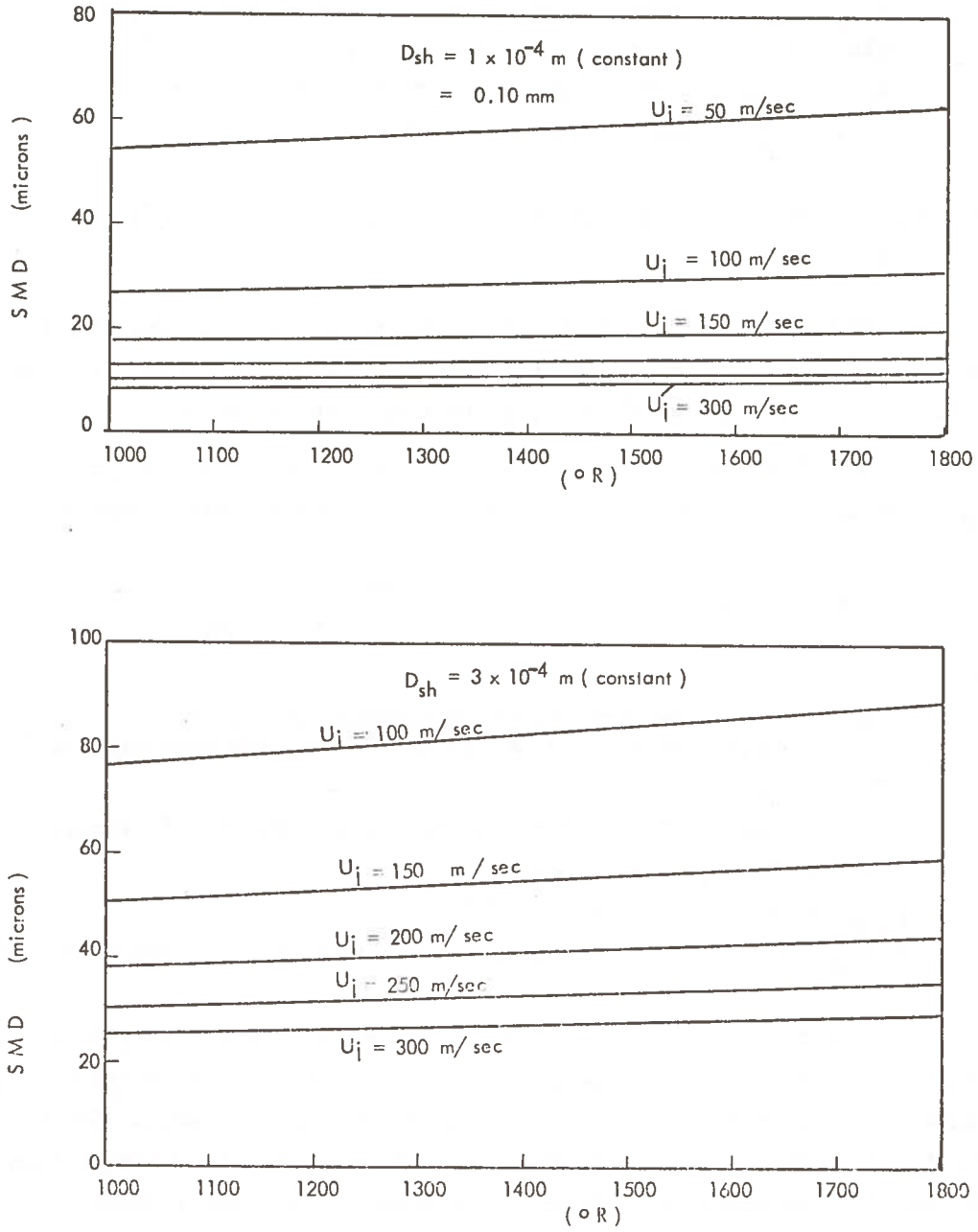

FIGURE 11. EFFECT OF CHARGE TEMPERATURE ON DROPLET MEAN DIAMETER

where :

SMD = Sauter Mean Diameter produced at atomisation (m)

D_{sh} = Diameter of the spray hole (m)

Surten = Surface tension (kg/m) - suggested value = 0.0029kg/m

U_{orel} = Relative velocity (m/sec)

D_{eng} = Density of the surrounding (cylinder) gas (kg/m^3)

Denlf = Density of the liquid fuel (kg/m^3)

Vislf = Viscosity of the liquid fuel (kg/m^2)

g = Acceleration due to gravity = 9.81 (m/sec^2)

N.B. Most of the above names are Fortran (computer) names, chosen for easy identification.

Equation (13) is said to be valid for an injection lasting about 3 to 8 milliseconds. Figures 10, 11 illustrate the Sauter Mean Diameters calculated at different conditions, using the above equation.

Knight's equation (ref. 4 introduced a multiplying factor, $|A_{orf}/A(t)_{eff}|^{0.916}$ into Knight's equation below) on the other hand is:

$$SMD = 220(\Delta P)^{-0.458} (Q)^{0.209} (KV)^{0.215} (A_{orf}/A_{(t)_{eff}})^{0.916} \qquad (14)$$

and:

ΔP = The difference between instantaneous injector pressure and instantaneous cylinder gas pressure (psi)

SMD = in microns

Q = Mass flow rate through the nozzle (orifice) (lb/hour)

KV = Kinematic viscosity of fuel (cs)

A_{orf} = Exit orifice area (in^2)

$A(t)_{eff}$ = Effective orifice area across which P is measured (in^2).

According to reference (14), for a properly designed injector nozzle of an automotive high speed engine, an SMD of about 50 microns should be expected. However, for a typical injection pressure of about 3500 psi (KV = 5 centistokes and D_{sh} = 0.38mm), The SMD calculated from equations (10) and (11) respectively is 65 and 21 microns. From experimental and theoretical information available at present (refs. 15, 16) it appears that the former equation is more likely to predict an SMD, which would be very close to a practical case.

Droplet Size Distribution

A number of empirical mathematical expressions for size-distribution have been proposed and used for liquid sprays. No criterion has been established for choosing the preferred distribution function.

For convenience, the distribution suggested by Whitehouse and Way (ref. 5) is used in this simulation and its mathematical formulation is shown in equation (15) below and is explained in Appendix A.2.

$$F(Do) \approx 100 \left| Exp\ (-3.125(D_o - D_{av})^2)/D_{av}^2 \right| dD_o \qquad (15)$$

where:

$F(D_o)$ = The mass percentage of each droplet size of diameter between D_o and $D_o + dD_o$ injected

D_o, D_{av} = The initial diameter of the droplet size and the mean diameter of the whole spray respectively.

dD_o = width

Exp = Base "e"

Nine droplet sizes are considered and the proportion of the total mass of fuel corresponding to each droplet size is assumed to follow a truncated Gaussian distribution with a standard deviation of 0.4 times the mean diameter. Moreover, the realistic assumption that the maximum diameter of the droplets in any fuel spray is approximately twice the SMD (ref. 11) is also incorporated into this modified size distribution analysis.

4.1.2 Droplet Jet Mixing and Vapour Jet Mixing Without Chemical Reaction

After the atomisation process, the droplets may exist in liquid form for an appreciable period of time to diffuse into the charge air in the form of a spray or jet. The smaller droplets in the fuel spray, however, are rapidly decelerated by the aerodynamic force and give away their mass and completely vaporise faster and travel a shorter distance through the combustion chamber than the large droplets. A cloud of vapour due to the smaller droplets is thus rapidly formed and is then diffused outwards into the charge air and at the same time diluted to form a mixture which is initially too lean (i.e.below inflammable limit or stoichiometric ratio) to initiate an auto-ignition or support a flame propagation. In fact, the reason for the formation of the above lean mixture is that the smaller

droplets being only a small fraction of the total fuel injected and also the earliest to be completely vaporised, have the longest mixing time. More important, perhaps, part of this lean mixture if unable to mix further with pockets of air/vapour of higher concentration, especially at light engine operating conditions, may constitute one source of the unburned hydrocarbons in a diesel engine (ref.17).

Furthermore, the vapour due to the droplets of the next size is also quickly formed but at a slower rate and the mass of more concentrated vapour (due to increased droplet surface temperature) given away by the incoming larger droplets, is added to it. Simultaneously, the droplets which have vaporised also leave concentrated regions of vapour, which may exist for an appreciable period of time while further diffusing into the charge air. At different points in the combustion chamber, pockets of nearly stoichiometric mixture of air and vapour are formed and are ready for ignition. In the absence of an external ignition source, these pockets of mixture must be further heated up by the charge air until the self-ignition temperature is reached, if combustion is to occur.

Finally, in support of Lyn, the essential criteria are that these pockets of vapour-air mixture within the inflammable limits must be formed and maintained within these limits for a sufficient length of time to allow the chemical ignition delay period to lapse before they are over-diluted.

4.1.3 Vaporisation of Droplets without Chemical Reaction

Droplet vaporisation influences combustion efficiency, the heat release course and the rate of pressure rise in an i.c. engine to an important degree. As a result of its importance, vaporisation has been a subject of both theoretical and experimental studies. Droplet vaporisation in a gas stream with relative motion as defined in many works, involves heat and mass transfer theory and many experimental investigations have been conducted by suspending droplets on spherical thermocouple junctions exposed to a gas stream. Differential vaporisation equations are given in (18, 19) and (20, 21). The equations proposed by Wakil (22) when combined with an appropriate droplet aerodynamic drag coefficient, allow a step-by-step computation of droplet histories, when a droplet with given initial conditions moves in a gas stream of known velocity field. Calculations of a single droplet mass, temperature and velocity history are shown in Figures 12, 13, 14 and in more detail in ref. 23.

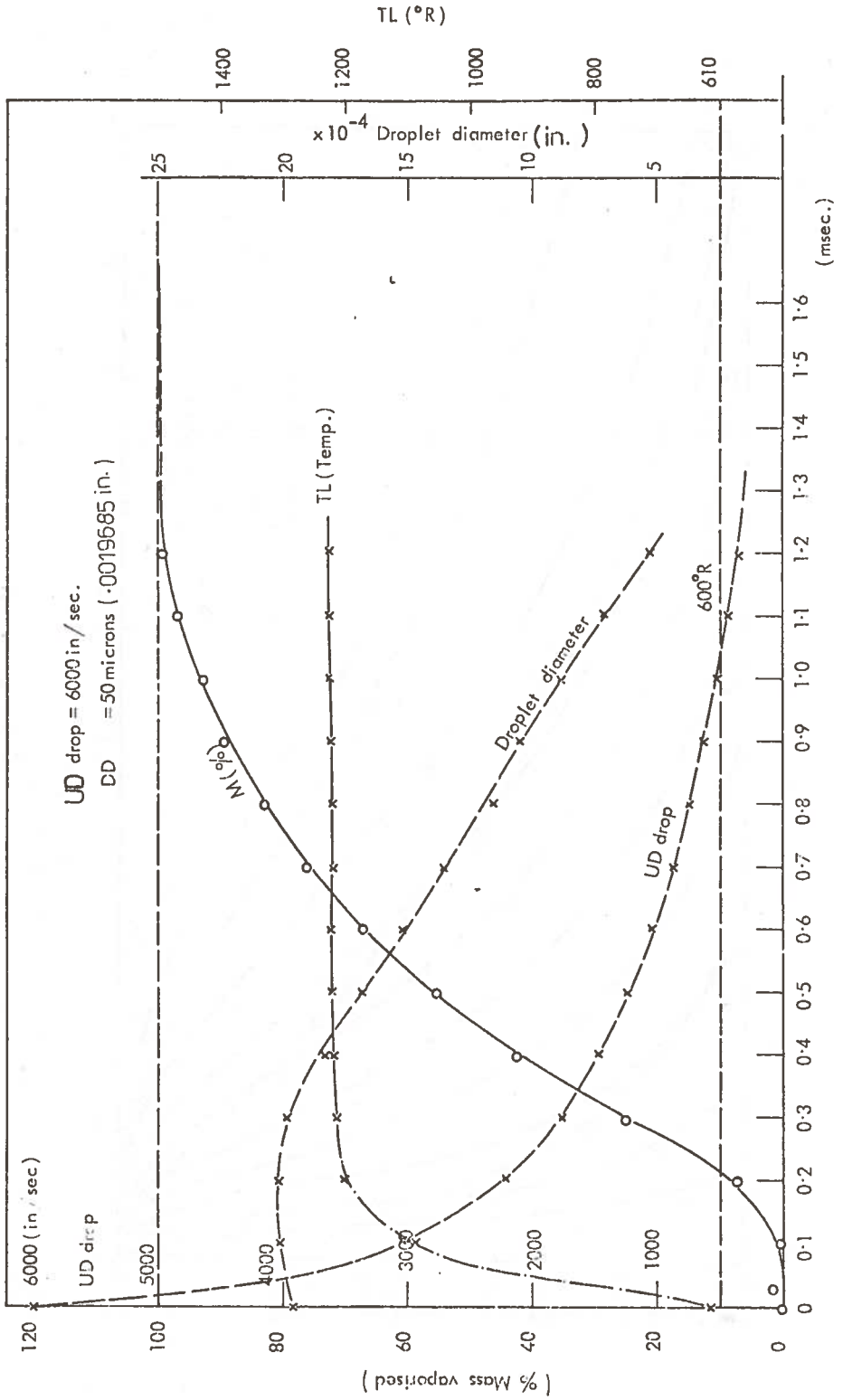

FIGURE 12. DROPLET HISTORIES

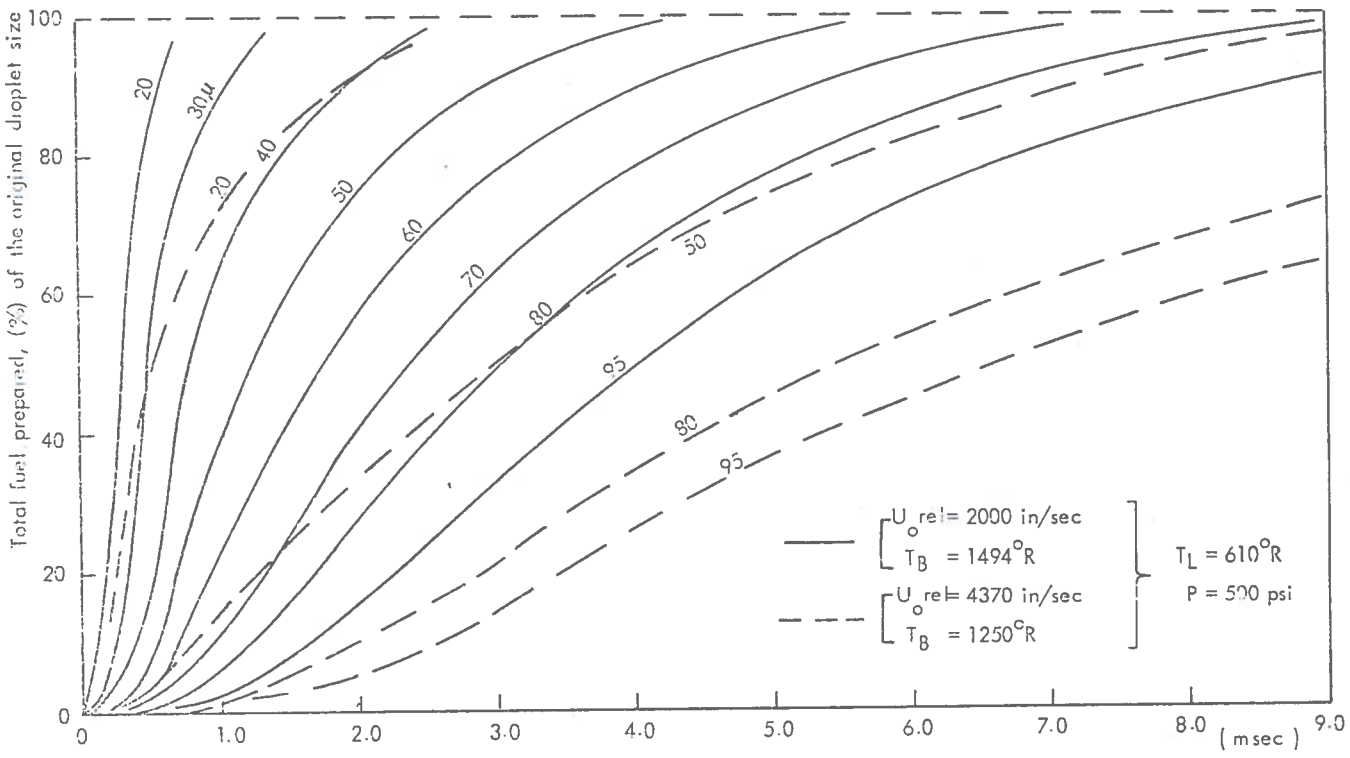

FIGURE 13. PREPARATION HISTORIES OF THE DROPLET SIZES

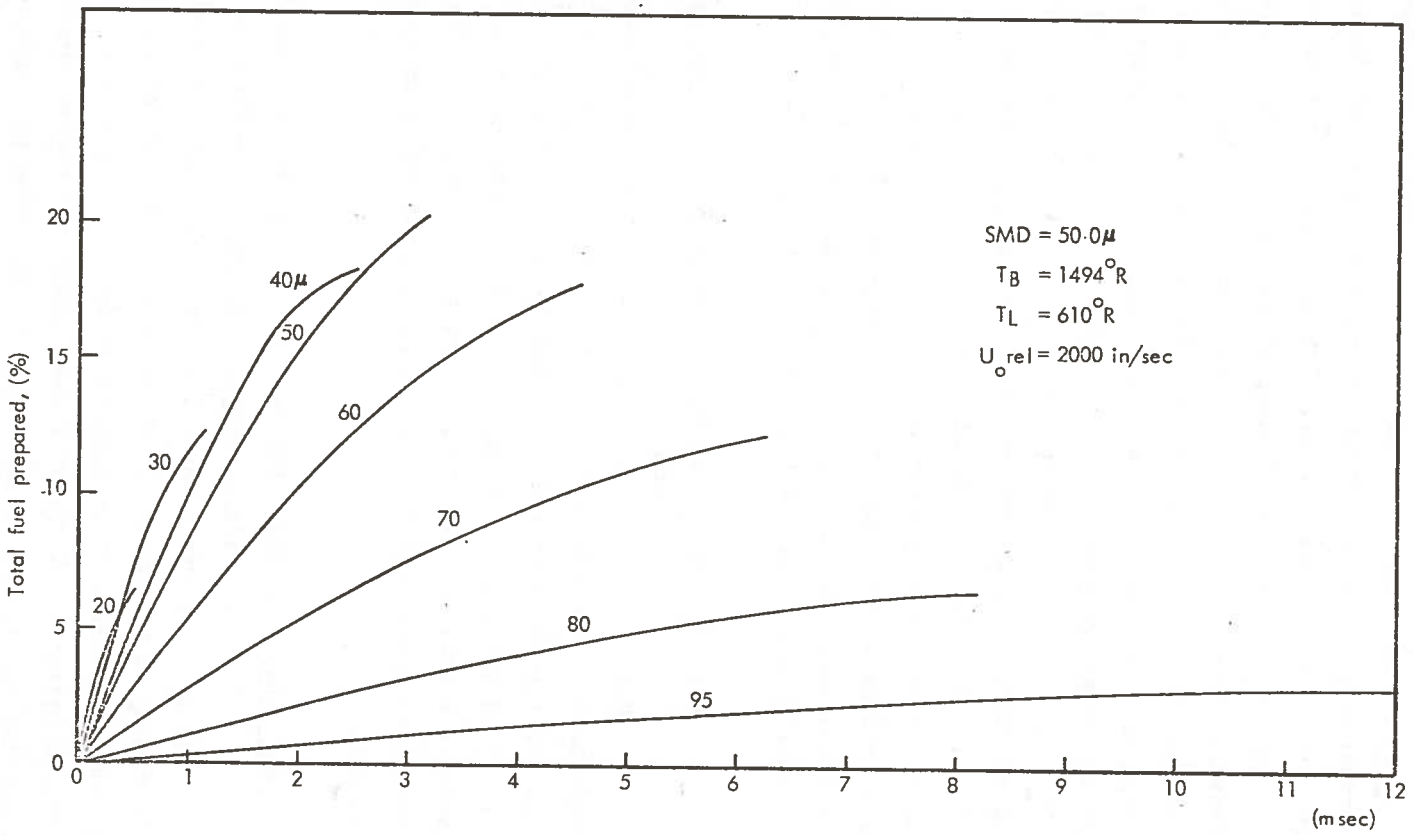

FIGURE 14. TOTAL FUEL PREPARED IN TERMS OF THE ACTUAL MASS OF THE SIZE GROUP IN THE FUEL SPRAY

While it is common to divide the vaporisation time into two different parts, namely the unsteady (non-equilibrium) and steady period, up to date there has been no theory which can be used to determine the exact relative magnitude of the two components. The first theoretical and experimental investigations of the unsteady period (heating-up period) were carried out by Wakil et al, although these investigations were not specifically directed towards droplet vaporisation in a diesel engine. Moreover, their calculations indicate that the heating-up portion of the total vaporisation time is of great importance in most cases especially at high air temperatures, high pressures, etc. It is further suggested that the larger droplets would be expected to reach the combustion zone while still in the heating-up state. Above all it appears from these findings that the vaporisation time, considering only the steady state cannot represent the total true vaporisation time. But since the size of the droplet is continuously decreasing with time, a quasi-steady state theory may therefore be applicable to small droplets (10 to 100 microns). Under such a condition, however, the total vaporisation time is underestimated by approximately 20 per cent according to Williams (24).

4.1.4 Discussion of Single-droplet Theories and Droplet-Cloud Theories

Most of the single-droplet and droplet-cloud theories reported in literature are scarcely applicable (ref.14) to the case of very fine droplet in an air stream under very high temperature and high pressure conditions as exist in the engine cylinder. Therefore, some empirical adjustments, discussed below, are required, in order to be able to utilise the above theoretical background for simulating experimental observations in diesel engines.

(a) Fuel Spray As indicated earlier in this chapter, the fuel spray in any diesel engine consists of droplets of varying sizes. These sizes on the other hand, vary from one engine to another and depend principally on the diameter of the injector nozzle and on the fuel injection pressure. However, it is safe to assume that the droplet distribution given in Appendix A.2 typifies most modern automotive diesel engines. This means that the effect of any change in injection pressure either as a result of the engine speed or fuel pump, geometry of the spray nozzle, instantaneous cylinder conditions, fuel properties, etc. is considered to affect only the

SMD, which affects in turn both the degree of fineness and the uniformity of the spray atomisation. The above mode of thinking is closely in line with the results presented in Figure A.2.1 and in reference 25.

Initial analyses had demonstrated that the fuel mass distribution with time within certain limits had no appreciable influence on the heat release diagrams. Thus, what is significant is the SMD of the whole spray, which determines not only the surface area of the droplet exposed to the cylinder gases but also the mass of each droplet prepared and its burning time, Figure 14. As a result a 60 micron SMD was calculated using equation (60) and a trial and error method allowing the above calculated SMD to vary in a step of 10 microns (ranging from 40 to 70 microns) was adopted in this model. A 70 micron SMD gave a burning time consistent with most heat release analyses previously conducted. This size has therefore been used in most of the calculations.

(b) Droplet Relative Velocity : Since the droplet sizes (probably ranging from 5 to 140 microns) in a diesel fuel spray are distributed, it is similarly logical that their relative velocities will be distributed as well. Unfortunately, the problem which is still unsolved at present is how to predict these velocities. However, it is accepted that the smaller the droplets, the higher their initial relative velocities. Since the smaller droplets, owing to their size, almost immediately become airborne and give up their vapour in a very short time, Figure 14 , these high initial relative velocities are of little importance. The larger droplets which are major contributors of heat release are formed on the other hand at the beginning of fuel injection owing to their size as well (though with lower initial relative velocities), also loose their initial velocities rapidly and become airborne shortly afterwards. In view of the uncertainty in the determination of the droplet relative velocity-distribution and in view of the results presented in the above Figures, it was assumed that all the droplets were injected initially at the same relative velocity. Subsequently, however, the rate at which this velocity is impacted to the cylinder charge, then depends on the droplet size.

(c) Single Droplet: In Section 4.2.4, equilibrium (wet-bulb) temperatures are mentioned and it is noted that these conditions only occur as long as a dynamic equilibrium exists between the heat transferred from air to the liquid surface of the droplet and the mass transferred out. In other words, the droplet temperature has attained a value (due to its high vapour pressure and mass transfer) that the diffusing vapour superheat Q_s, and the latent heat of vaporisation, Q_{LAM}, balance the heat transfer from the air, Q (i.e. $Q = Q_s + Q_{LAM}$ or $Q_{LAM} = Q_v$). Of course, the above analysis is based on the fact that the average cylinder gas temperature (typical value $\sim 1494^{\circ}R$) and pressure (~ 500 psi) during vaporisation process remain essentially unchanged. Moreover, it is also valid for a single droplet burning in an environment which has an abundant quantity of air and in which the droplets do not interact or the interaction is very weak.

However, for the diesel fuel spray, opinions are still divided as to whether interaction between droplets has a large effect on the temperature and fuel vapour concentration in the surrounding cylinder gas or not. But, according to reference (23) the rapidity with which an adiabatic saturation or a thermodynamic equilibrium (a condition in which the cylinder gas cools down to approach the droplet temperature and consequently whereby vaporisation slows down rapidly) is reached as a result of droplet interaction, depends on the air-fuel ratio. Their calculations based on experimental spray formation indicate that adiabatic saturation is approached very closely at very rich mixtures (i.e. in the spray core) and less rapidly at very weak mixtures (i.e. away from the spray centre to the spray edge).

There are quite a number of engine design parameters which can render the effect of droplet interaction less significant. The continuous bringing in of fresh hot air into the spray centre by macroscopic turbulence, the turning effect applied on the fuel spray by the air swirl coupled with spray dispersion and the high overall air/fuel ratios normally employed in diesel engines, tend to keep the cylinder gas temprature and pressure approximately constant during the vaporisation process.

(d) Effect of Radiation: In this model, the heat transfer by radiation from the combustion chamber walls and flame to the liquid droplets has been neglected because it cannot be estimated accurately enough. Moreover, since the influence of radiation is to reduce the effective

value of the total convective heat, Q, required to evaporate any droplet size. Reference (26) has made a simple calculation to amplify its magnitude. According to his calculation, the heat transfer by radiation from a surrounded transmitting and non-reflecting shell (flamefront), having a temperature of 2000°K to a droplet of 0.00142cm (i.e. 14.2 microns) diameter, contributes only 0.2 per cent of the total heat, Q required. Furthermore, the results of his calculation (although it does not include black body radiation from soot) suggest that the effect of radiation decreases in direct proportion to the droplet size and absorptivity. That is, the radiation heat transfer decreases with decreasing droplet size and absorptivity. Of course, the latter parameter is not constant but will decrease as the droplet size decreases. In fact, some similar findings and estimates have been reported by Reference (27).

It is to be noted that the above estimate given by reference (26) is only qualitative, for it is valid for one single droplet whose own radiation loss is neglected. Moreover, for several droplets and carbon particles found in diesel engines, the above analysis may not hold. Until sufficient information is available about carbon particle or droplet radiation, much cannot be said at the present stage. However, radiation is likely to be negligible until the diffusion flame predominates, that is after the time period of present interest.

4.1.5 Chemical Kinetics and its Application to Diesel Combustion

Although the nature of the physical processes discussed previously has been fairly well established, the uncertainty and complexity of the chemical reactions involved in diesel engine combustion have hindered a vigorous application of reaction rate theories. During the delay period, that is before ignition occurs, chemical reaction rates are very important because the temperature is still very low. After ignition, characterised by a measurable pressure-rise, there is generally an extremely rapid reaction of at least all the thoroughly prepared combustible mixture of fuel and air vapour. At high temperatures and pressures, corresponding to the main period of combustion, treatment of subsequent chemical reaction rates may reasonably be simplified to a burning droplet or burning particle theory (as explained later) because the chemical reaction rates are very fast and consequently the reaction times may be neglected.

Comprehensive theories and experiments of reaction mechanisms for combustion processes, particularly for hydrocarbon oxidation are given in Lewis and von Elbe*. With the possible exception of the oxidation of relatively simple compounds (such as H_2 and CO), the detailed reaction mechanism is not well understood. Quantitative knowledge about the specific rate constants is also deficient. However, there is now a general acceptance of chain reactions, in which free radicals form and are propagated and then destroyed due to the effect of promoters or inhibitors. The gas analysis carried out by Jackson (28) in a diesel engine has helped to establish both the oxidation type of chain and thermal cracking mechanisms. These findings have been supported by other co-workers. On the other hand, thermal cracking of fuel vapour molecules has been evaluated theoretically and experimentally by Wakil et al (22). The conclusion is that with light diesel fuels, thermal cracking is insignificant.

Moreover, for a single step reaction involving binary collisions between molecules of two species A and B, according to the classical thermal theory of combustion, the general reaction rate, k_i given in literature (29, 30) is as follows:

$$k_i = Z B_c T^{\alpha} \mathrm{Exp}(-E/R_u T) \qquad (16)$$

where:
- B_c = Frequency factor (is proportional to $C_A C_B \sqrt{T}$)
- E = Activation energy of the reaction
- R_u = Universal gas constant
- T = Absolute temperature
- α = constant ($0 \leq \alpha \leq 1$)
- Z = Steric factor (to account for unfavourable collisons, $Z \leq 1.0$)
- C_A = Concentration of species A
- C_B = Concentration of species B.

The parameter, α, is usually of the order of unity and can reasonably be set equal to zero by modifying slightly the two temperature-

*Lewis, B and Elbe, G "Combustion, Flames and Explosions of Gases" 2nd Edition, New York and London, Academic Press, 1961.

independent parameters, B_c and E. With $\alpha = 0$ equation (16) reduces to the classical Arrhenius equation for the specific reaction rate of this form:

$$k_{iA} = Z\, B_c\, \mathrm{Exp}(-E/R_u T) \qquad (17)$$

However, because of lack of sufficient knowledge in the determination of the activation energies or specific reaction rates, the theory of chemical reaction rates can only be applied to combustion reactions empirically at the present time.

One of the empirical equations suggested and used by Whitehouse et al (5) in calculating the reaction rate in a diesel engine is as follows:

$$R = \frac{K' P_o}{N\sqrt{T}} \int (P-R)\, d\theta\, \left|\mathrm{Exp}(-act/T)\right| \qquad (18)$$

where:

"act" comes directly from Arrhenius equation

= Activation energy

K' = Coefficient in reaction rate

$\int (P-R)\, d\theta$ = The quantity of fuel in the cylinder that has been prepared but not yet burned

N = Engine speed

P_o = Partial pressure of oxygen

T = Gas temperature

$d\theta$ = Crank angle step size.

It is to be noted that a rigorous calculation of reaction rate in premixed fuel-vapour/air in a diesel engine combustion requires above all the exact composition of the fuel used and the instantaneous local temperature.

4.1.6 Ignition Delay Studies

Ignition delay has been defined as the period extending from the beginning of needle lift to measurable combustion. Because of the complex interactions of processes occurring in this period, it is always difficult to measure the point where combustion begins. To overcome this, ignition delay is commonly divided into two different parts, namely the physical and the chemical delay, although there is no accurate theory to show which is rate-determining. However, the physical delay period is defined as the time required for the physical changes to occur to the fuel from its liquid phase

at the injection temperature to the preparation phase at the self-ignition temperature. In other words, it is the time to inject fuel, to atomise to vaporise and to mix the vapour with the cylinder charge. The chemical delay on the other hand, is defined as the period during which local concentrations of product which are capable of self-ignition reactions are made. That is, the period which elapsed from the end of the physical delay period to the beginning of ignition. In most cases, these periods may overlap.

Relatively simple correlations of the ignition delay with physical parameters such as injection characteristics, compression temperature, pressure, engine speed, etc., have been made in diesel cylinder engines by Lyn and Valdmanis (ref. 31), Henein and Bolt (ref.32) and in bombs by Yu and Uyehara (ref.33), Wakil et al (ref. 23), Wolfer (ref.34), etc. Detailed ignition correlations are discussed in the above references and only a brief summary will be given below.

A pressure rise delay (defined as the time that elapses between the beginning of needle lift and a measurable pressure rise due to combustion) correlation for combustion in two different constant volume bombs was given by Wolfer as :

$$I.D_p = \frac{0.44}{p^{1.19}} \quad Exp(4650/T) \qquad (19)$$

where p is the pressure in atmospheres, $I.D_p$ the pressure rise delay in milliseconds and T is the temperature in degrees Kelvin. The above equation is said to be fairly accurate for all the fuels having a cetane number greater than 50. The shape of combustion chamber, the fuel/air ratio, the spray characteristics and the fuel temperature, if not initially higher than 100°C, are claimed to have negligible effects. Small (ref. 35) extended the work of Wolfer a little further, and made two tests in sperical bombs. One test was with rotatable shells held stationary, the other with the shells rotating at 1000 rpm. The aim of these two tests in fact was to determine the effect of turbulence and finally, he reported no appreciable change in pressure rise delay.

Tao et al (ref. 36) on the other hand, obtained an empirical relationship for the temperature rise delay in a modified open chamber engine as follows:

$$I.Dt = 1000\ Exp(x) - 1000 \qquad (20)$$

where :

$$x = \frac{1}{1000}\left(\frac{123}{P} + 0.415\right)\left\{\left(-\frac{36.3}{T} + 0.222\right)N + \left(\left(\frac{47.45 \times 1000}{T}\right) - 26.66\right) + \left(\frac{T}{1000} - 1.45\right)\left(\frac{1000 - N}{60}\right)\right\}$$

It is to be noted that the formula above is the first to include the engine speed, N, as a factor affecting the delay period. Sitkei (ref.37) however, obtained the following expression for the illumination delay in a precombustion chamber :

$$I.Dil = 0.5 + \frac{0.135}{P^{0.7}}\ Exp(7800/RT) + \frac{4.8}{P^{1.8}}\ Exp\ (7800/RT) \qquad (21)$$

and I.Dil is the illumination delay in milliseconds.

Under normal operating conditions when ignition is far from marginal, compression temperature, pressure and injection timing are the major factors affecting the delay period (Figures 15,16). Wolfer's equation (19) was in fact used to assess the ignition delay history shown in the Figures above. Moreover, from the above definitions, it is obvious that the delay period cannot be reduced to zero, partly because even if the fuel on entry were already at its ignition temperature, the fuel and air must mix to a certain degree before combustion can occur, and this will require a certain amount of time. On the other hand, sufficient heat must be released to make the ignition delay's presence felt and again some time is required.

Figure 17 and Appendix A.6 compare the ignition delay period calculated from equations (19) and (20) respectively with experimental data at different engine speeds. The comparison is better using Wolfer's equation. However, since these equations are highly empirical, a more proper selection of expressions for ignition delay is required to account for changes (increase) in cylinder gas compression temperature and pressure (see Figure 16) as well as injection pressure due to increase in engine speed. Above all, the calculated delay period must be compared with the measured and probably modified before it is finally utilised.

To conclude, it is now accepted (references 6, 16) that the quantity of the combustible mixture which reacts

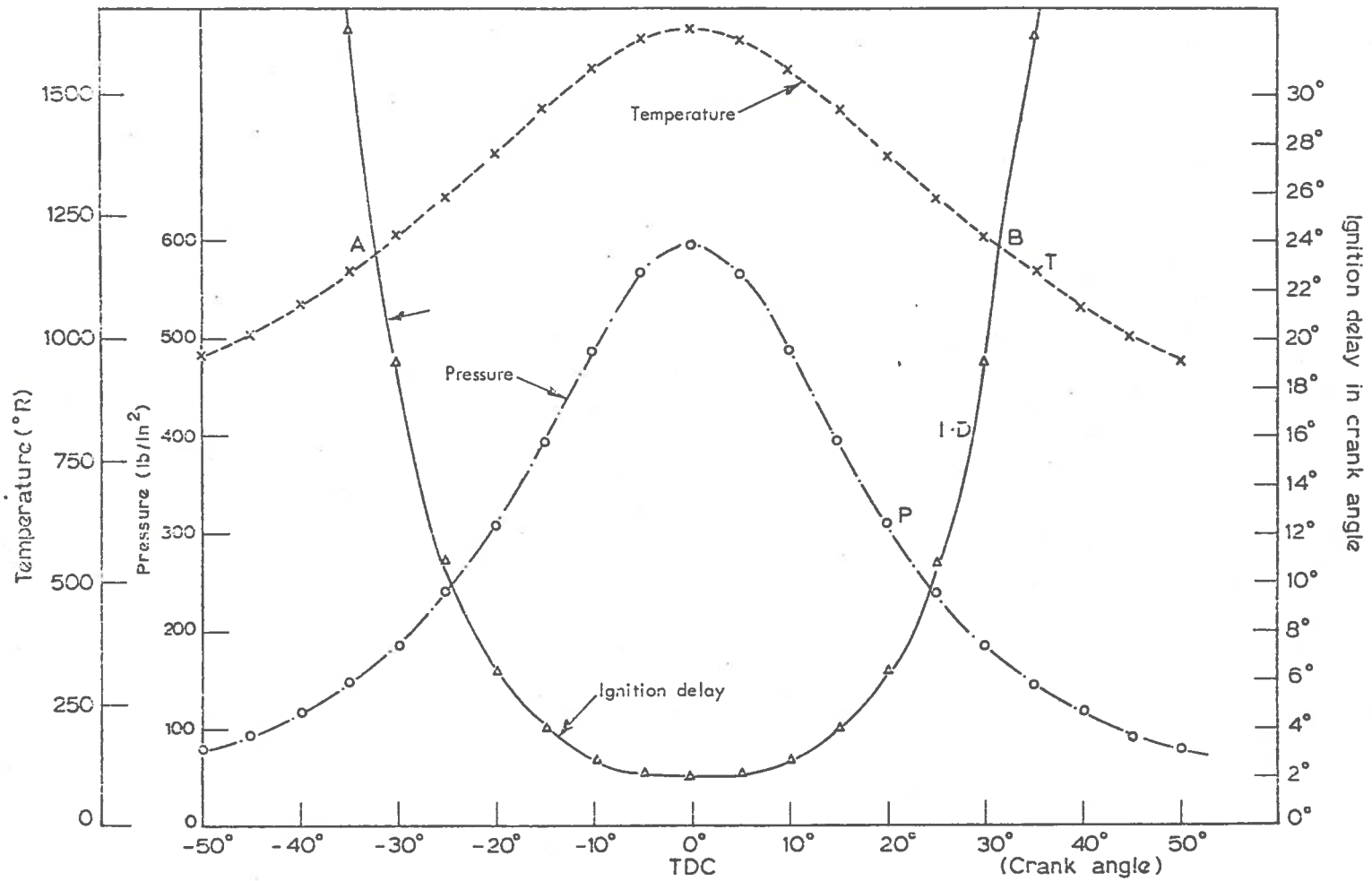

FIGURE 15. VARIATION IN DELAY PERIOD WITH COMPRESSION TEMPERATURE AND PRESSURE

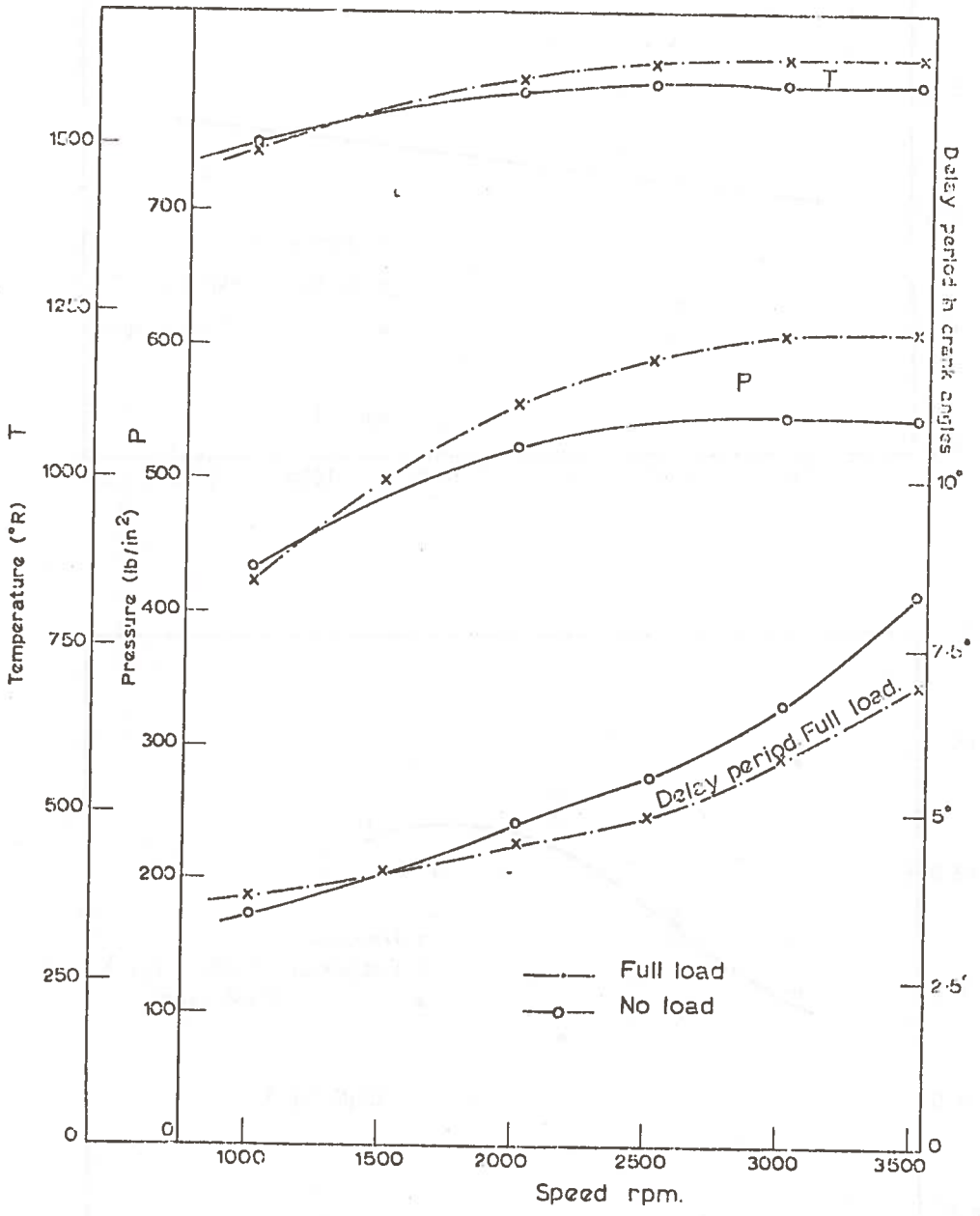

FIGURE 16. VARIATION OF COMPRESSION PRESSURE AND TEMPERATURE AND OF DELAY PERIOD WITH SPEED IN AN INDIRECT COMBUSTION CHAMBER ENGINE. BMC.

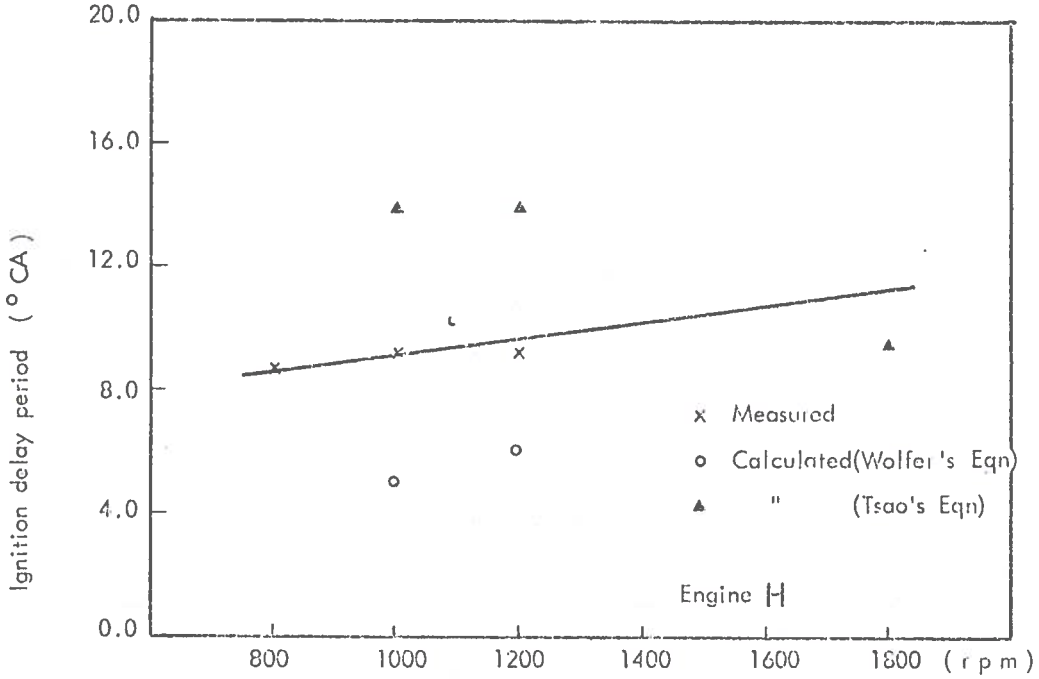

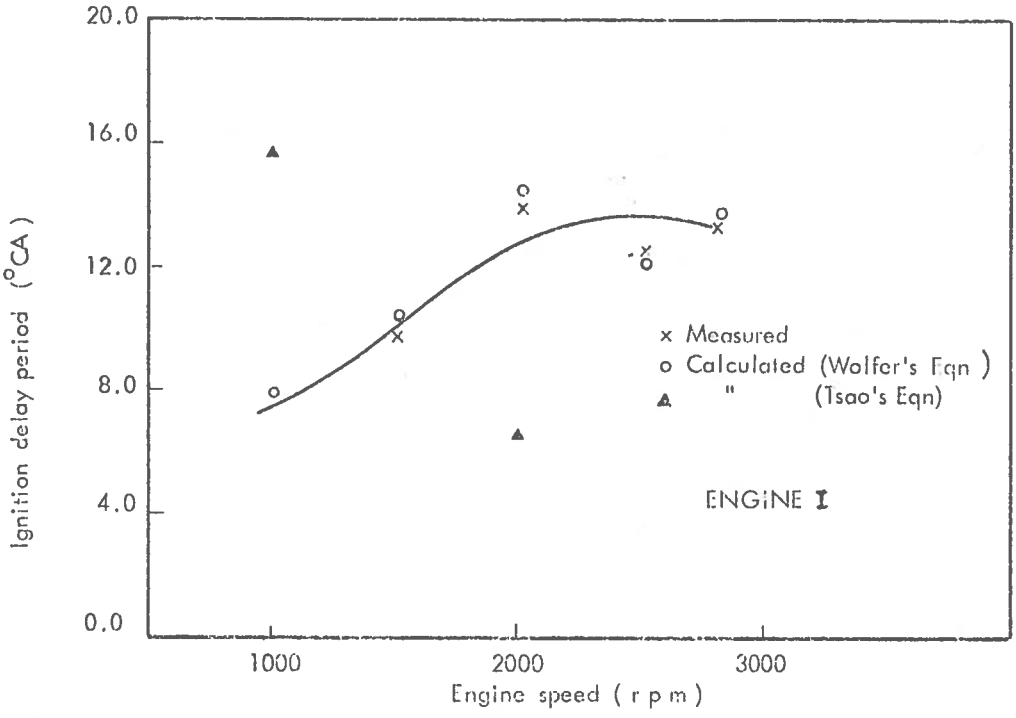

FIGURE 17. MEASURED AND CALCULATED IGNITION DELAY PERIOD

in a rapid uncontrolled manner after ignition delay may not have any relation with the delay period itself at all. The ignition delay period of the MAN engine in Figure 18 is much longer than other conventional engines at different speeds, yet the MAN engine has a lower initial heat release, (Figure 4). .However, with the same engine (or provided wall impingement does not occur) it is logical to assume that the initial heat release, the rate of pressure rise and hence combustion induced noise will increase as the delay period becomes longer.

4.1.7 Burning Droplet or Particle Combustion

After the period in which the physical and chemical processes are the rate controlling, that is after the rapid combustion of suitably premixed fuel vapour/air, the remaining fuel may burn in the form of a droplet or particle. Combustion rate of fuel droplet burning steadily in an oxidising atmosphere has been studied theoretically and experimentally by Godsave (Ref.26), Spalding (ref.38), Wakil et al (ref.20), etc., and corresponding burning droplet equations based on heat and mass transfer are also presented by these workers. Since it is possible that the rates of mass and heat transfer will be increased by the effects of convection, a lower limit for the burning rate of the bulk diffusion flame could be expected, for example in the work of Godsave (in which the convection of hot gases over the fuel droplet was neglected) according to reference (18).

In a diesel engine, combustion in the form of droplet or particle may be sometimes of great interest because the cylinder temperatures and pressures shortly after auto-ignition may be very high so that vaporisation is insignificant. As a result of this, Spalding has suggested a theory (which is explained in Section 4.2.5) by which the burning rate of a carbon particle, a limiting case for the form of hydrocarbon fuel may be estimated. In fact, the combustion of the complete range of forms of hydrocarbon fuels ranging from a carbon particle, heavy fuel droplets, gas oil droplet to a light gasoline droplet, can be considered as a single family, having a progressively increasing transfer number.

4.1.8 Heat Transfer to the Cylinder Walls

Absolute heat release analysis requires an estimate of instantaneous heat transfer rate to the cylinder walls. Since little is known about the pattern of the gas flow remaining after induction stroke, or its concentration

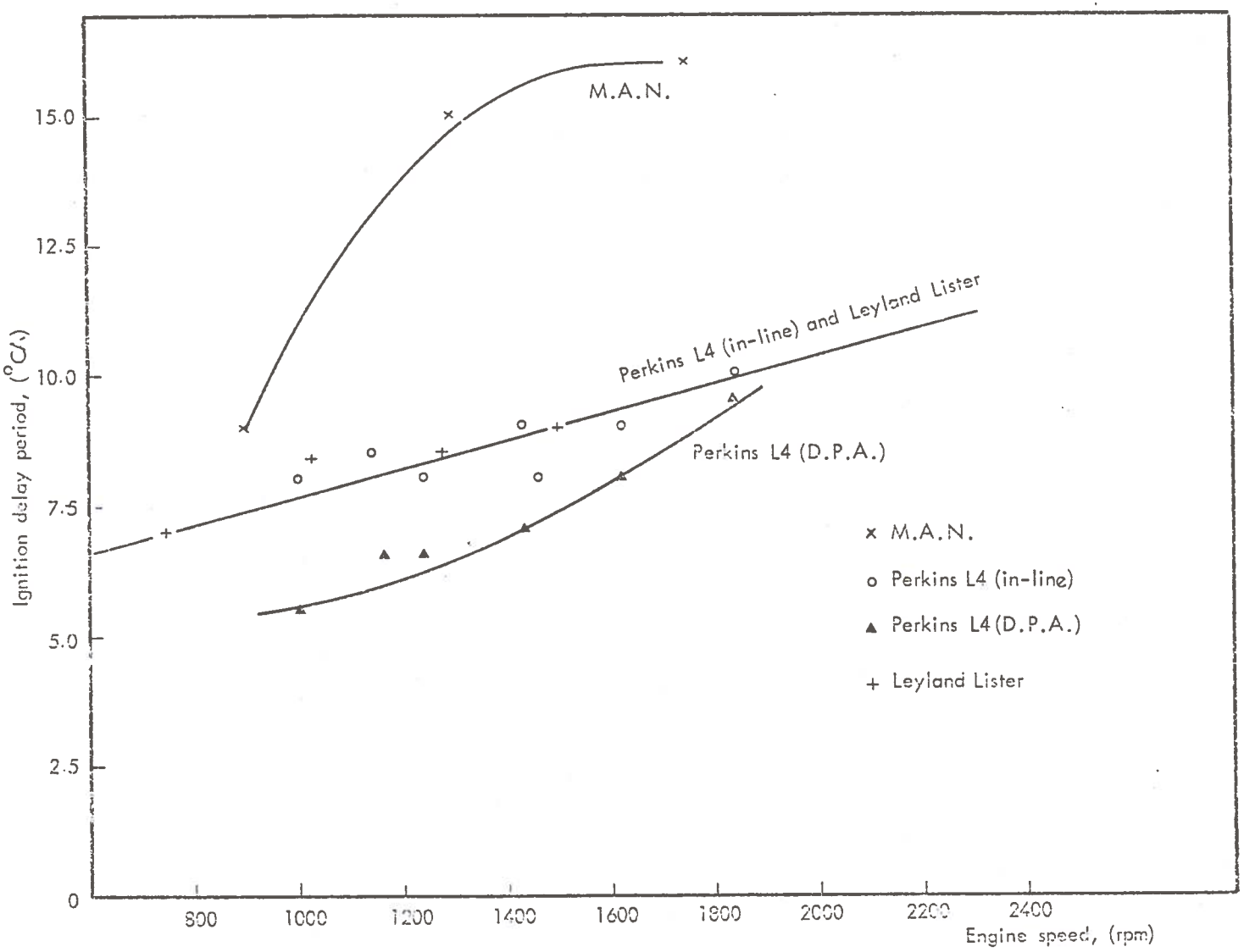

FIGURE 18. DELAY PERIOD AT FULL LOAD AND STANDARD TIMING (LYN)

and turbulence spectrum and also the intensity of flame radiation, which depends on the structure of the flame, so it is impossible to calculate the heat transfer rate accurately. In view of the lack of further data, Eichelberg (ref. 39) or Annand's (ref. 40) empirical equation is still widely used for the calculation of heat transfer in internal combustion engines. According to Eichelberg, the heat transferred from the working gas to the cylinder walls in a small interval of time, δt in a naturally aspirated engine may be evaluated as :

$$\delta Q_{\ell} = H_{\ell} A_{\ell} (T_c - T_{\ell}) \delta t \qquad (22)$$

and

$$\delta Q_{p} = H_{p} A_{p} (T_c - T_w) \delta t \qquad (23)$$

where:

$H = H_{\ell} = H_p$ = Heat transfer coefficient (Btu/sq.in.hour ^{o}R)
$= 1.05 \times 10^{-4} (V_m)^{1/3} \sqrt{P_c T_c}$

δQ , δQ_p = Heat transferred to the liner and piston crown during δt respectively (Btu)

δt = time increment (sec)

A_{ℓ}, A_p = Respective surface areas (sq.in)

T_{ℓ}, T_p = Respective area mean surface temperatures (^{o}R)

V_m = Mean piston speed (in/sec)

P_c = Cylinder gas pressure (psi)

T_c = Cylinder gas temperature (^{o}R)

Annand, on the other hand, abandoned Eichelberg's relation entirely and replaced it by an empirical expression, treating separately the convective and radiative transfer. Thus, his equations for the total heat transfer increment are given by :

$$\delta Q_{A\ell} = A_{\ell} \left| \frac{aK_A}{D} (Re)^{b} (T_c - T_{\ell}) + c(T_c^4 - T_{\ell}^4) \right| \delta t \qquad (24)$$

and

$$\delta Q_{A_p} = A_p \left| \frac{aK_A}{D} (Re)^{b} (T_c - T_p) + c(T_c^4 - T_p^4) \right| \delta t \qquad (25)$$

where:

b = index relating Nusselt number (Nu) to Reynolds number (Re)

a = factor that varies widely with intensity of charge motion, it increases with increasing intensity of motion in the region considered ($a \simeq 0.35$–0.80)

c = coefficient of radiant heat transfer
= 6.875×10^{-12} (Btu/sq.in.hour $^{o}R^{4}$) for diesel engines.
= 9.03×10^{-13} (Btu/sq.in.hour $^{o}R^{4}$) for spark ignition engines - during combustion.
= 0 during compression

Re = Reynolds Number
$= \frac{D_{eng} V_m D}{Visc}$

D = bore of the engine, (in)

Visc = dynamic viscosity of fluid (lb/in.sec)

K_A = thermal conductivity of fluid (Btu/ft.sec.^{o}R)

Moreover, Annand suggested the following values for a and b :

a = 0.38 for the two-stroke
a = 0.49 for the four-stroke
b = 0.70.

From equations (22) or (25) it is readily apparent that Annand's formula for calculating heat transfer is quite sensitive to the exponent b. In other words, the optimum value of b is likely to be obtained through trial and error. However, it was decided to use Eichelberg's correlation because of its simplicity. Of course, for each of the above equations, a multiplying factor is required in order to give the overall percentage heat transfer of the correct order by comparison with estimates from the steady-state heat balance.

4.1.9 General Description of the Model

With the aid of all the processes described above, the Model finally developed may be explained as follows:

(a) The trapped charge which may consist of air contaminated with products of previous cycle, the degree of contamination, charge pressure, temperature and induced charge motion depending on the gas exchange process, is compressed in the cylinder with heat transfer from the surrounding walls initially to it.

(b) Compression of the charge is followed by injection of relatively cool fuel into the chamber. The resultant fuel spray is broken up at once into discrete individual spherical droplets, which are distributed into nine size groups, covering a 5 to 130 microns spread. The initial percentage

by weight of each size group follows a truncated Gaussian Distribution Law and each size group is in turn represented by a single droplet size, which is chosen as some average of the range of its particular size group.

(c) As soon as the droplets are formed, they will start to evaporate and the amount vaporised from each size group is obtained as a function of time (degree crank angle). Similarly, the total amount of vapour formed from the fuel spray is then obtained by adding the properly weighted vaporisation due to each size group.

(d) The total vapour formed will mix homogeneously with part of the air in the combustion chamber. Then it will undergo slow preliminary reactions which take place during the so-called "delay period", although these preliminary reactions are considered for simplicity to be insignificant.

(e) The chemical reactions, which give rise to an appreciable rate of heat release will start when an overall air-vapour mixture of combustible strength (close to stoichiometric) of the droplets injected into the cylinder have undergone the delay period. The temperatures and pressures are well above that necessary to support chain reactions so that ignition of any fuel element does not require energy transfer from adjacent elements, although it may be assisted by such transfer.

(f) The prepared mixture (i.e. homogeneously mixed vapour) formed before combustion and any gaseous fuel present (as a result of previous cycle) before injection is initiated, will start to burn from a number of regions in the combustion chamber. The rate of heat release will be proportional to the concentration of the prepared mixture, the temperature and the oxygen available in the chamber. The heat released from these reactions will alter the temperature and pressure of the gas within the cylinder and the chemical reactions will alter the mean concentration of the cylinder.

(g) The reactions after ignition delay will give rise to high local temperatures around the burning droplets and eventually decrease the delay period considerably for all the droplets then in the combustion chamber. All these droplets will start to burn almost immediately and all droplets subsequently injected will start to burn as they enter the combustion chamber if enough oxygen is nearby. Therefore, the combustion rate of the droplets will depend on the size-distribution and the oxygen (air) supply.

(h) As burning proceeds, the oxygen supply in the combustion chamber decreases. It is probable that the first vapour formed will take priority in obtaining oxygen over the liquid droplets. Of course, during the premixed stage, combustion of both liquid and vapour will proceed simulataneously until either all the vapour or the droplets are burnt or all the oxygen available has been used up. This latter condition will give the maximum possible heat release from the cycle.

(i) Finally, if all the oxygen is used up before combustion is completed, some droplets will remain unburnt or partially burnt, giving rise to high exhaust smoke levels. The level of exhaust smoke will depend on the droplet size as well.

4.2 Theory

For the sake of completeness, the theory of simultaneous mass and heat transfer proposed in references (15, 20) is summarized below. Some modifications (such as droplet-size distribution, drag coefficient, air swirl velocity, etc.) are introduced so that the above theory may be extended directly to a diesel combustion simulation.

Figures (19a) and (19b) show the spray model and a schematic diagram of heat transfer to vapour film and liquid droplet. The spray consists of discrete spherical droplets, grouped into nine droplet sizes. Each size-group is represented by a single droplet size, which is chosen as some average of the range of its particular size group. This single spherically symmetrical droplet size is shown in Figure 19c to be surrounded by a film containing an air-fuel vapour mixture.

N.B. The film is assumed spherically symmetric, despite relative motion.

At any one instant, the mixture concentration varies from a maximum at the droplet surface to a minimum at the outer edge of the film. The shape of the temperature gradient curve depends on the relative temperatures of the fuel droplet and air and the mass of vapour being diffused out at that instant. For simplicity, it is convenient to divide vaporisation process into three parts, namely the heat transfer, the mass transfer and the velocity change.

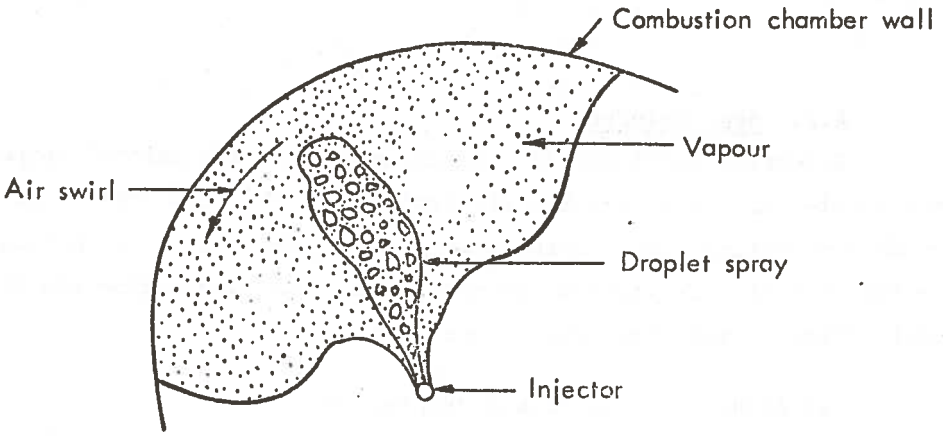

FIG. 19a. SPRAY MODEL

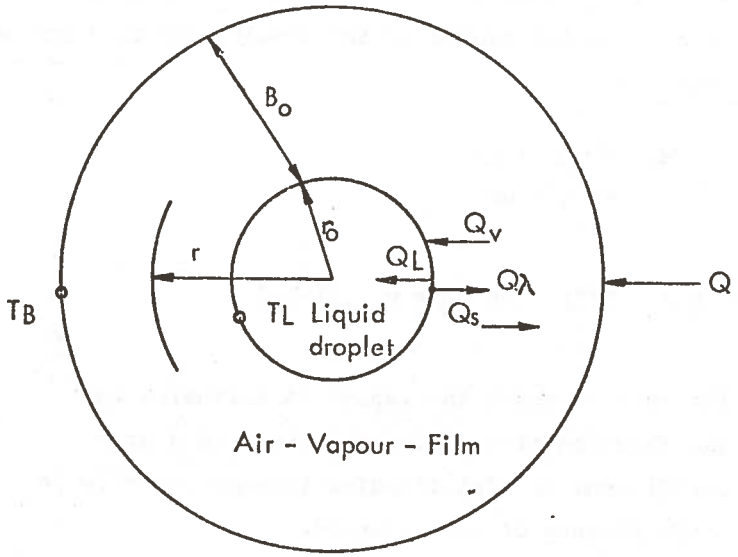

FIG. 19b. HEAT TRANSFERRED TO DROPLET

Where: Q = Total heat transferred from air to droplet

QL = Sensible heat received by droplet

Qs = Diffusing vapour superheat

Qv = Heat received at droplet surface = $Q_L + Q\lambda$

$Q\lambda$ = Heat of vaporisation

Bo = Film thickness

T = Temperature

B, L = Gas, liquid

FIG. 19c. COMBUSTION MODEL.

4.2.1 Heat Transfer

Referring to Figure 19 and assuming that the initial temperature of the droplet is lower than the air temperature (T_B) and lower than its own wet-bulb temperature (equilibrium temperature), which is true in c.i. engines, the total heat transfer, Q, from the air to the film surrounding the liquid droplet, prior to ignition, goes three ways

(a) to heat up the liquid droplet, QL
(b) to vaporise the liquid , Qλ
(c) to be carried back with the diffusing vapour in the form of superheat, Qs

(N.B. Q does not include radiant heat transfer. Justification is explained already)

If at any instant during vaporisation, a point in the air-vapour film at a radius r, from the centre of the droplet and at temperature T is considered, then,

$$Q_y = QL + Q\lambda$$
$$= Q - Qs \qquad (26)$$

but

$$Q = h A_o \, dT/dy \quad \text{and} \quad Q_s = w_{cpf}(T-T_L) \qquad (27)$$

where

w = the rate at which the vapour is diffusing out
y = the fraction of the film thickness (B_o) at r
h = coefficient of heat transfer through the film in the absence of mass transfer
cpf = the specific heat of the fuel vapour
T = the temperature of the mixture at position y
T_L = the temperature of the surface of the droplet
A_o = the surface area of liquid droplet

Substituting equation (27) into (26) and rearranging it, equation (26) becomes

$$dy = \frac{h A_o}{Q_y - w_{cpf} T_L + w_{cpf} T} \, dT \qquad (28)$$

Integrating across the film between y=0 (at r=ro) to y=1 (at r=ro+B_o) where $T=T_L$ to $T=T_B$ and considering the specific heat of the fuel vapour, cpf to be constant at some mean value, it follows:

$$\int_0^1 dy = \int_{T_L}^{T_B} \frac{h\,A_o}{Q_v + w_{cpf}\,(T-T_L)}\,dT$$

$$|y|_0^1 = \frac{h A_o}{w_{cpf}}\,\ell n\,|Q_v + w_{cpf}(T-T_L)|_{T=T_L}^{T=T_B}$$

$$1 = \frac{h\,A_o}{w_{cpf}}\,\ell n\left|\frac{Q_v + w_{cpf}\,(T_B-T_L)}{Q_y}\right|$$

or by rearranging the above equation and expressing it in an exponential form :

$$Exp(w_{cpf}/h\,A_o) = \frac{Q_v + w_{cpf}\,(T_B-T_L)}{Q_y}$$

and defining z as $w_{cpf}/h\,A_o$, then

$$Q_y = \frac{w_{cpf}\,(T_B-T_L)}{Exp(z) - 1} = h\,A_o(T_B-T_L)\;\; z/|Exp(z) - 1|$$

$$Q_y = Q\;|z/\{Exp(z) - 1\}| \qquad (29)$$

Thus the factor $z/|Exp(z) - 1|$ represents the fraction of the total heat transfer Q from the air that finally arrives at the surface of the liquid droplet and supplies the latent heat of vaporisation for the vapour diffusing out as well as the sensible heat added to the liquid droplet itself. The above factor therefore represents a correction factor to the heat transfer coefficient, h, without mass transfer from the droplet.

Correlation for the Nusselt number, NN_u for heat transfer is given by reference 41 (for spheres at moderate NR_e):

$$NN_u = \frac{h(2ro)}{K_m} = 2 + 0.6\,(NP_r)^{1/3}\,(NR_e)^{\frac{1}{2}} \qquad (30)$$

From the above equations, it can be seen that a calculation of the heat transfer through the film at any instant during the vaporisation process of the droplet would require the knowledge of the temperatures on both sides of the air-vapour film surrounding the droplet, of the velocity of the droplet relative to the air and its radius, which is dependent on the mass transferred up to that point and on the droplet temperature (see Figures 12,13).

4.2.2 Mass Transfer

Neglecting thermal diffusion and assuming all diffusion to result from the driving force of concentration or partial pressure gradient which exists in the direction of diffusion, the following equations are obtained for counter diffusion systems (ref.39).

$$\frac{dP_f}{dr} = -\frac{X}{R_u T}\ (rf\ P_a - v_a\ P_f) \qquad (31)$$

and $$X = (R_u T)^2/D_y\ P_T \text{ or } D_y = (R_u T)^2/\ X\ P_T \qquad (32)$$

where:

P_f = average partial pressure of fuel vapour in film

P_a = average partial pressure of air in film $(=P_T - P_{fL}/2)$ (P product is assumed very small and thus negligible)

rf = molal rate of diffusion of fuel vapour in equimolal diffusion, based on surface area of liquid droplet, A_o

r_a = molal rate of diffusion of air in equimolal diffusion

X = proportionality factor

D_y = diffusion coefficient of air-vapour system

R_u = universal gas constant

P_T = total pressure

Substituting for X in equation (31) with the aid of (32), then:

$$\frac{d\ P_f}{dr} = -\frac{R_u T}{D_y P_T}\ (r_f\ P_a - r_a\ P_f) \qquad (33)$$

Since in most cases of a fuel droplet vaporising in air, a uni-directional diffusion takes place, that is, there would be diffusion of the fuel vapour away from the droplet, while the rate of diffusion of the air in the opposite direction towards the droplet is usually insignificant and may considered zero, then:

$$r_a = 0 \qquad (34)$$

Therefore, equation (34) becomes:

$$\frac{d\ P_f}{dr} = -\frac{R_u\ T}{D_v\ P_t}\ r_f\ P_a \qquad (35)$$

From the total pressure, $P_T = P_f + P_a$ and substituting for P_f in equation (35) it follows that :

$$\frac{d P_f}{dr} = \frac{d(P_T - P_a)}{dr} = \frac{R_u T}{D_y P_T} r_f P_a \qquad (36)$$

or

$$\frac{d P_T}{dr} - \frac{D P_a}{dr} = - \frac{R_u T}{D_y P_T} r_f P_a$$

Since P_T is assumed constant throughout the film, equation (37) is then :

$$\frac{d P_a}{dr} = \frac{R_u T}{D_y P_T} r_f P_a \qquad (37)$$

Again, D_y and T are also considered constant at their instantaneous mean values. By integrating the above equation between $r = r_o$ and $r = r_o + B_o$, where $P_a = P_{aB}$, then

$$\int_{P_{aL}}^{P_{aB}} \frac{d P_a}{P_a} = \frac{R_u T}{D_y P_T} r_f \int_{r_o}^{r_o+B_o} dr$$

$$\left(\frac{P_a B}{P_{aL}}\right) = \frac{R_u T}{D_y P_T} r_f (r_o + B_o - r_o) = \frac{R_u T}{D_y P_T} r_f B_o$$

Therefore:

$$r_f = \frac{D_v P_T}{R_u T B_o} \ln \left(\frac{P_{aB}}{P_{aL}}\right)$$

$$r_f = \frac{D_v}{R_u T B_o} (P_{aB} - P_{aL}) \frac{P_T}{\frac{P_{aB} - P_{aL}}{\ln (P_{aB}/P_{aL})}} \qquad (38)$$

In order to maintain the total pressure, the following conditions must be satisfied, i.e.:

$$P_T = P_{aB} + P_{fB} \quad (\text{at } r = r_o + B_o)$$

or

$$P_T = P_{aL} + P_{fL} \quad (\text{at } r = r_o)$$

With the above boundary conditions and assuming further that the partial pressure of the fuel vapour at the outer edge of the film, P_{fB} is zero, then the rate of diffusion of the fuel vapour can be written in terms of partial pressures in the film as follows:

$$r_f = \frac{D_v}{R_u T B_o} P_{fL} \frac{\frac{PT}{P_{fL}}}{\ell n \left| P_T/(P_T - P_{fL}) \right|} \qquad (39)$$

or

$$r_f = \frac{D_v P_{fL}}{R_u T B_o} \times \text{ALPHA} \qquad (40)$$

where

$$\text{ALPHA} = \frac{\frac{P_T}{P_{fL}}}{\ell n \left| P_T/(P_T - P_{fL}) \right|}$$

Equation (40) states that the unidirectional diffusion of the fuel vapour into the air equals the equimolal rate of the concentration, times the factor ALPHA (which is greater than unity). This increase in rate represents a correction for the fact that the net rate of movement of the air is zero, while the diffusion velocities of the fuel vapour and the air relative to each other must be maintained.

Because the physics of the factors determining B_o are very difficult to evaluate (ref.15), a semi-theoretical relationship is set up for mass transfer on the basis that the mass of fuel vapour diffused out per unit time according to ref.39 is given by :

$$w = A_o \, kg \, P_{fL} \, \text{ALPHA} \qquad (41)$$

where kg is the mass transfer coefficient for the film in the case of equimolal diffusion, which is generally estimated from the equation of Ranz (34) :

$$NNu' = \frac{2 r_o P_a kg}{D_{vx} \, Denm} = 2 + 0.6 \, (NS_c)^{1/3} (NR_e)^{\frac{1}{2}} \qquad (42)$$

and Denm is the average density of the air-vapour mixture in the film.

It can be seen again from the above equation that to calculate the mass transfer at any instant, a knowledge of the heat transfer and of the radius and velocity of the droplet at that instant is essential (Figs.12,1

It is to be noted that the difference between equations (30) and (42) lies in the cube root of Prandtl number (NP_r) and Schmidt number (NS_c) respectively. At high gas temperatures, $NP_r \approx NS_c$ according to Spalding (38). In other words, the Nusselt number correlation for heat transfer (NNu) is equal to that of mass transfer (NNu'), that is NNu $\approx$ NNu'.

4.2.3 Velocity Equation:

Calculation of both the heat and mass transfer at any instant, requires the knowledge of the velocity of the droplet at any instant during the vaporisation process, since it enters into both correlations. The droplet is considered to be injected with a certain initial velocity relative to the air (i.e. Uo_{rel}). Aerodynamic drag forces will then either decelerate it or accelerate it so that its velocity approaches that of the air in a very short time. The less the density of the air, that is, the lower its pressure and the higher its temperature, the less effective the drag forces and the greater and more rapid the penetration through the combustion chamber.

From the theory of aerodynamics, the drag force exerted by a moving fluid upon an immersed body may be calculated from the equation:

$$F = -\frac{m}{g}\frac{dU_{rel}}{dt} = C_D \frac{A_c}{g} Denm \frac{U_{rel}^2}{2}$$

$$F = C_D \frac{\pi}{8} D_o^2 Denm U_{rel}^2 \qquad (43)$$

where C_D is the coefficient of drag for the given body form and is a function of the Reynolds number; A_c the cross sectional area of the body ($\pi/4\ D_o^2$) and Denm is the density of the air. But m is the mass of the body (Denl x $\frac{\pi}{6} D_o^3$); D_o is the initial diameter of the body and Denl is the density of the body. Then,

$$m\frac{dU_{rel}}{dt} = Denl \times \frac{\pi}{6} D_o^3 \frac{dU_{rel}}{dt} = -C_D \frac{\pi}{8} D_o^2 Denm U_{rel}^2$$

In general:

$$\frac{dU_{rel}}{dt} = -\frac{3}{4} C_D \frac{Denm}{Denl} \frac{U_{rel}^2}{D} \qquad (44)$$

During vaporisation, the correlation proposed by Sami (42) for C_D is considered valid and given by:

$$C_{Dv} = \text{Betav}\ (0.4 + 50/NR_e) \tag{45}$$

where $(5 < NR_e < 10{,}000)$

Similarly, during the burning period, C_D is:

$$C_{Db} = \text{Betab}\ (20/NR_e^{0.6}) \tag{46}$$

where $(1 < NR_e < 600)$.

It is noted above that the drag coefficient (C_{Dv} and C_{Db}) of the droplet during the vaporisation and the burning period are Betav and Betab times those for the solid spheres respectively. Moreover, the dragforce consists of the forces due to skin friction and form drag. When vapour projects from the droplet surface, the skin friction decreases due to the thickened boundary layer, and the form drag decreases as a consequence of weakened Karman vortices. Betav and Betab being correction factors when considering the effects of vaporisation and combustion, their numerical values are smaller than 1. Because of the lack of sufficient information, these factors are assumed to be constant at each instant during vaporisation and combustion respectively. However, the following values are suggested (ref.42) for the above factors:

$$\text{Betav} = 0.85$$
$$\text{Betab} = 0.40.$$

In any case, the drag coefficient is evaluated at the Reynolds number (NR_e) for which the calculation is performed. It is again evident that to calculate the deceleration of the droplet at any instant, a knowledge of both the heat and mass transfer is essential.

On the whole, the droplet relative velocity, the rate of heat transfer from the charge to the droplets and also the rate of heat interchange between the charge and the cylinder walls, etc., will be affected by the turbulence of the charge. On the other hand, since generation of turbulence in a combustion chamber is a design problem, and since it varies from chamber to chamber, it is difficult at this stage to say precisely how it affects the factors above. However, what can be said is that part of its bulk effect is embedded into the ignition delay period. That is, the delay period is known to decrease as turbulence increases.

Also, turbulence is known to play a significant role in spray formation and disintegration, especially at high engine speeds.

4.2.4 Droplet Temperature

The droplet temperature is determined from the energy balance applied (based on average bulk gas temperature, T_B) at the liquid droplet surface (equation 26), i.e.

$$Q_L = Q_y - Q\lambda \tag{47}$$

The heat, Q_L for raising the liquid temperature is expressed by equation (47) above. The values of Q_y and w are already given by equations (29) and (40) respectively and the heat of vaporisation Q_{LAM} (i.e. $Q\lambda = w \times Q_{LAM}$) is determined by the temperature of the liquid droplet (T_L).

By assuming that the temperature of the droplet is uniform over a very small time interval, which implies infinite thermal conductivity or very fast heat circulation within the droplet, the change in droplet temperature is related to the heat as follows:

$$Q_L = m C_{pL} \frac{dT_L}{dt} \tag{48}$$

or

$$\frac{dT_L}{dt} = \frac{1}{mC_{pL}} (Q_y - w \times Q_{LAM}) = \frac{1}{mC_{pL}} (Q_y - Q\lambda) \tag{49}$$

where m and C_{pL} are the mass and the specific heat at constant pressure of the liquid droplet respectively.

From equation (48), to estimate the rate of change of the droplet temperature, requires a knowledge of the instantaneous heat transfer rate, mass transfer rate, droplet temperature and droplet size. If the heat transfer rate, Q_y is larger than the rate at which heat is carried away, by the vaporising liquid, $Q\lambda$, the droplet temperature will increase. If Q_y is lower, the droplet temperature will decrease. At some point, the heat transfer rate may equal the heat carried away by the vapour and the droplet temperature will then remain constant. This in fact corresponds to a droplet "wet-bulb" (equilibrium) temprature and consequently all the heat that arrives at the droplet surface will be carried away as vaporising liquid.

4.2.5 Droplet or Particle Burning:

Shortly after the droplet temperatures reach the thermodynamic critical temperature, Tl_c (which can be estimated), the vaporisation process is considered to be insignificant any further. This is because the latent heat of vaporisation is virtually zero and very high vaporisation rates are expected, and what would be even higher droplet burning rates. As a result of this and from the knowledge gained from other previous work, it becomes evident that some other mechanism is controlling combustion after the auto-ignition (see Section 4.4).

To this end, an assumption similar to that of Greeves (43) is made. The droplet vaporisation process is allowed to persist up till the end of the premixed combustion after which the droplet burns according to a modified particle theory of Spalding in this form :

$$\frac{dM_p}{dt} = 2 \frac{D_p D_v}{AUC} \text{Denm } \ell n (1+BxBfac) \left|1 + 0.276(NR_e)^{\frac{1}{2}}(NS_c)^{1/3}\right| \qquad (50)$$

where

$$B = 12 \times 0.232 (1-F_R/F_{st})/ \left|32(1+F_R)\right| \qquad (51)$$

and

AUC = a constant (to be determined by comparison with experimental heat release period)

M_p, D_p = droplet or particle mass and diameter respectively.

Denm, D_v = Average density and diffusion coefficient of the combustion gases controlling mass transfer

B = transfer number for burning droplet (in low temperature regime)

F_R, F_{st} = overall and stoichiometric fuel/air ratio respectively

B_{fac} = transfer number multiplying factor (suggested by ref.43 and to be determined by comparison with experimental results).

4.3 Method of Calculation

Because of the dependence of the heat transfer, mass transfer and velocity equations upon each other and the complexity of these equations, a stepwise integration process is necessary, where the values required are evaluated over a small period of time during which the properties of the droplet and the charge are assumed to be constant. The process of calculation is as follows:

The liquid spray emerges from the injector hole with initial temperature TL_o and an average initial velocity U_o, the latter being estimated from equation (52) below:

$$U_o = Q_{inj}/(DenL \times A_{sh} \times C_{dis} \times T_{inj}) \qquad (52)$$

where

U_o = average initial velocity (in/sec)
Q_{inj} = total mass of fuel injected (lb) - Appendix A.3
A_{sh} = area of spray hole (sq.in)
C_{dis} = discharge coefficient
DenL = density of the fuel (lb/cu.in)
T_{inj} = injection period (sec.)

The actual initial velocity of the fuel spray relative to that of the swirling charge, U_{orel} is given by :

$$U^2_{orel} = U^2_o + U^2_{swrl} \qquad (53)$$

where U_{swrl} is the product of the swirl angular velocity and the cylinder radius (i.e. $U_{swrl} = 2\pi\ r_b\ k\ N/60$ and r_b, k and N are the cylinder radius, the swirl ratio and engine speed respectively). This means that a value for k and hence the swirl angular velocity during fuel injection can be obtained from the estimated trapped swirl rpm and engine rpm. The mean droplet diameter, SMD of the whole spray is calculated (and modified) from equation (13), though equation (53) has been substituted for the relative velocity in equation (13). Moreover, the fuel spray is assumed to consist of nine droplet size groups and the diameter of a single droplet representing each size group is determined from SMD with the aid of the truncated Gaussian distribution in Appendix A.4. Each droplet then with the initial conditions given above, is considered to move through a uniform gas field with an initial relative velocity, U_{orel}, uninfluenced by the presence of the neighbouring droplets.

Preparation histories of the droplets are determined by solving equations (41), (44), (45) and (49) until the end of the premixed stage is reached when the remaining mass of the droplet then burns according to equations (44), 46) and (50).

A satisfactory method of solving the above equations is by generating a very small time step. For instance, the time increment, dt, is defined as follows :

(a) dt = 0.000010 sec (until the preparation time of 0.00050 sec is reached)

(b) dt = 0.00010 sec (up till the end of the premixed combustion stage and throughout the droplet burning period)

These small time increments are necessary because the small droplets give off their vapour in a very short interval of time.

According to Wakil et al, NR_e, NP_r and NS_c, which are the droplet Reynolds, Prandtl and Schmidt numbers, should be evaluated on the basis of mean gas-vapour envelope properties (as defined in Appendix A.I taken at temperature, T_m. An attempt has been made to obtain estimates of a the required diesel fuel vapour property functions (see Appendix A.I) although in some cases the assumption that the dodecane fuel ($C_{12}H_{26}$, the principal ingredient of diesel fuel) properties are representative of diesel fuel has to be made.

At the end of the calculations, the computation is organised to sum up all the preparation rates (i.e. P_R) at each crank angle (each step) and multiply it by a local oxygen-supply factor, F_{loc}. In other words, the actual total preparation rate, P_{rtot}, is mathematically expressed thus:

$$P_{rtot} = F_{loc} \sum_{n=1}^{9} P_{rn} = F_{loc}\, P_R \qquad (54)$$

where P_{rn} is the preparation rate of each droplet size group at each step or crank angle and F_{loc} is defined as :

$$F_{loc} = \frac{M_{oav} - M_{uti}}{M_{oav}} = 1 - \frac{M_{uti}}{M_{oav}} \qquad (55)$$

where M_{oav} and M_{uti} are the volume (mass) of oxygen available in the cylinder for combustion and the volume (mass) of oxygen utilised or entrained respectively. The latter is calculated using a jet model (for details, see Appendix A.2). From equation (55) it can be seen that as M_{uti} increases as a result of combustion, the local oxygen supply factor, F_{loc} decays for a constant supply of oxygen.

Furthermore, for the premixed burning stage, two simple modes of calculation are used, purely on comparison grounds. In the first case, the burning rate during the above stage is allowed to follow a triangle rate Law (ref.44) with 6 degrees crank angle base. In the second case, heat is released according to a modified type of Arrhenius equation (65) in Section 4.1.4, in this form :

$$R = K' \frac{F_{loc}}{\sqrt{T}} \int (P_R - R)\, d\theta \; |Exp(-act/T)| \qquad (56)$$

where nearly all the terms above have already been defined. T is the instantaneous average cylinder gas temperature, obtained from the heat release analysis and of course, taking into account the heat transferred to the cylinder walls. The value of $K' = 3.0 \times 10^6$ once determined for one engine, is never varied but used for correlation over a wide range of operating conditions for different engines. On the other hand, a constant value of 2.7×10^4 is assigned to "act" in equation (56) as suggested by ref.(45).

It is to be noted however, that for the two cases considered above, a preparation efficiency of about 88 per cent is selected and compared with experimental heat release analysis. This efficiency allows for the fact that some air-vapour pockets in the cylinder are too lean or have not been thoroughly mixed or both and therefore cannot take part in the reaction process during the premixed burning stage. In other words, 88 per cent of the total fuel prepared during the delay period is assumed to be ready for burning during the above stage.

After rapid heat release, characteristic of the above first stage, the subsequent processes contributing to the bulk of heat release last for longer periods and the combustion of the fuel proceeds essentially via the mechanism of droplet (particle) diffusion burning. The rate of heat release is given by equation (98) multiplied by the fuel calorific value. This rate of heat release will obviously depend on the total heat released during the premixed stage, the droplet size distribution and the availability of oxygen in the cylinder.

Figure 20 shows a Flow Chart of the simulation.

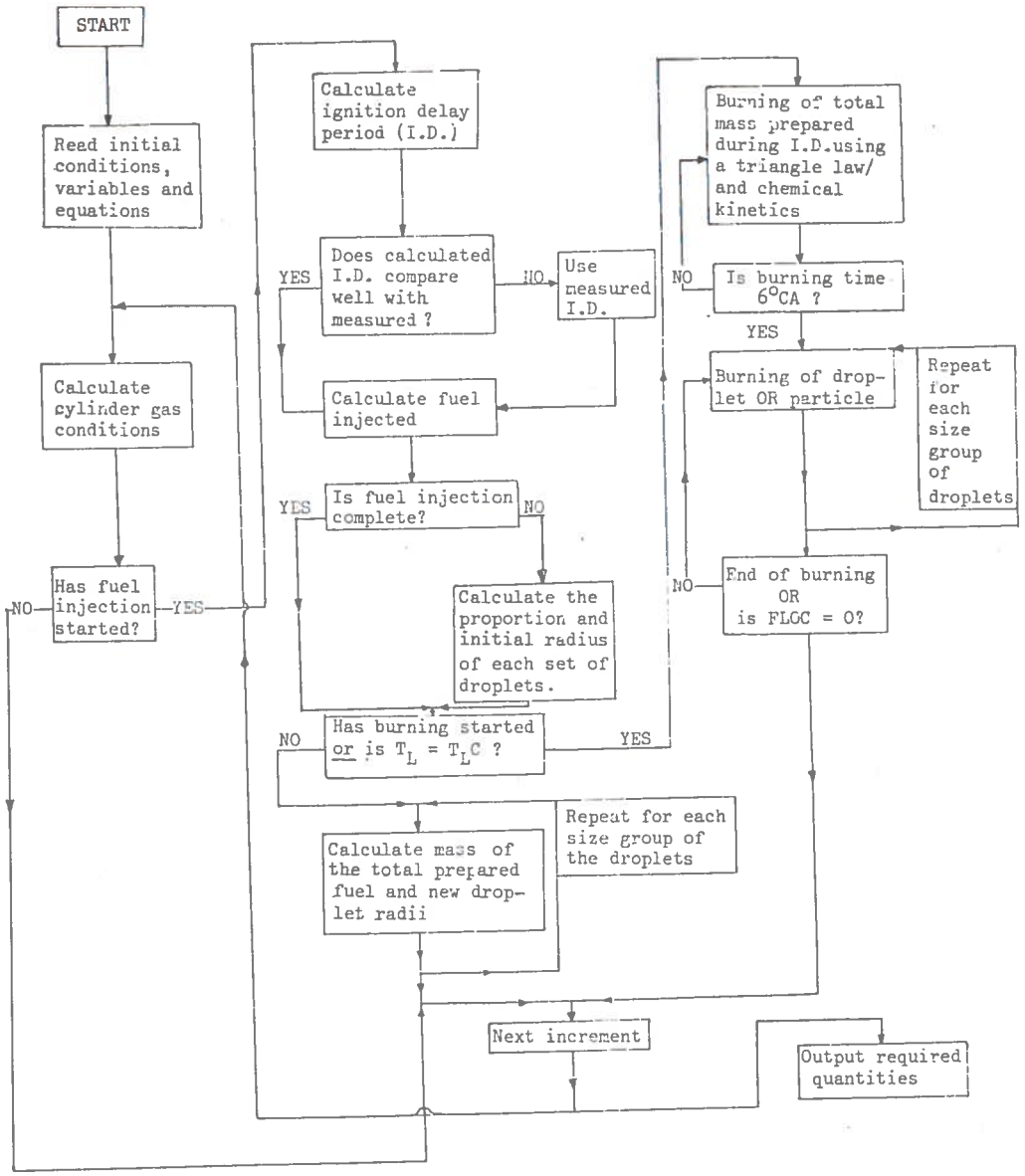

FIGURE 20. COMBUSTION SIMULATION FLOW CHART

4.4 Results and Discussions

Before this theoretical combustion model could be used to predict and describe engine performance, it was found necessary to make some simplified assumptions (section 4.1.4) and to assign values to some constants, for the mathematical solutions to be possible.

Some of the assumptions in Sections 4.1 and 4.2 require further amplifications. It is mentioned in Section 4.2.5 that the vaporisation process is insignificant or ceases after the droplet temperatures reach their thermodynamic critical temperature, $T_{\ell c}$, which is known quite reasonably (ref.14) for most of the pure hydrocarbons. For the dodecane ($C_{12}H_{26}$) on the other hand, which is considered to be the principal ingredient of diesel fuel, $T_{\ell c}$ is 1340°R (ref.14). However, for all the calculations made using the approach in Section 4.3, the droplet wet-bulb temperatures never exceeded 1236°R and even then the smaller droplets (< 50 microns in diameter) attained this latter temperature during the ignition delay period and the larger droplets (> 50 microns) after the premixed burning stage has expired, according to the preliminary experimental results carried out. Since there are several uncertainties concerning vaporisation of a multi-component fuel like diesel as $T_{\ell c}$ (which is unfortunately is not known precisely) is approached, one would expect a difference in the measured $T_{\ell c}$ and the calculated droplet wet-bulb temperatures and also in the calculated and measured auto-ignition temperatures. In spite of these, the assumption that vaporisation process is to be allowed to continue up to the end of the premixed burning stage is probably nearer to reality, for it is known in general that combustion begins long before vaporisation is complete.

Although the droplet sizes ranging from 5 to 140 microns are found to give burning times comparable with experimental analysis and hence used in most of the calculations reported in this report yet it is possible that the largest droplets found in the actual diesel spray are bigger than 140 microns (perhaps up to 250 microns according to ref.41). Even so, there will be a few of these judging from Table A.2.1 and the graph of the droplet distribution, Figure A.2.1. Furthermore, from the trend of the values of the spray penetration presented in Table A.4.1, coupled with the calculation of the droplet histories in Figure 13, droplets larger than 50 microns would be likely to impinge on the walls of a diesel engine having approximately a 5 inch bore. Of course in practice, because of the high combustion temperatures in the cylinder, the droplet life times

would be shorter than those calculated and consequently only larger droplets (>>50 microns) would be expected to hit the cylinder walls.

Some of the input data to the theoretical combustion model could only be found by guesswork and comparison between theoretical calculations and experimental results. The data input includes:

(a) The initial fuel temperature (TL_o): The liquid spray is assumed to emerge from the injector hole with initial temperature of 610°R.

(b) The initial average relative velocity of the fuel spray (U_{orel}): The total fuel, Q_{inj} injected (a method of calculating Q_{inj} is shown in Appendix A.3) during an average injection period of 20 degrees crank angle is 70 mm^3. The discharge coefficient, C_{dis} on the other hand is taken as 0.70. This value is obtained by summing all the C_{dis} values given in reference 44 and building a mean value (The value is then compared with the calculated C_{dis} in the Appendix above). There is a slight implication for adopting the above method, for C_{dis} is known to depend on the geometry of the injector nozzle and on the Reynolds number. This means, even for one particular injector, one will expect C_{dis} to vary throughout the injection period since the injection pressure (hence the injection velocity, of course, instantaneous) varies. Since the total fuel injected is not very critical as previously explained in Section 4.1.4, the average value for C_{dis} quoted above, is accurate enough for the present purpose.

For the injector nozzle, a diameter of 0.32 mm (Appendix A.3) is assumed and using equation (A.I.1) to calculate the density of the fuel, the spray is calculated to emerge with an average initial velocity of 1900 in/sec (∿48 m/sec) into a cylinder swirling charge having a swirl ratio, k, of 2.5. The value of k in fact is obtained from the empirical expression of ref.(46). Except for the Leyland 8.61 engine (denoted by engine H) in which a higher value of k (i.e. k=16.0 and the corresponding U_{orel} = 4370 in/sec) is used as explained later, the average initial relativ velocity of the fuel spray with respect to the swirling charge is thus 2000 in/sec (∿51 m/sec), and this then becomes the figure used in most of the calculations.

(c) The cylinder charge pressure and temperature: The charge pressure and temperature during the preparation stage are assumed constant and to be 500 psi and 1494°R respectively (section 4.1.4).

(d) The value for AUC: The value for AUC in equation (94) is kept constant at 50.0. This figure is arrived at by trial and error method. It is to be noted that AUC controls both the heat release period and the second peak in the heat release diagram. If AUC is less than 50.0, the second peak becomes higher and the heat release period becomes shorter. The opposite effect is true for AUC more than 50.0.

(e) Ignition delay periods: Ignition delay periods at different engine speeds as previously warned are calculated from Wolfer's equation in Section (4.1.5) and in Appendix A.6. The average measured ignition delay periods used in the program to control the calculated values are as follows:

At 1000 rpm	FL :	ignition delay period	= 8.0°CA
1500			= 10.0°CA
2000			= 12.0°CA
2600			= 13.0°CA
3000			= 13.5°CA

N.B. If the difference between the average calculated and measured ignition delay periods is more than 0.05°CA at any engine speed, the computer uses the latter value automatically.

Although it should be recalled that the input data given above are used throughout the testing of this theoretical combustion model because they were found during the model's initial development tc give reasonable results compared with experimental results, Figures 31-36, yet it was still considered necessary to vary some of these input data in order to assess their effects on the fuel preparation and hence heat release diagrams. The effect of increasing the initial fuel temperature from 560°R to 710°R; the air swirl ratio from 0 to 7.5 and the cylinder pressure during the preparation stage from 300 psi to 600 psi on fuel preparation diagrams, Figures 21-24, is somehow small. On the other hand, this model is very sensitive to the average cylinder temperature (during the preparation stage) and to the droplet size distribution as illustrated in Figures 25 , 26 .

All the above effects are summarised in Figures 29 , 30 and Table 1, in terms of the total fuel prepared during the ignition delay period, initial heat release peak, rate of pressure rise and combustion induced noise level. The latter is calculated from the total fuel prepared during the delay period and hence the initial heat release peak and the rate of

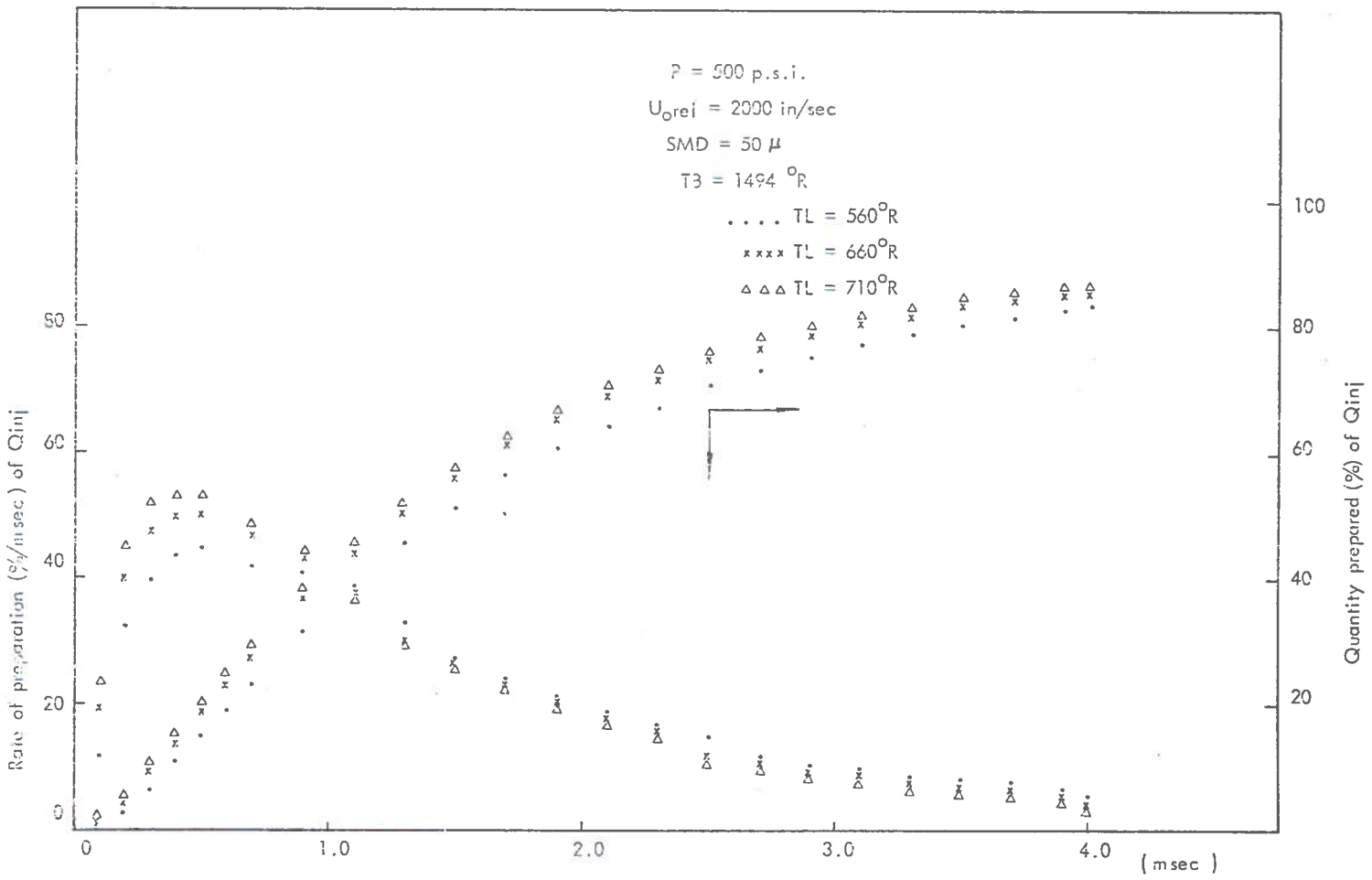

FIGURE 21. EFFECT OF INITIAL FUEL TEMPERATURE ON FUEL PREPARATION

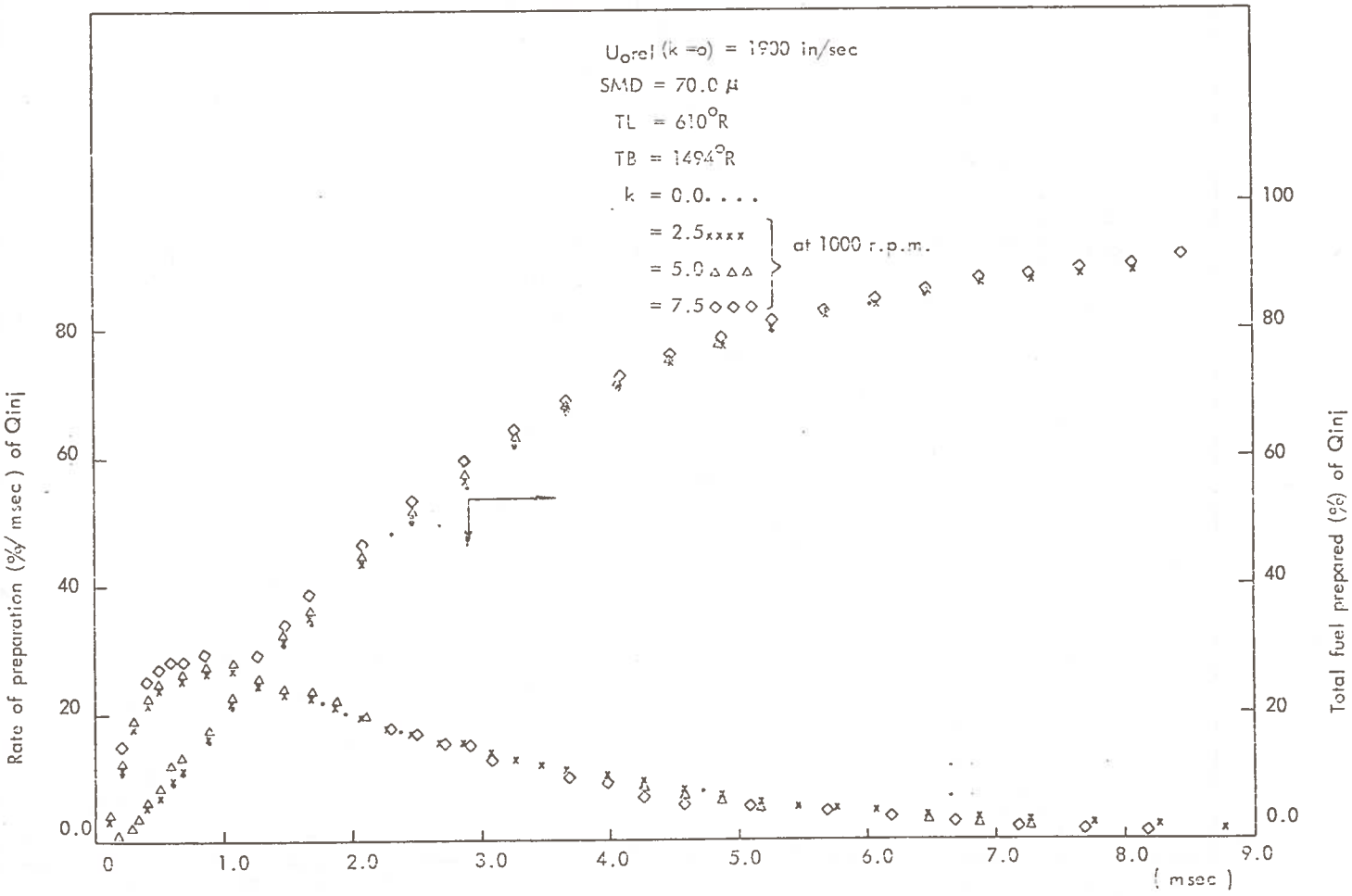

FIGURE 22. EFFECT OF AIR SWIRL RATIO ON FUEL PREPARATION

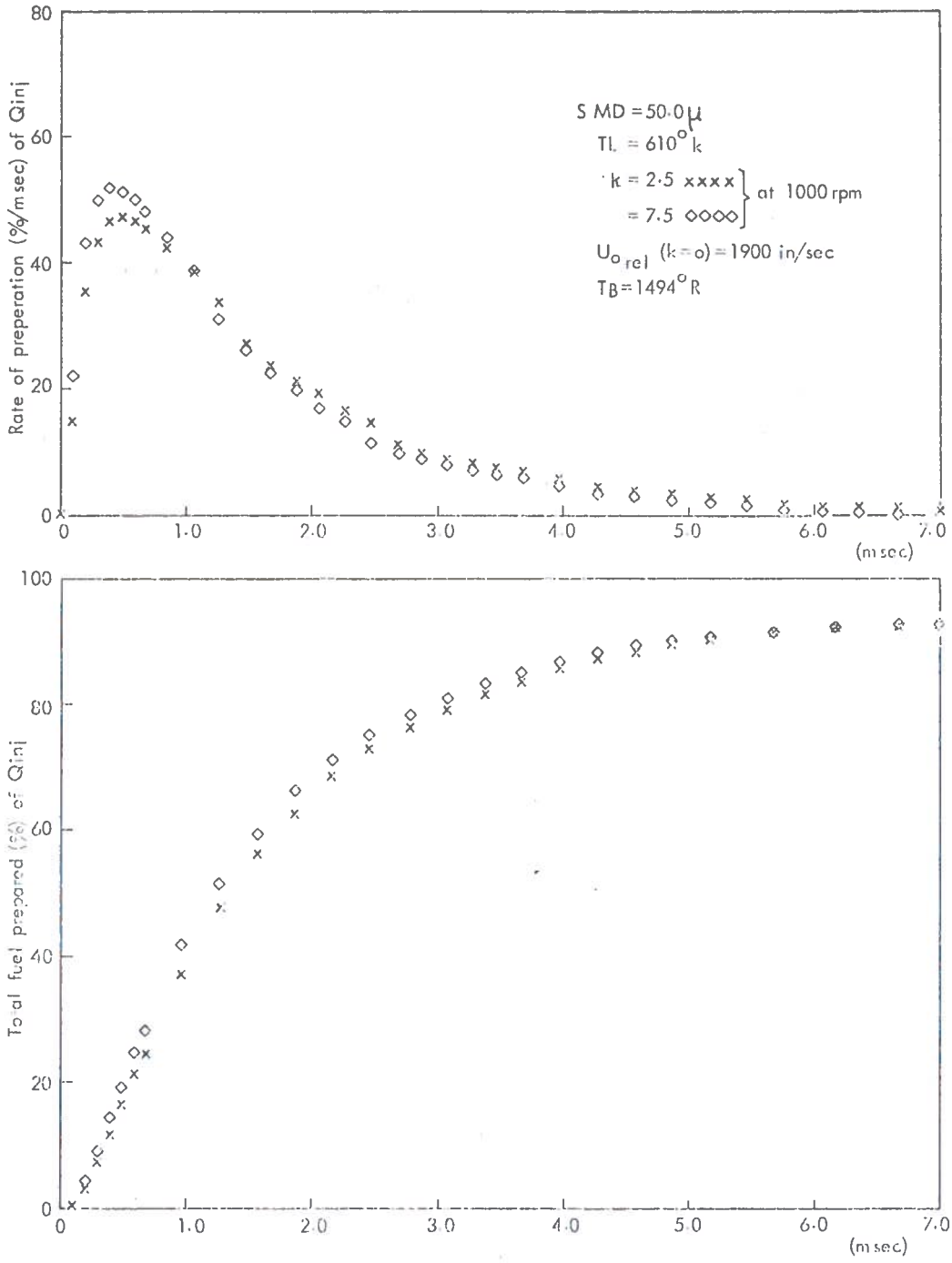

FIGURE 23. EFFECT OF AIR SWIRL RATIO ON FUEL PREPARATION

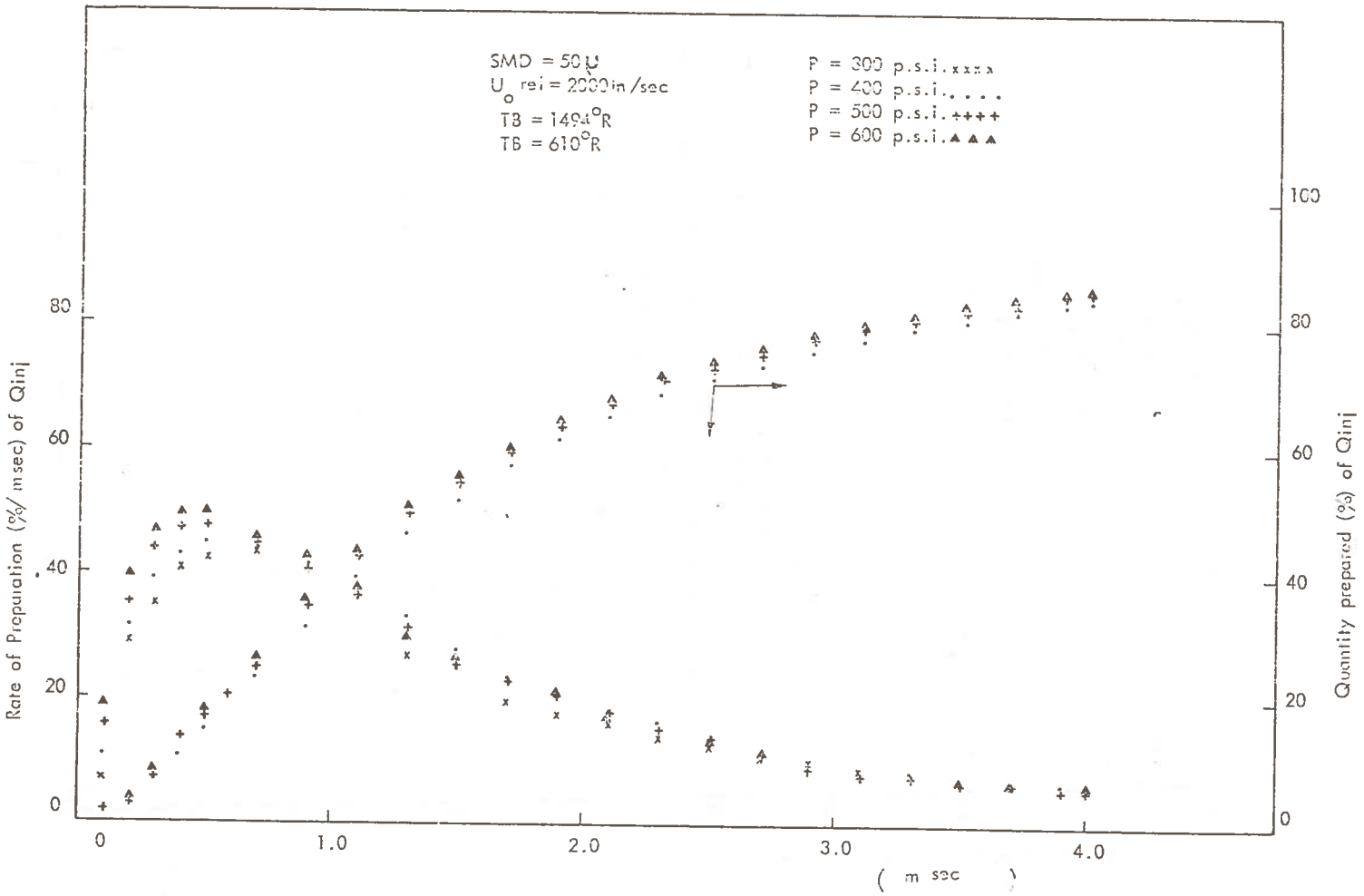

FIGURE 24. EFFECT OF CYLINDER PRESSURE ON FUEL PREPARATION

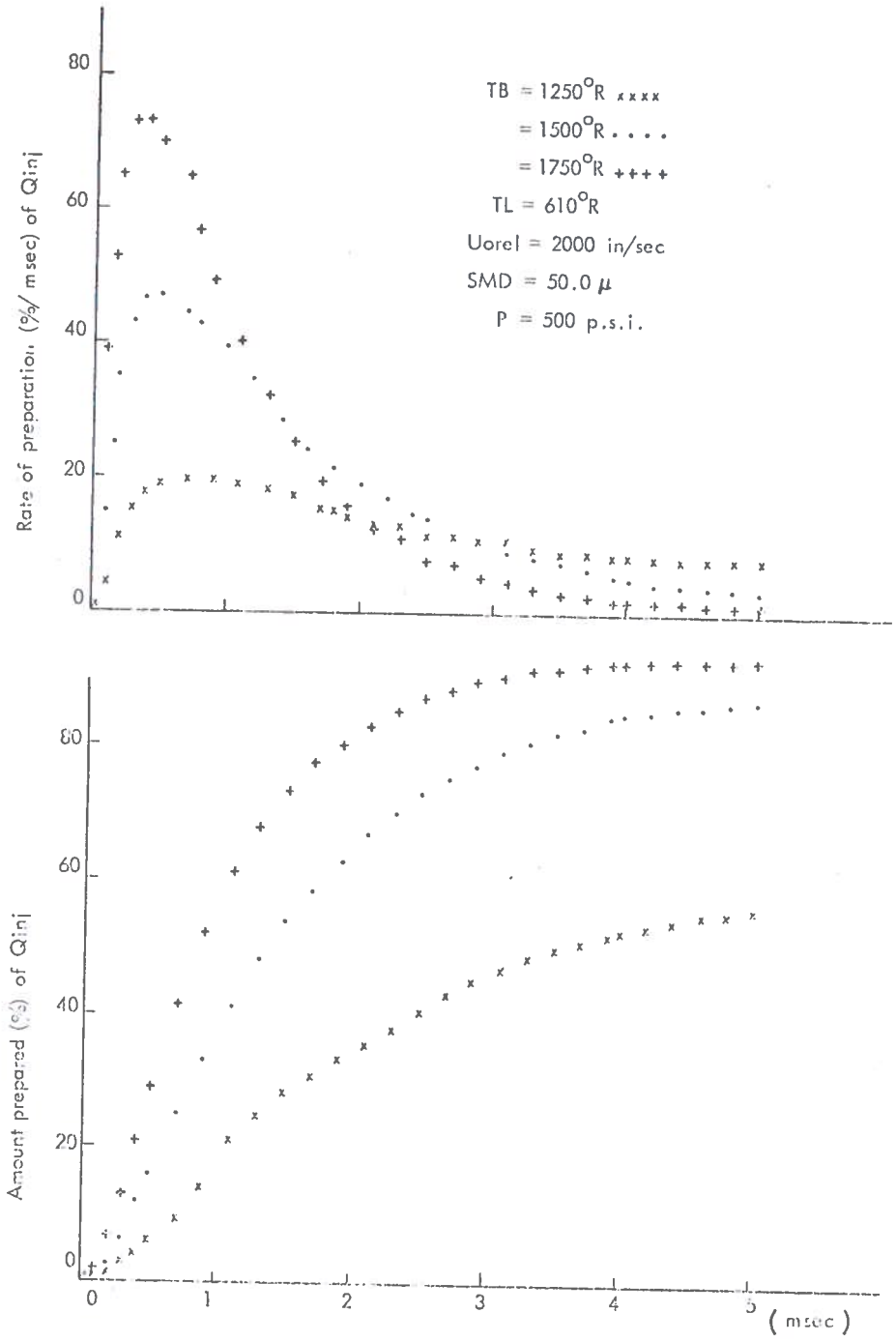

FIGURE 25. EFFECT OF CYLINDER GAS TEMPERATURE ON FUEL PREPARATION

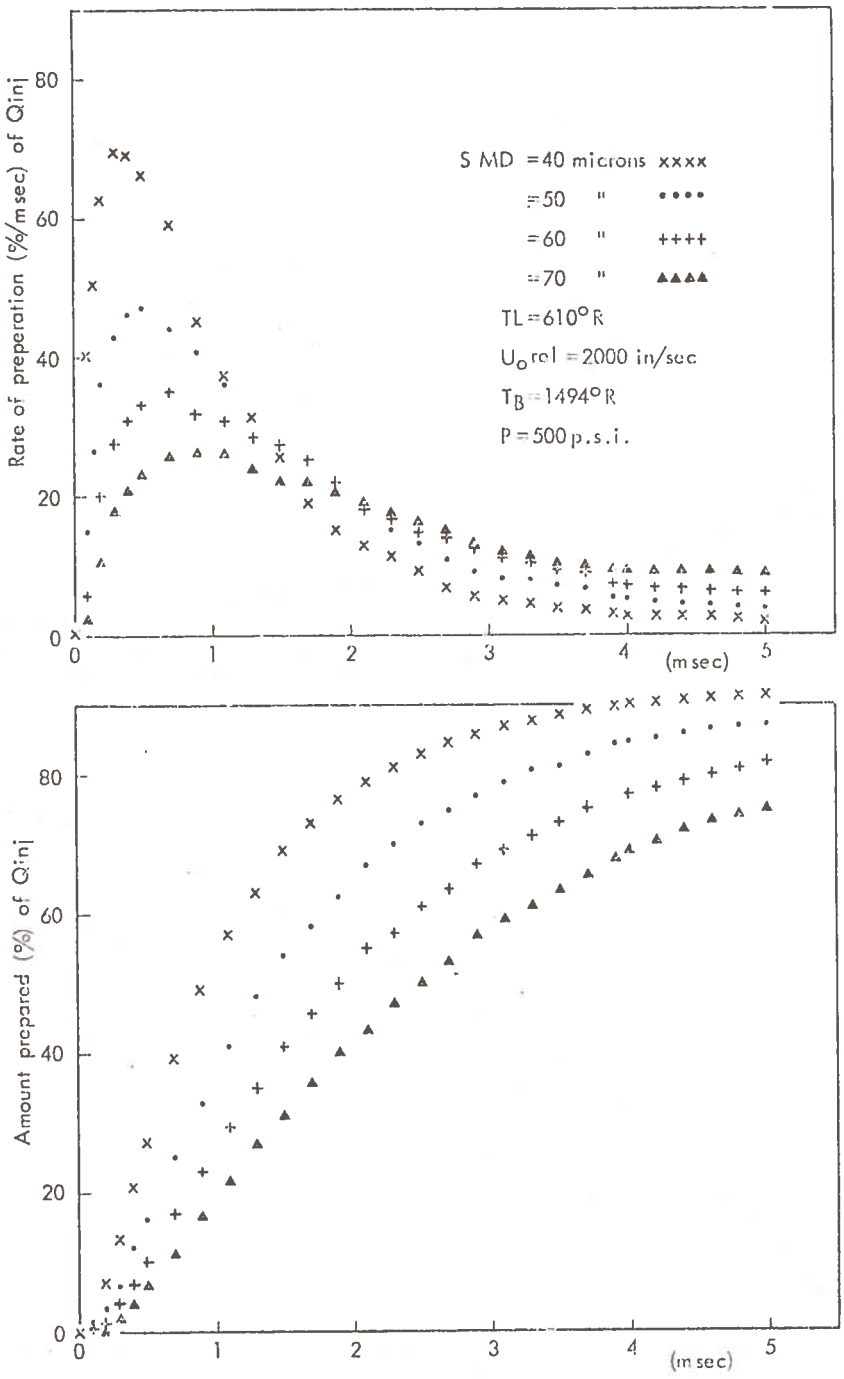

FIGURE 26. EFFECT OF DROPLET MEAN DIAMETER FUEL ON PREPARATION

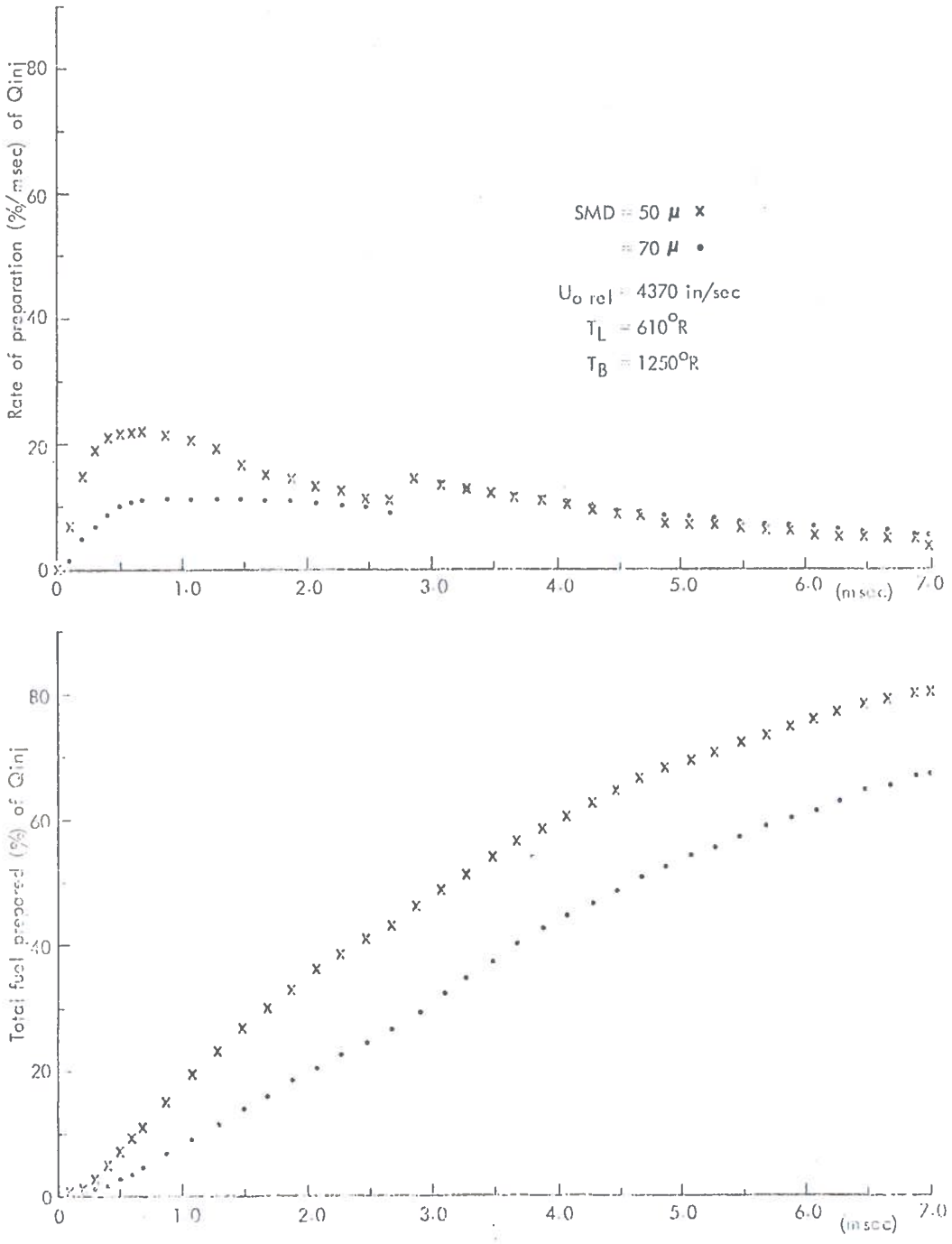

FIGURE 27. EFFECT OF TEMPERATURE ON DROPLET PREPARATION HISTORY

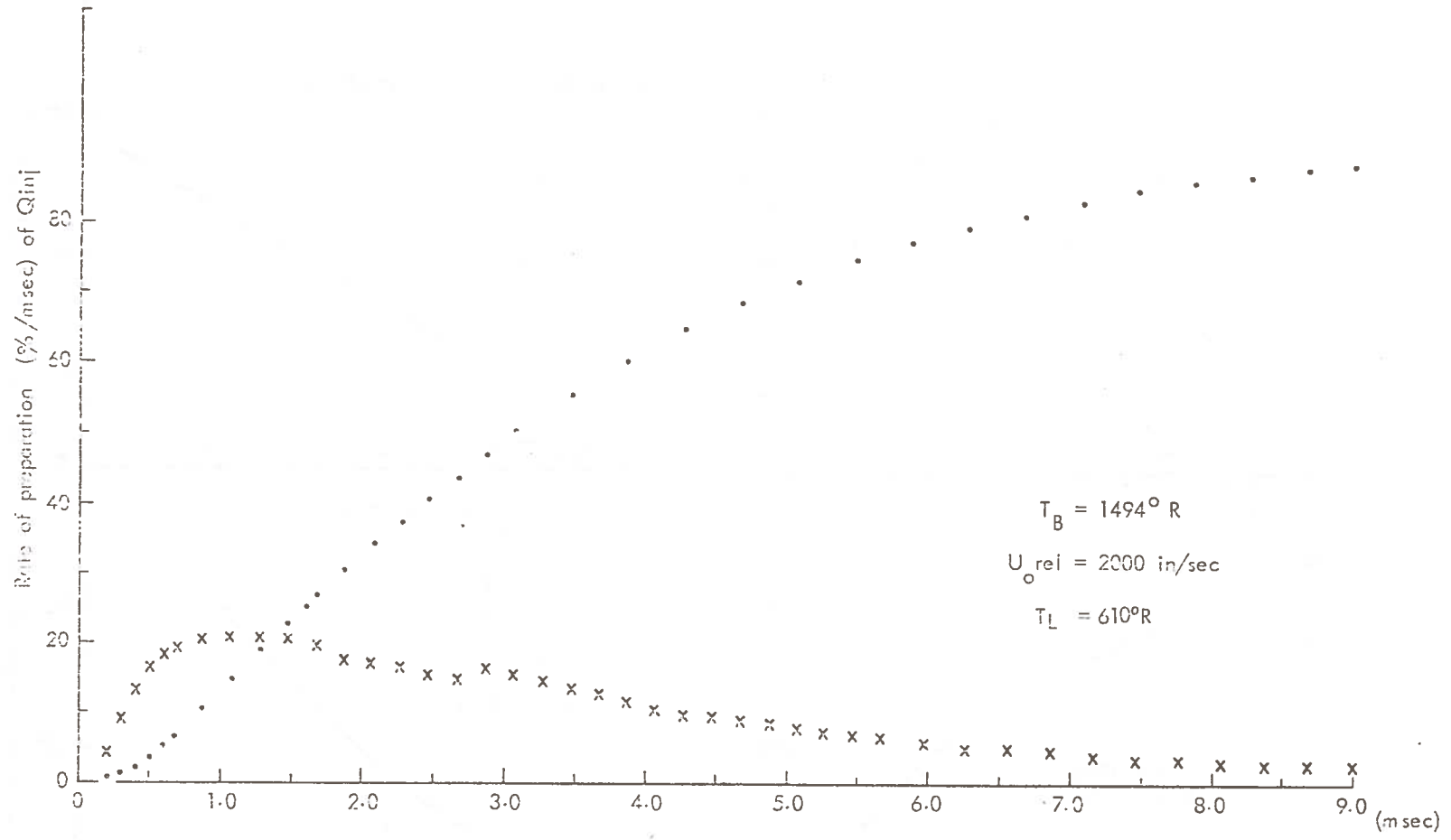

FIGURE 28. PREPARATION HISTORY OF AN 80μ - SMD FUEL SPRAY

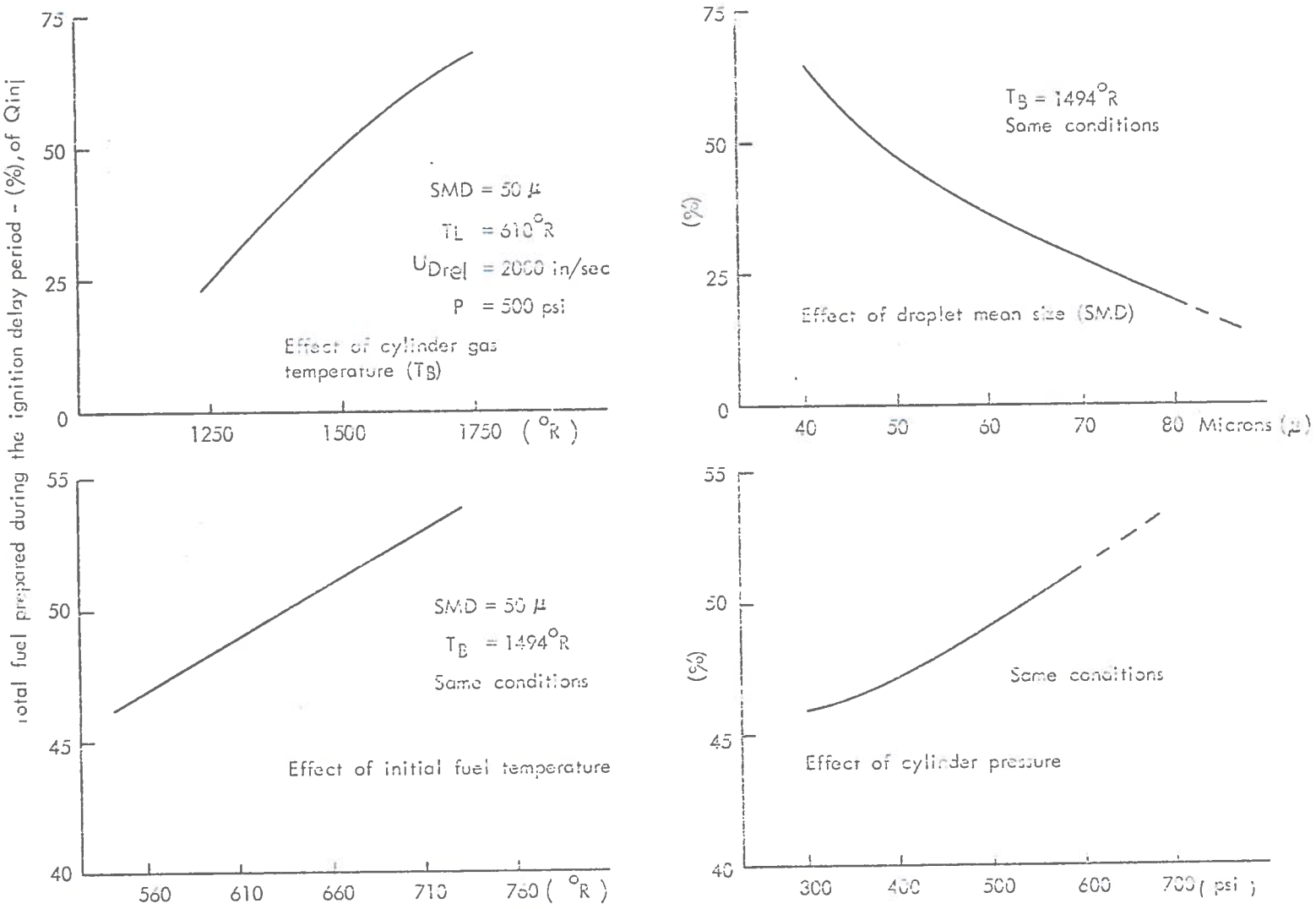

FIGURE 29. EFFECT OF PHYSICAL PARAMETERS ON THE TOTAL FUEL PREPARED DURING THE DELAY PERIOD AT 1000 RPM FL.

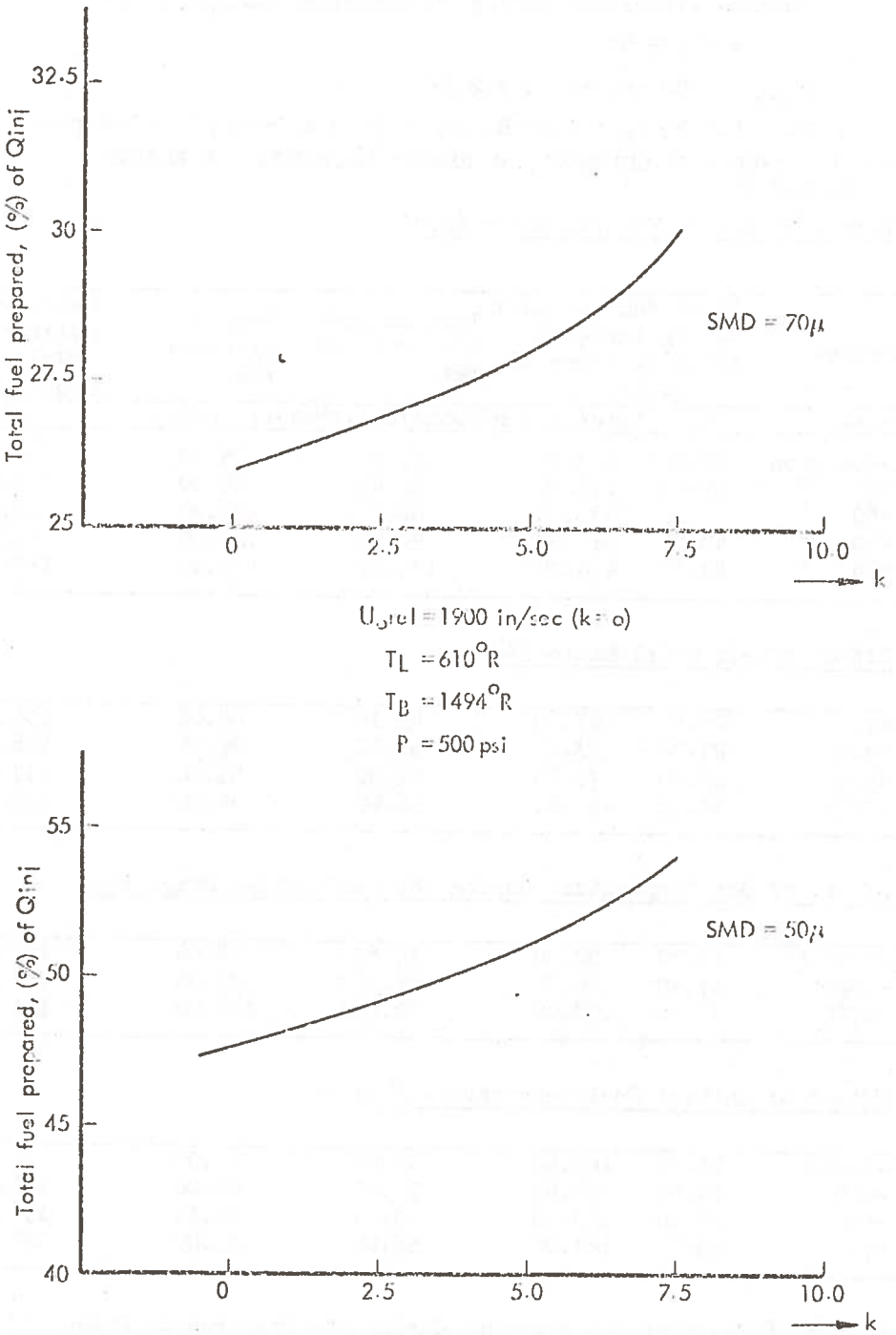

FIGURE 30. EFFECT OF AIR SWIRL RATIO (k) ON THE TOTAL FUEL PREPARED DURING THE DELAY PERIOD AT 1000 RPM FL

Q_{inj} = 750 Btu/lb Air (i.e. 70 mm^3)

Burning efficiency during the premixed burning stage

= 85.75 %

U_{orel} = 2000 in/sec (k = 2.5)

TL = 610°R; T_B = 1494°R; SMD = 70.0 microns; P = 500 psi.

TABLE 1. EFFECT OF CHANGING THE DESIGN PARAMETERS ON ENGINE A AT 1000 RPM FL

(a) Effect of Sauter Mean Diameter (SMD)

Parameter	Total fuel prepared during ignition delay(in terms of Q_{inj})	Initial peak heat release rate	Rate of pressure rise	Calc.Averaged cylinder press. level at 500Hz-3000Hz.
Units	(%)	(Btu/lb air)	(Btu/lb air/°CA)	(psi/°CA)	(dB)
SMD=80microns	20.00	128.50	37.60	75.00	152.35
=70 "	27.00	173.40	51.00	89.00	156.50
=60 "	36.25	233.00	68.50	104.00	161.00
=50 "	48.75	313.00	92.00	120.00	166.00
=40 "	63.75	410.00	120.00	135.00	170.30

(b) Effect of Air Swirl Ratio (k)

k=0	26.00	167.00	49.10	88.00	156.00
=2.5	27.00	173.40	51.00	89.00	156.50
=5.0	28.00	179.80	52.90	91.00	157.20
=7.5	30.00	192.60	56.60	94.50	158.20

(c) Effect of Gas Temperature During the Preparation Stage (T_B)

T_B=1250°R	13.70	88.00	25.875	58.00	147.00
=1500	27.40	176.00	51.750	90.00	157.00
=1750	37.00	238.00	70.000	105.00	161.50

(d) Effect of Initial Fuel Temperature (TL)

TL=560°R	25.90	166.50	49.00	88.00	156.00
=610	27.00	173.40	51.00	89.00	156.50
=660	28.10	180.30	53.00	91.10	157.21
=710	29.20	187.20	55.00	93.00	157.70

(e) Effect of Cylinder Gas Pressure during the Preparation Stage (P)

P=300psi	25.40	163.00	48.00	86.00	155.50
=400	26.20	168.00	49.40	88.35	156.30
=500	27.00	173.40	51.00	89.00	156.50
=600	28.30	182.00	53.50	92.00	157.40

pressure rise with the aid of Figures 52 and 53. For instance, changing the SMD from 80 microns to 70 or to 60 microns produces an increase in the rate of pressure rise from 75 psi/^{o}CA to 89 psi/^{o}CA and 104 psi/^{o}CA respectively. This increase in turn causes some average of 3 dB and 7.5 dB increase in the combustion induced noise levels at about 500 Hz to 3000 Hz respectively, etc.

Moreover, comparison in terms of heat release rates is shown in Figures 31-36. It will be remembered that a high value of k is used for engine H, Figure 36. Experience with this engine has indicated that the value of the swirl ratio calculated is a reasonable one. Because the wall impingement due to its only one spray is very severe, it was decided to use a lower average cylinder temperature of 1250^{o}R during the preparation stage. The comparison in terms of pressure versus crank angle (Figures 39-41.) is also encouraging, although there are some discrepancies between the measured and the predicted results. Some of these are partly due to timing inaccuracies, either caused by inaccuracy in reading or measuring the start of ignition or the difficulty in accurately locating the Top Dead Centre position in the cylinder pressure diagrams taken in the tests. Some on the other hand, are due to the average values rather than the actual values for the constants , ignition delay periods and variable, which were introduced in the calculation in an attempt to make the model widely applicable.

Finally, from the Figures above and Table 1, the following broad conclusions can be made:

(a) The amount of the fuel prepared during the ignition delay period depends primarily on the quantity of heat transferred from the cylinder gases to the droplets and the droplet size distribution. In other words, for constant gas temperature, the finer the droplet size distribution, or for a constant droplet size distribution, the higher the gas temperature, the higher the initial rate of heat release and also the rate of pressure rise. This is mainly due to the increased rate of preparation.

(b) Preheating of the liquid fuel before it enters the combustion chamber has the advantage of allowing the fuel to flow more easily within the pumps and injector nozzles and to produce a finer atomisation, which will undoubtedly increase the total amount of fuel prepared slightly during

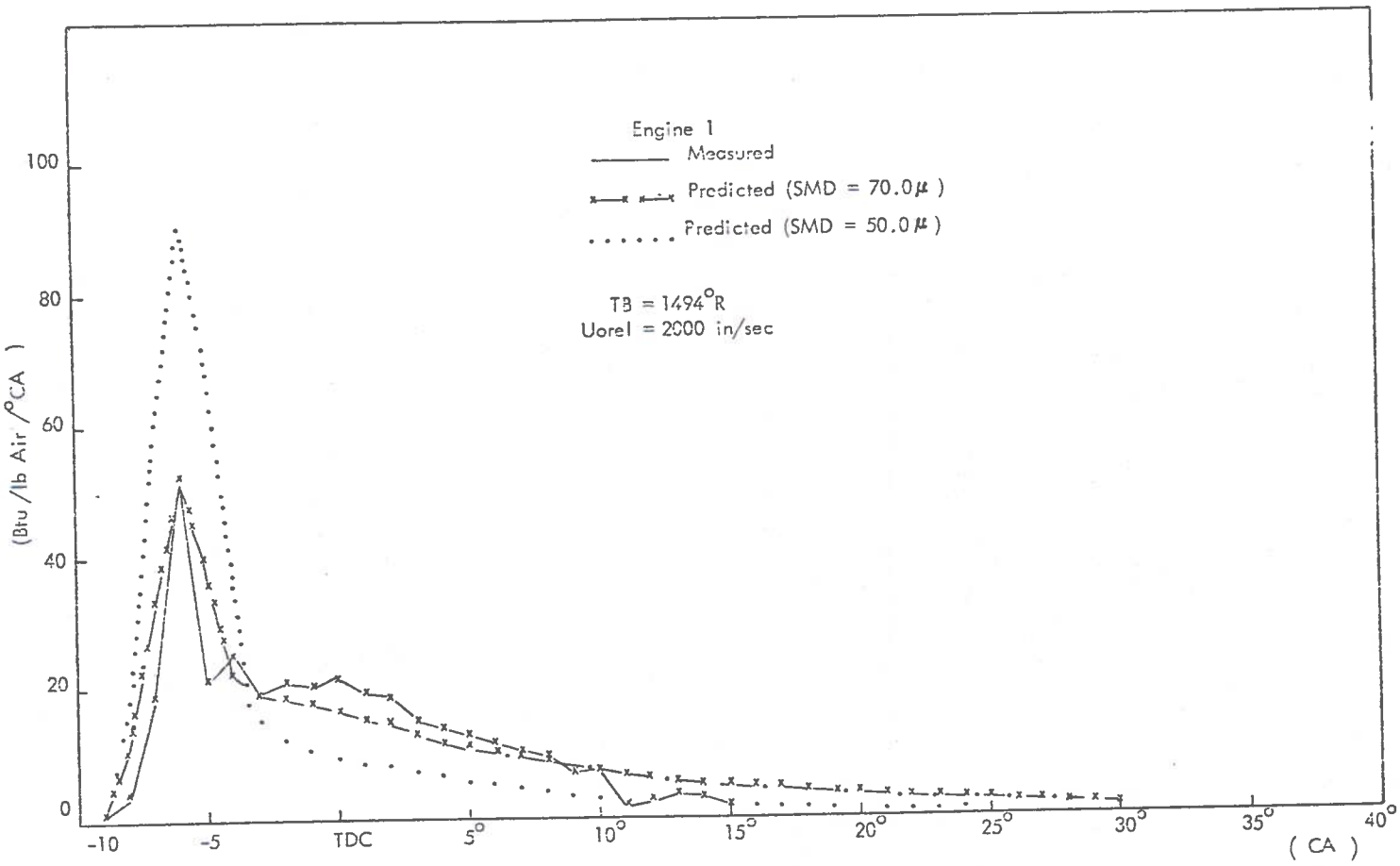

FIGURE 31a. MEASURED AND PREDICTED HEAT RELEASE AT 1000 RPM FL (INITIAL PEAK BASED ON CHEMICAL KINETICS)

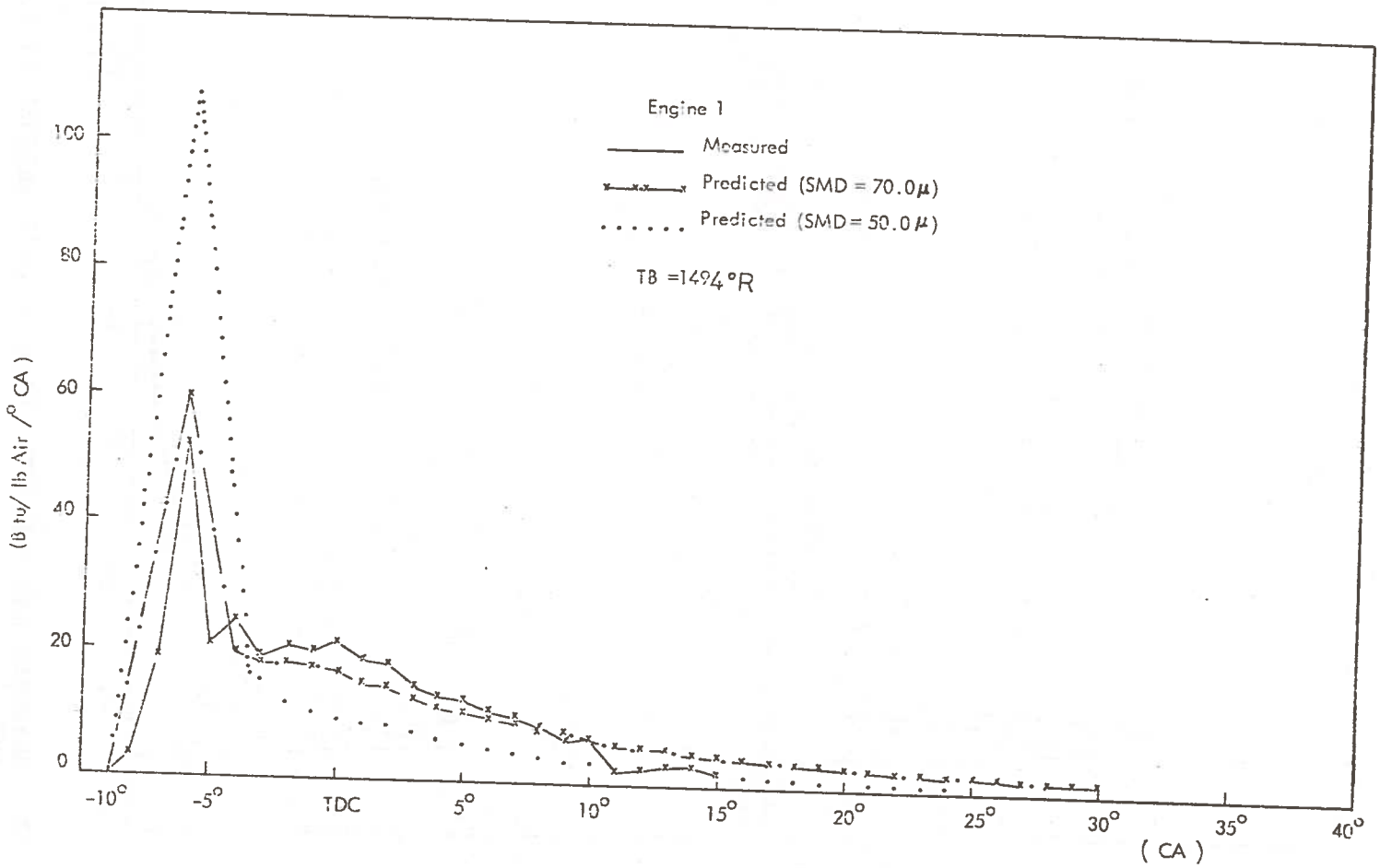

FIGURE 31b. MEASURED AND PREDICTED HEAT RELEASE AT 1000 RPM FL (INITIAL PEAK BASED ON TRIANGLE RATE LAW)

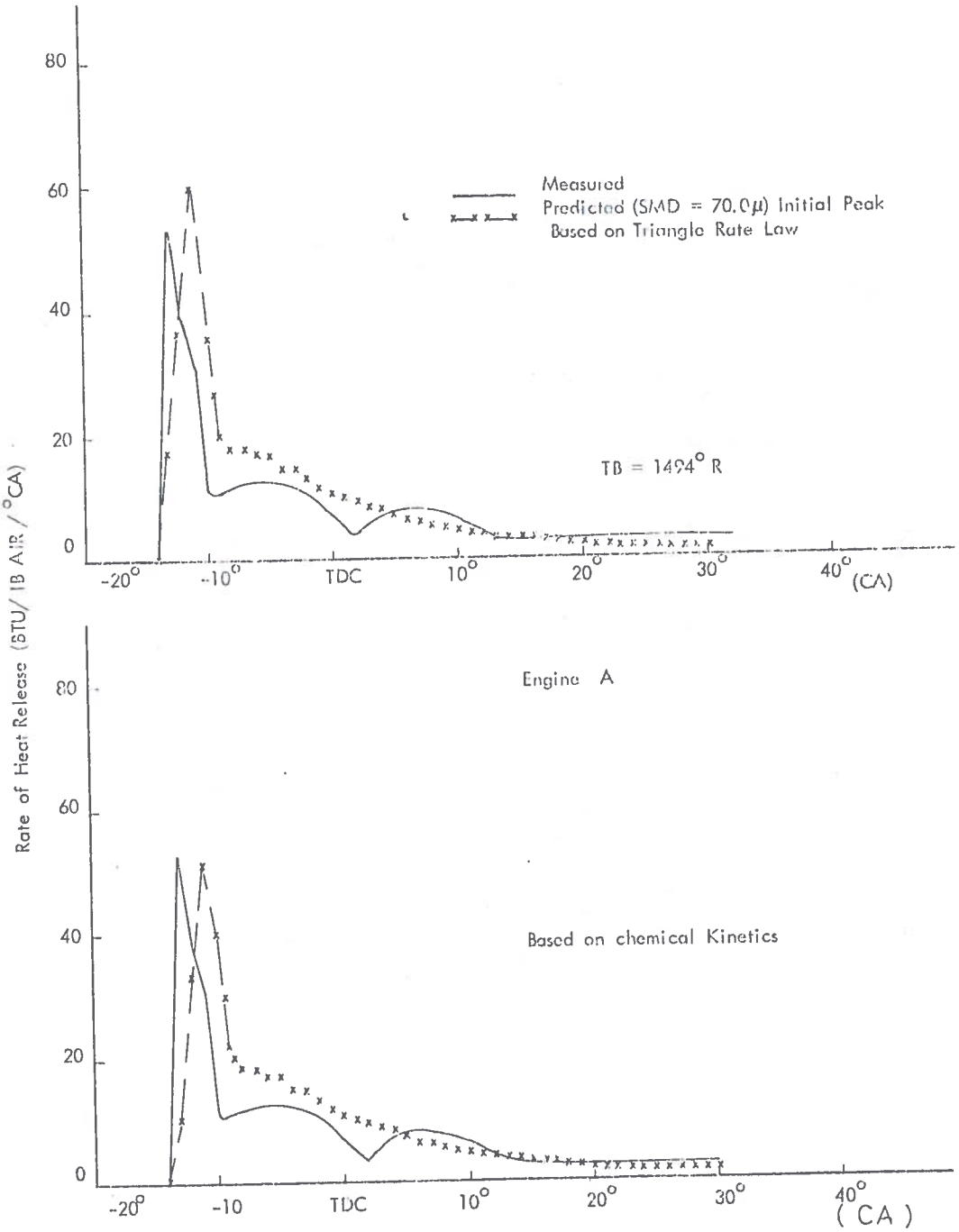

FIGURE 32. MEASURED AND PREDICTED RATE OF HEAT RELEASE AT 1000 RPM FL

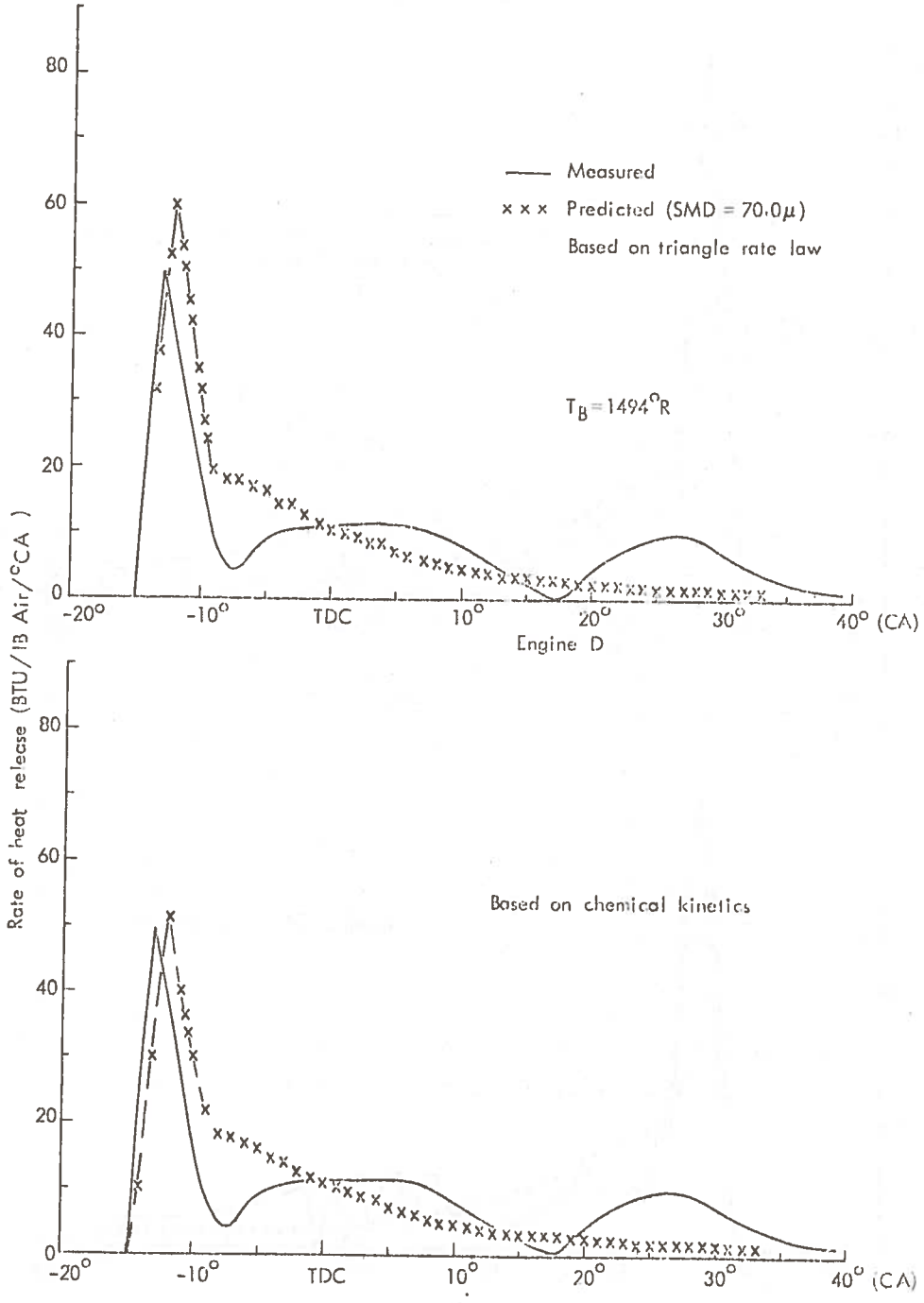

FIGURE 33. MEASURED AND PREDICTED RATE OF HEAT RELEASE AT 1000 RPM FL

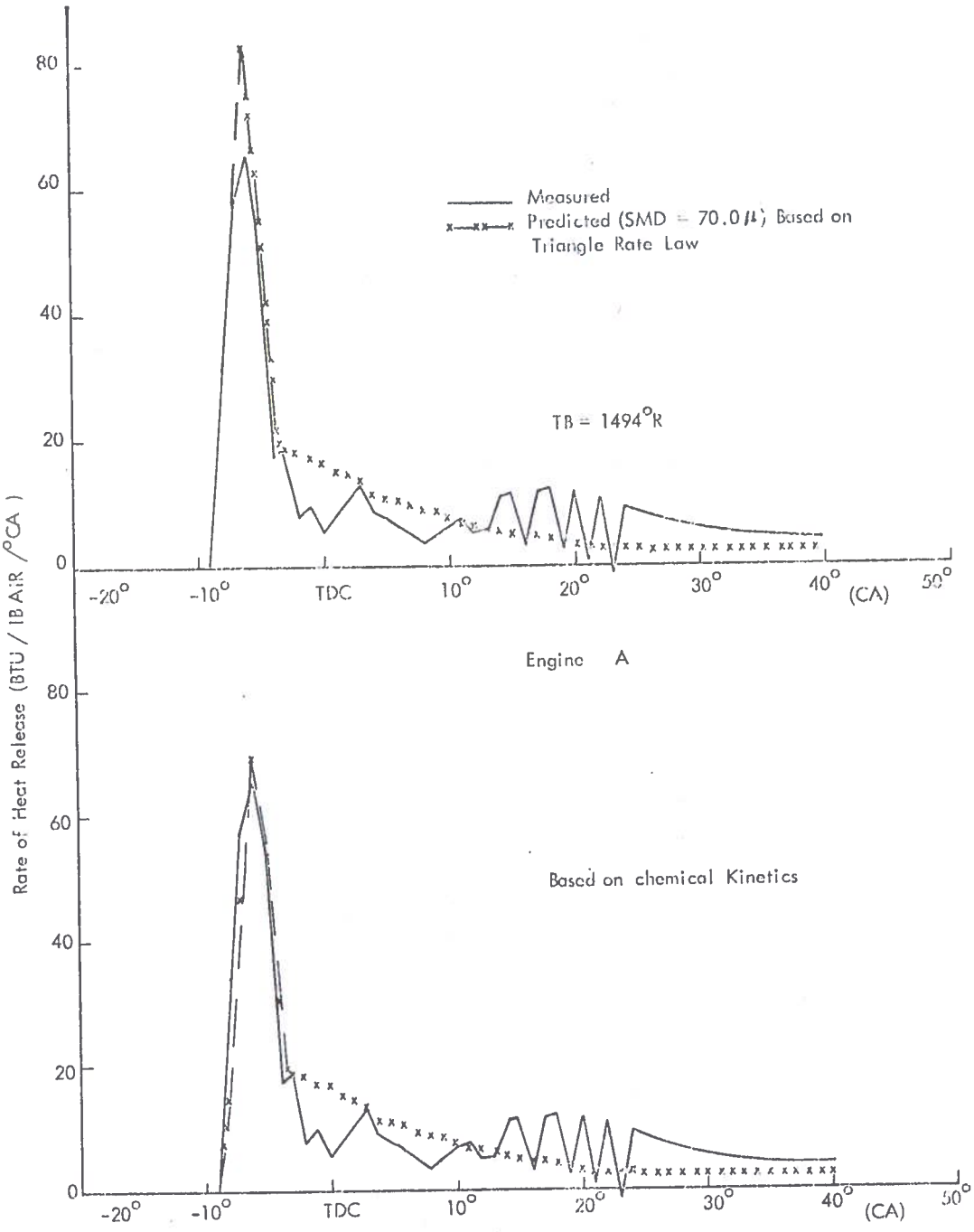

FIGURE 34. MEASURED AND PREDICTED HEAT RELEASE AT 2000 RPM FL

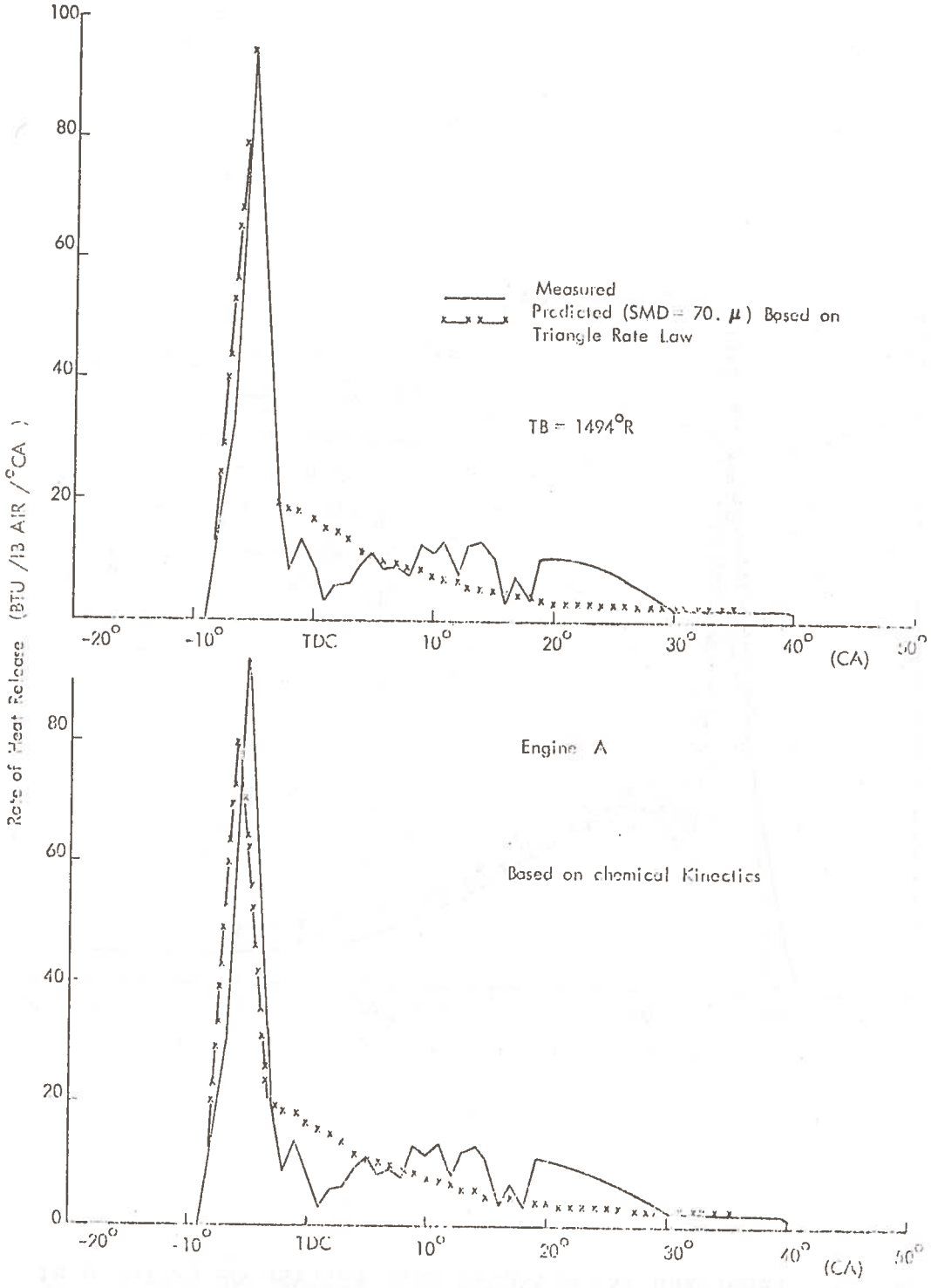

FIGURE 35. MEASURED AND PREDICTED HEAT RELEASE AT 2600 RPM FL

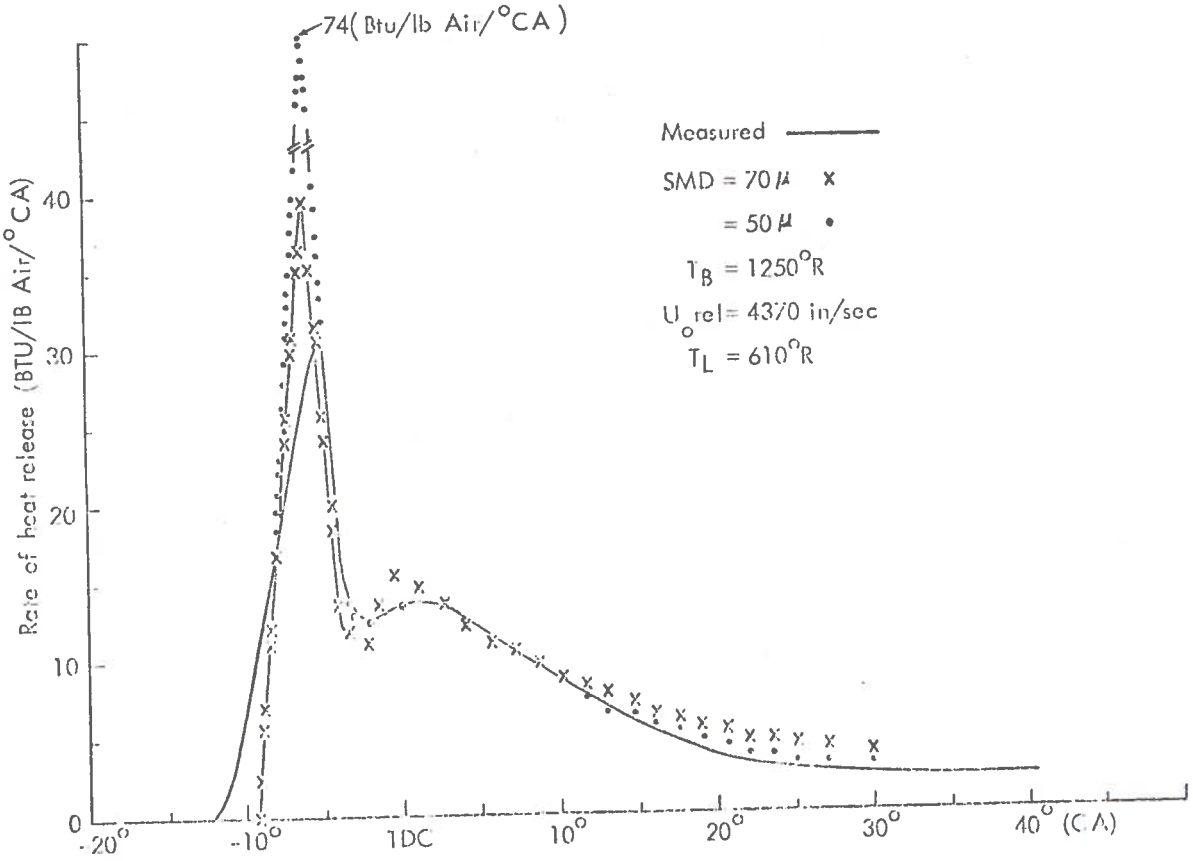

FIGURE 36. PREDICTED AND MEASURED HEAT RELEASE OF ENGINE H AT 1800 RPM FL

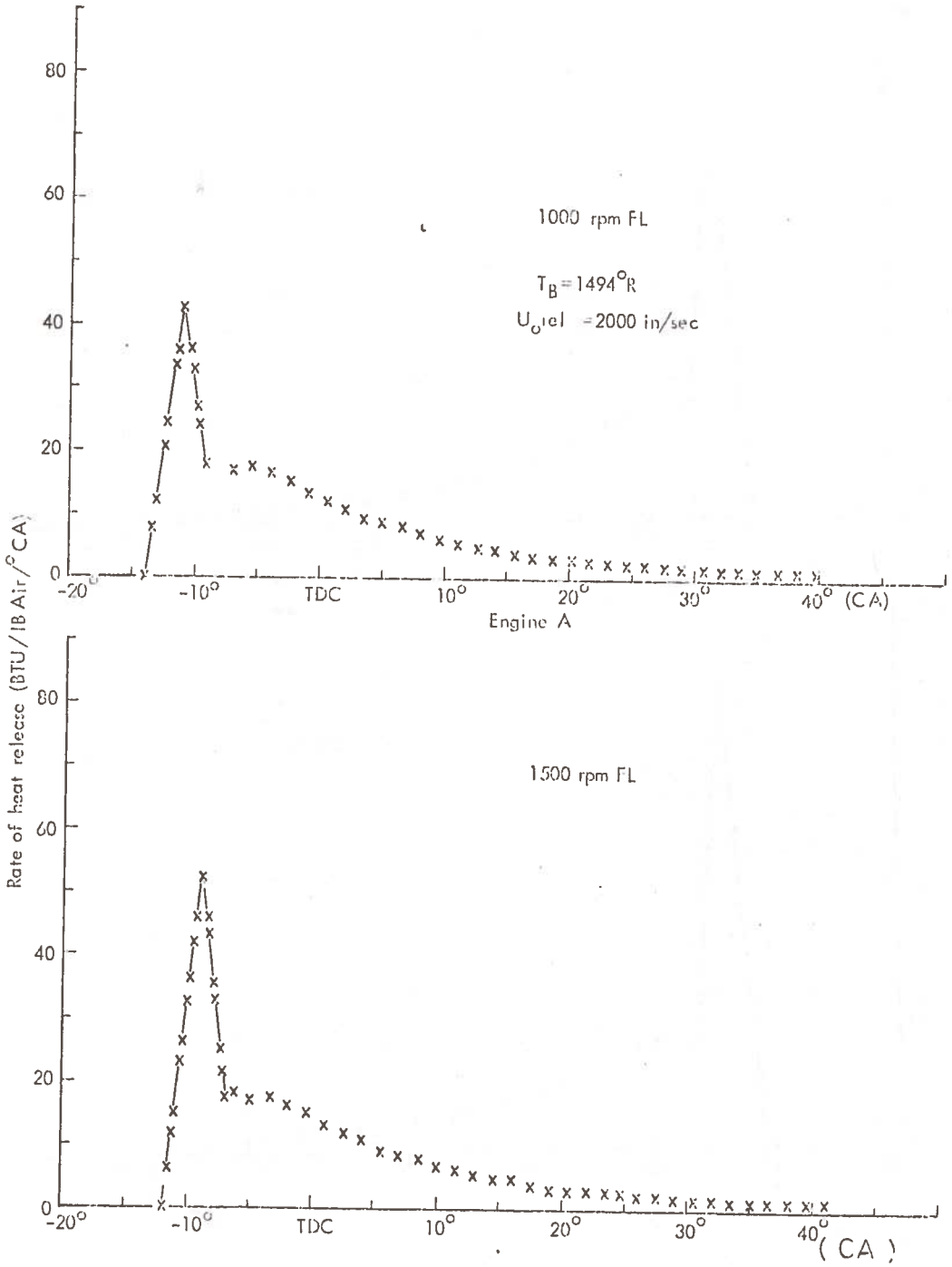

FIGURE 37. PREDICTED HEAT RELEASE RATES USING 80μ - SMD

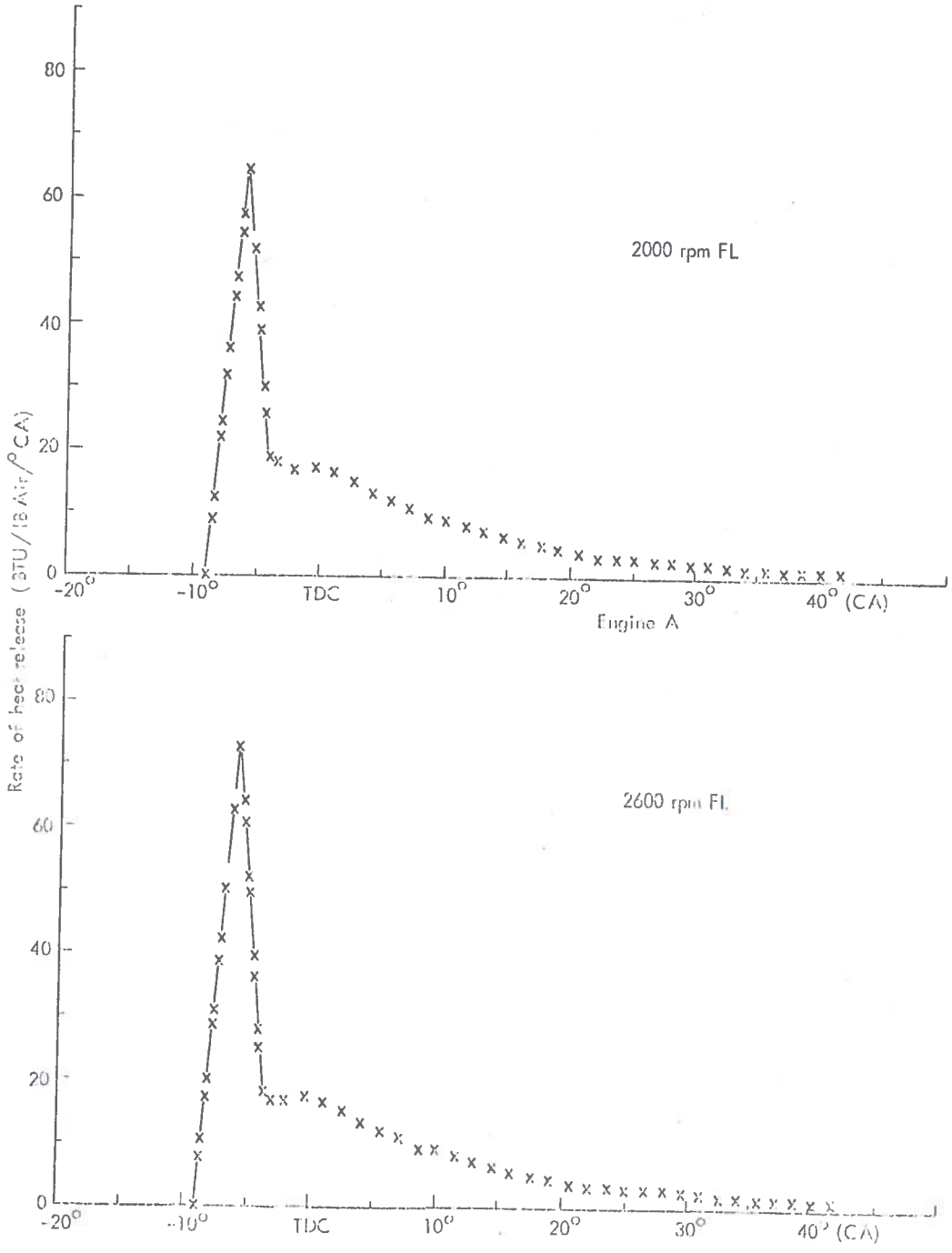

FIGURE 38. PREDICTED HEAT RELEASE RATES USING 80μ - SMD

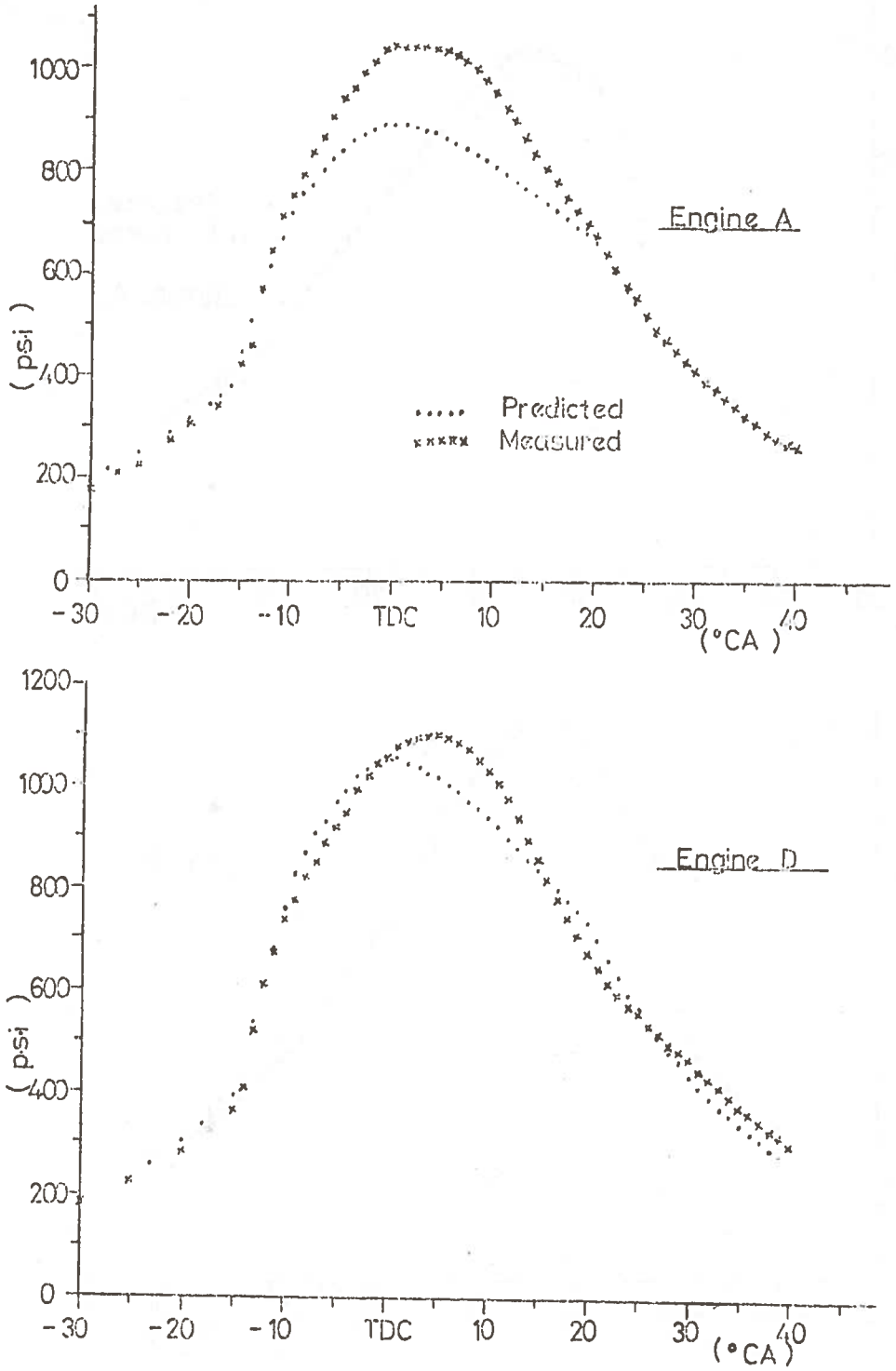

FIGURE 39. CYLINDER PRESSURE DIAGRAMS AT 1000 RPM FL

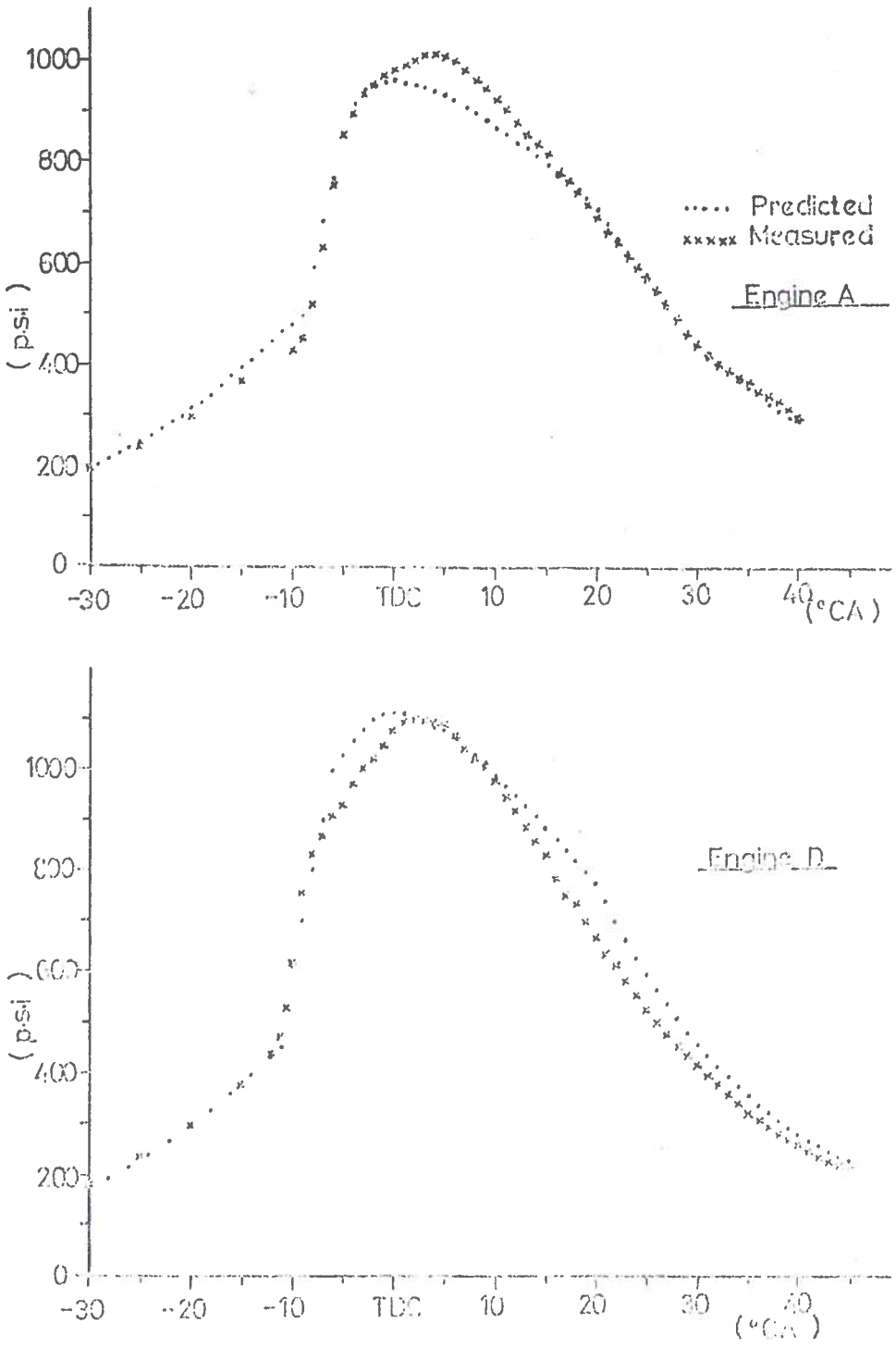

FIGURE 40. CYLINDER PRESSURE DIAGRAMS AT 2000 RPM FL

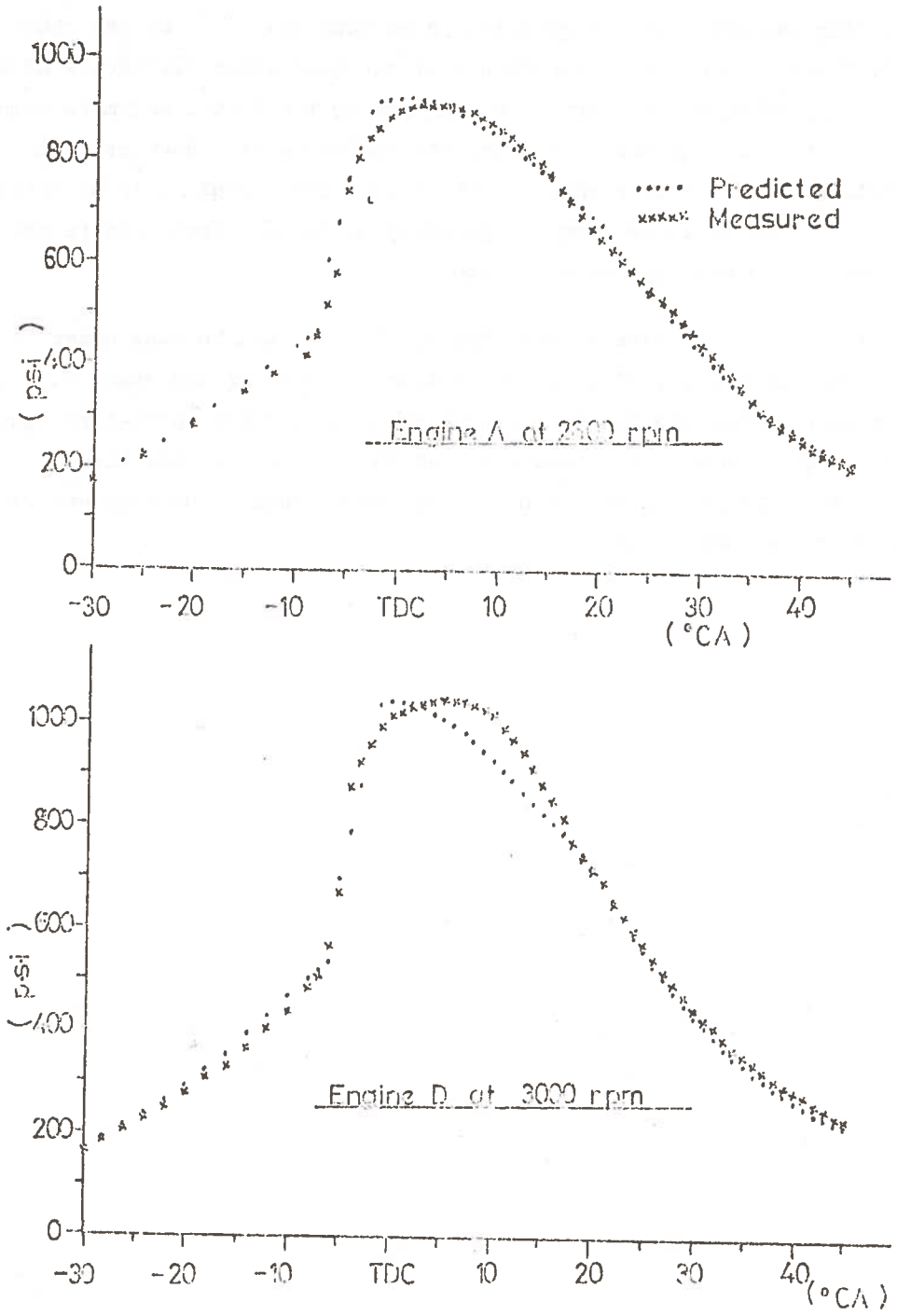

FIGURE 41. CYLINDER PRESSURE DIAGRAMS AT FL

the delay period. In fact there is a narrow limit in practice in which the temperature of the liquid fuel could be raised without adversely affecting its physical properties such as density. On the other hand, there is a strong indication that the combustion efficiency of a direct injection diesel engine is improved by the faster and more complete mixing caused by further increasing the engine swirl. However, this advantage like that of preheating the liquid fuel, could only be obtained at the expense of increasing the quantity of the prepared mixture prior to ignition as already explained above.

(c) The heat release rates during the premixed burning stage as calculated above, are close to the measured, both for the cases when heat is released according to the triangle rate law and Arrhenius-type equation. Of course, it should be remembered that the two methods are highly empirical. However, prediction of a cylinder pressure development was made from the latter case.

5. CORRELATION BETWEEN NOISE AND ITS COMBUSTION SYSTEM

To establish the relevant differences in noise characteristics of engines of different combustion systems a closer look has been made of all the different engines tested at I.S.V.R. laboratories over the past twelve years. On each engine gas force diagrams have been taken, and cylinder pressure noise and vibration analyses have been carried out. The overall noise in dBA at full load conditions of some 44 different engines is summarised in Figure 42. The noise of all the engines shows straight relationships with speed, except for some small high speed I.D.I. and petrol engines which show two slopes, a low rate of increase in the low speed range and a high rate in the high speed range. If the results are compared on the basis of constant speed the increase of noise with engine size is apparent. At the rated speeds, all engines (except the opposed piston two strokes) reach about the same level of noise within a band of some 10 dBA.

An attempt is also made to classify the engines in various groups according to combustion system and fundamental design principles. In each of these groups listed below, there are about seven engines -

1. Turbocharged in-line D.I.
2. Naturally aspirated in-line D.I.
3. Naturally aspirated Vee-form D.I.
4. Two stroke D.I.
5. Naturally aspirated I.D.I.
6. Spark ignition petrol.

In order to find some correlation with the simple combustion model the overall noise levels are plotted against engine bore diameter in Figure 43 at a constant speed of 2000 rev/min which represents a realistic speed for all the engines in this wide range.

It can be seen that the engines do fall into specific groups :

(a) All normally aspirated D.I. engines fit within a 3 dB band of slope $(\text{bore})^5$. It is clear that there are no differences between the noise of vee form and in-line engines. Some of the I.D.I. engines also fall within this same band;

(b) The turbocharged engines occupy a band just below.

(c) The remaining I.D.I. engines fall within a band some 8 dBA below the D.I. engines.

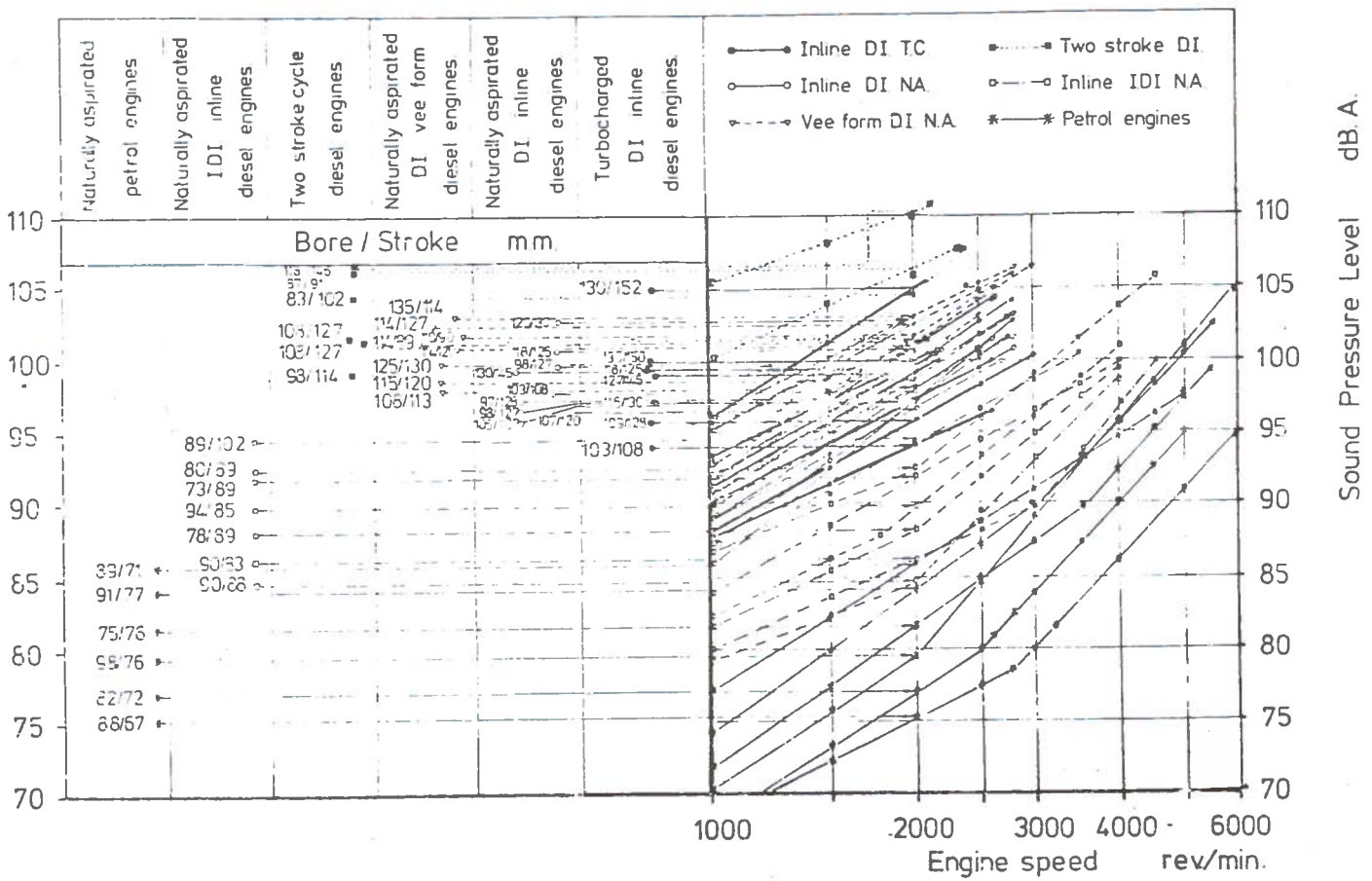

FIGURE 42. RELATIONSHIP BETWEEN NOISE AND ENGINE-DESIGN PARAMETERS-SHOWN FOR FULL LOAD CONDITIONS OVER THE SPEED RANGE.

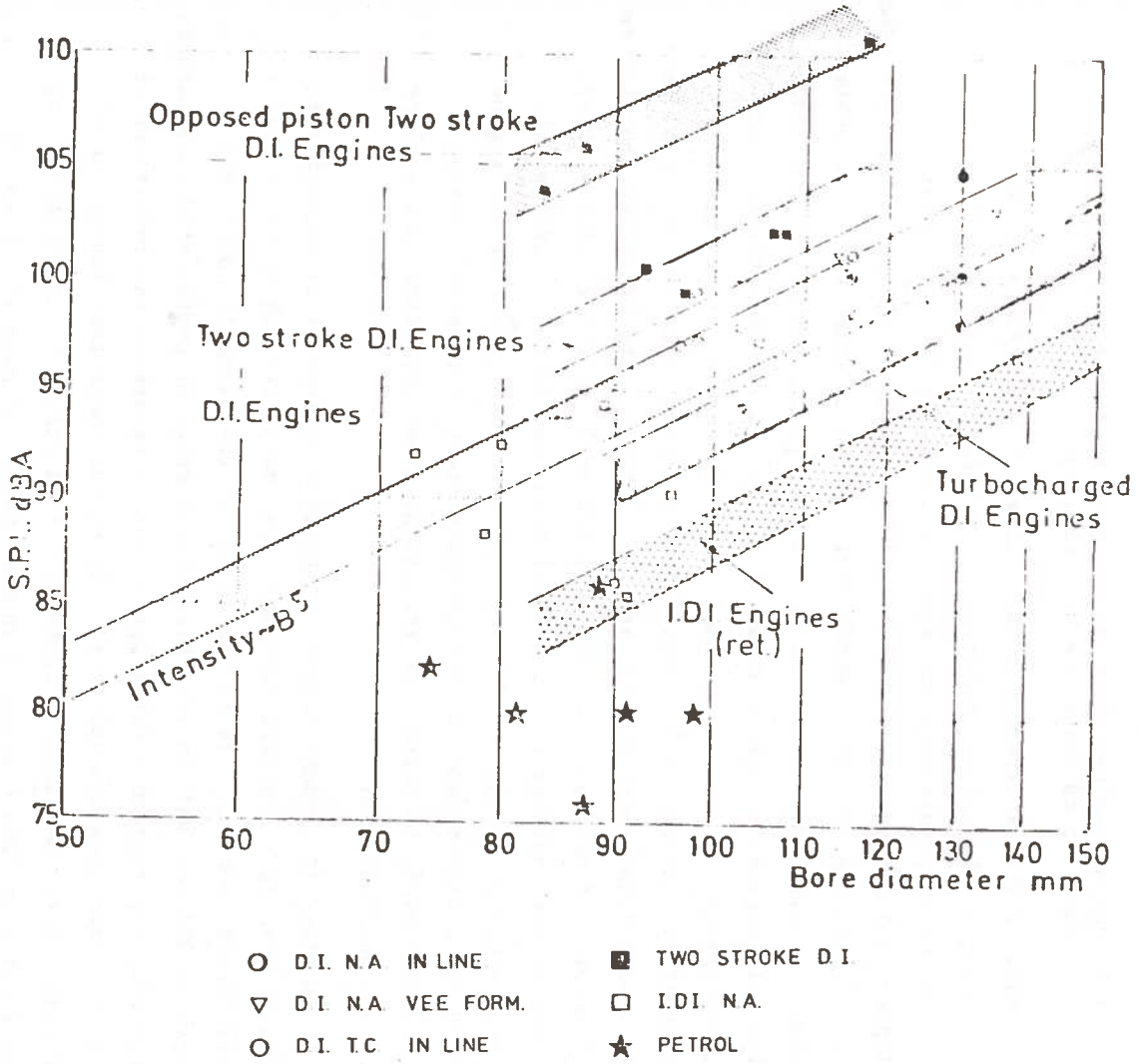

FIGURE 43. RELATION BETWEEN MEASURED OVERALL NOISE AND BORE SIZE OF ENGINES IN THE VARIOUS GROUPS AT 2000 REV/MIN

(d) Two stroke cycle engines fall within a band some 4 dB higher than the D.I. engines.

(e) Opposed piston two stroke cycle engines fall in a band 12 dBA higher.

(f) Petrol engines show considerable scatter but are about 15 dB below the D.I. engines.

Many of the differences between these various groups can be explained by the salient features of cylinder pressure development. Typical pressure diagrams are shown in Figure 44 for a normally aspirated D.I. engine, a turbocharged engine, both 'advanced' and 'retarded' type I.D.I. engines and a petrol engine. The diagram of the turbocharged engine is extremely smooth but with a high peak pressure of 100 - 135 bar. The D.I. engine pressure diagram is abrupt but the peak pressure is considerably lower at 65 - 80 bar. The advanced I.D.I. diagram is similar to that of the D.i. while the 'retarded' diagram has a flat peak or smooth double hump peaking at 65 - 75 bar. The petrol engine diagram is smooth and the peak pressure very low at 35 - 50 bar. The different forms of the cylinder pressure development can be fully described by their spectral analyses. The rate of increase of noise of the engine with speed also depends on the cylinder pressure form as cylinder pressure levels increase with increasing speed according to the slope of the spectrum (49).

In order to compare various combustion systems it is necessary to reduce them to a standard form which is independent of speed (simplified normalised spectra). It is the levels of the harmonic components between 800 and 3000 Hz (the predominant range of engine structure natural frequencies) that to a first approximation determine the importance of the cylinder pressure spectrum. Figure 45a shows that the cylinder pressure spectrum can be approximated to a straight line representing a best fit over this critical frequency range. Figure 45b shows this simplified spectrum normalised for engine speed which defines the cylinder pressure level as a function of both frequency and speed. Figure 45c shows measured cylinder pressure levels for a D.I. engine plotted on a base of normalised frequency. As can be seen all spectra are coincident in the important frequency range and can be approximated by a single straight line.

Such spectra have been derived for each engine tested and the results grouped according to their various combustion systems, are summarised in Figure 46.

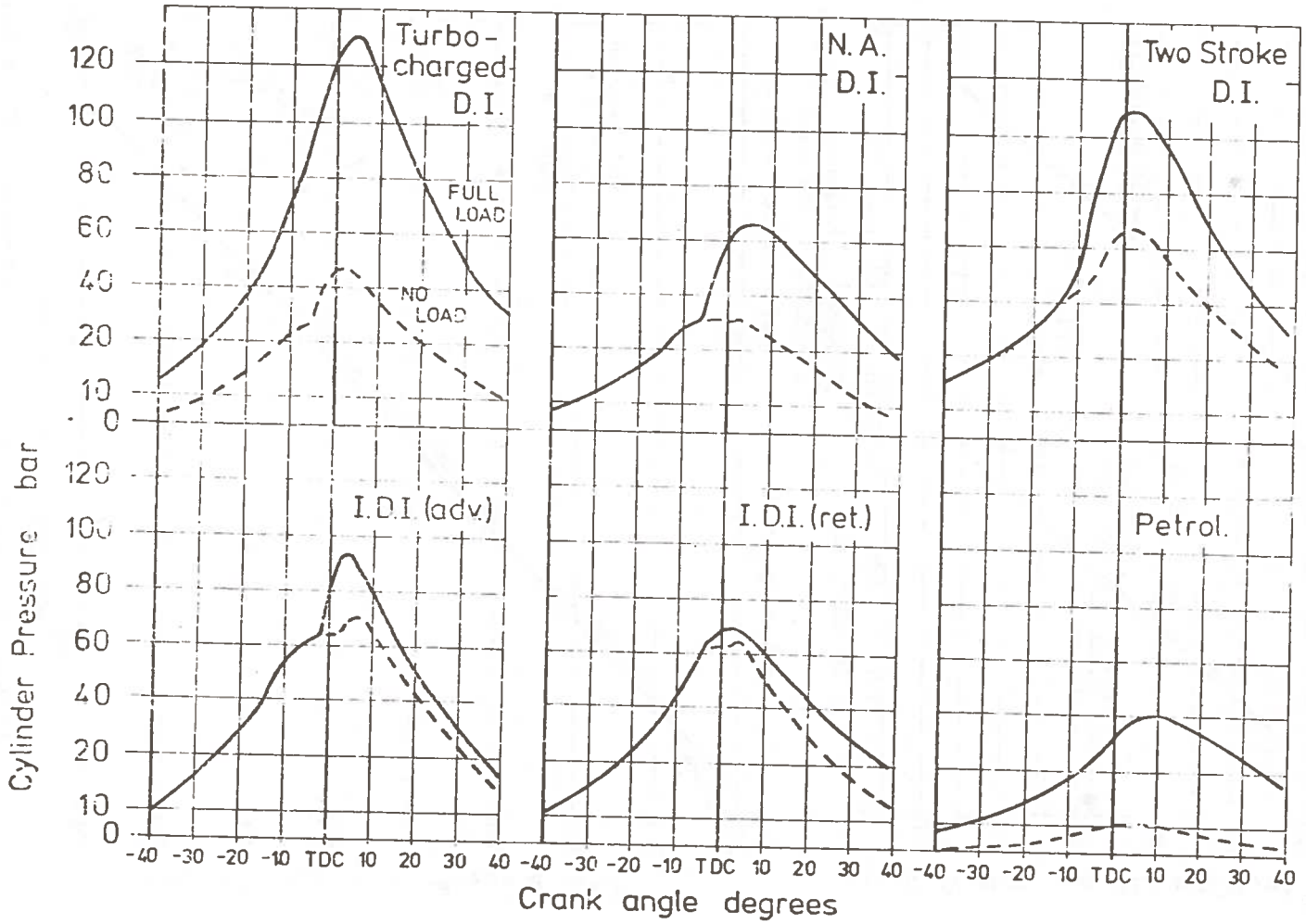

FIGURE 44. TYPICAL CYLINDER PRESSURE DIAGRAMS FOR VARIOUS COMBUSTION SYSTEMS

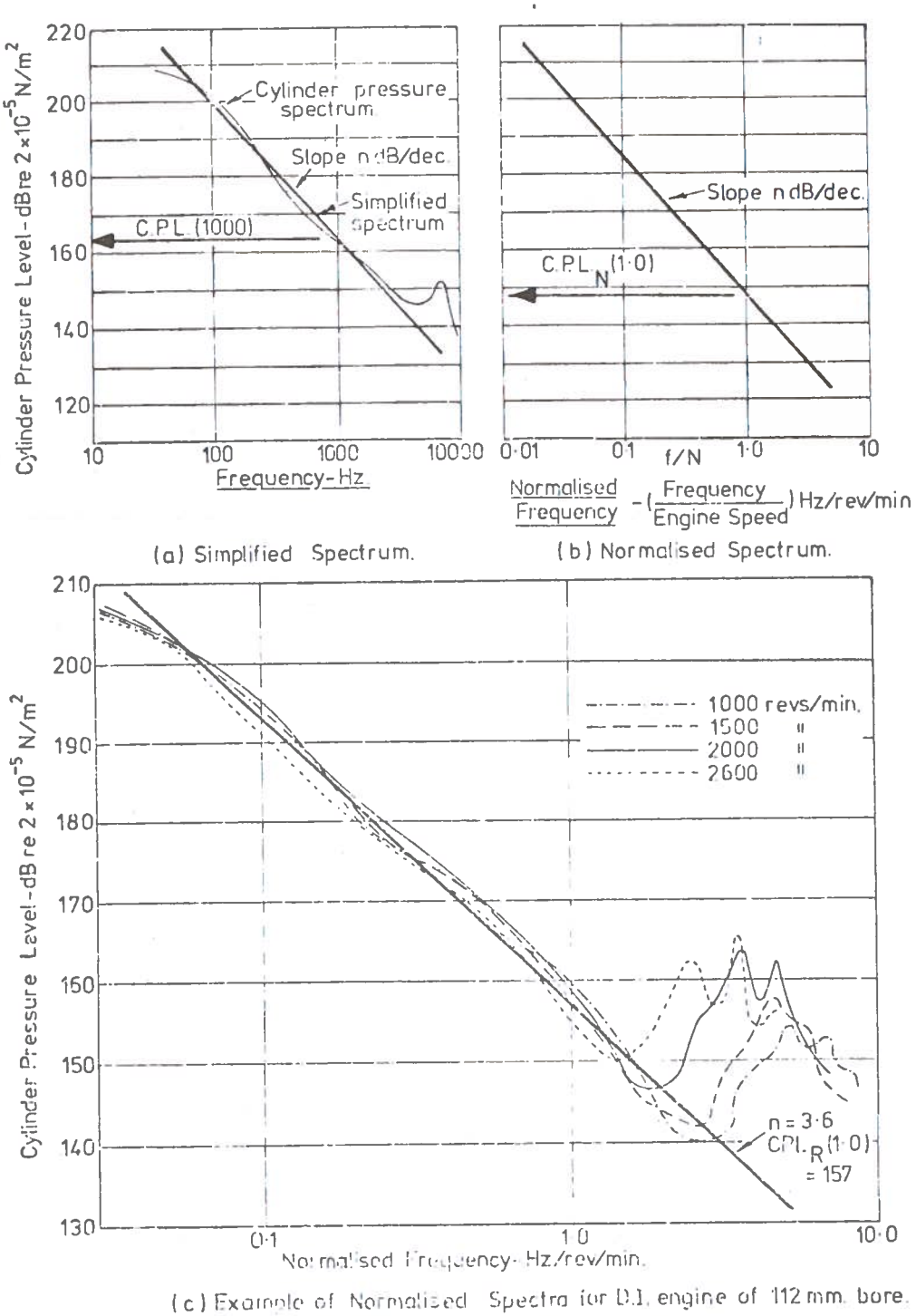

FIGURE 45. NORMALISED AND SIMPLIFIED CYLINDER PRESSURE SPECTRA

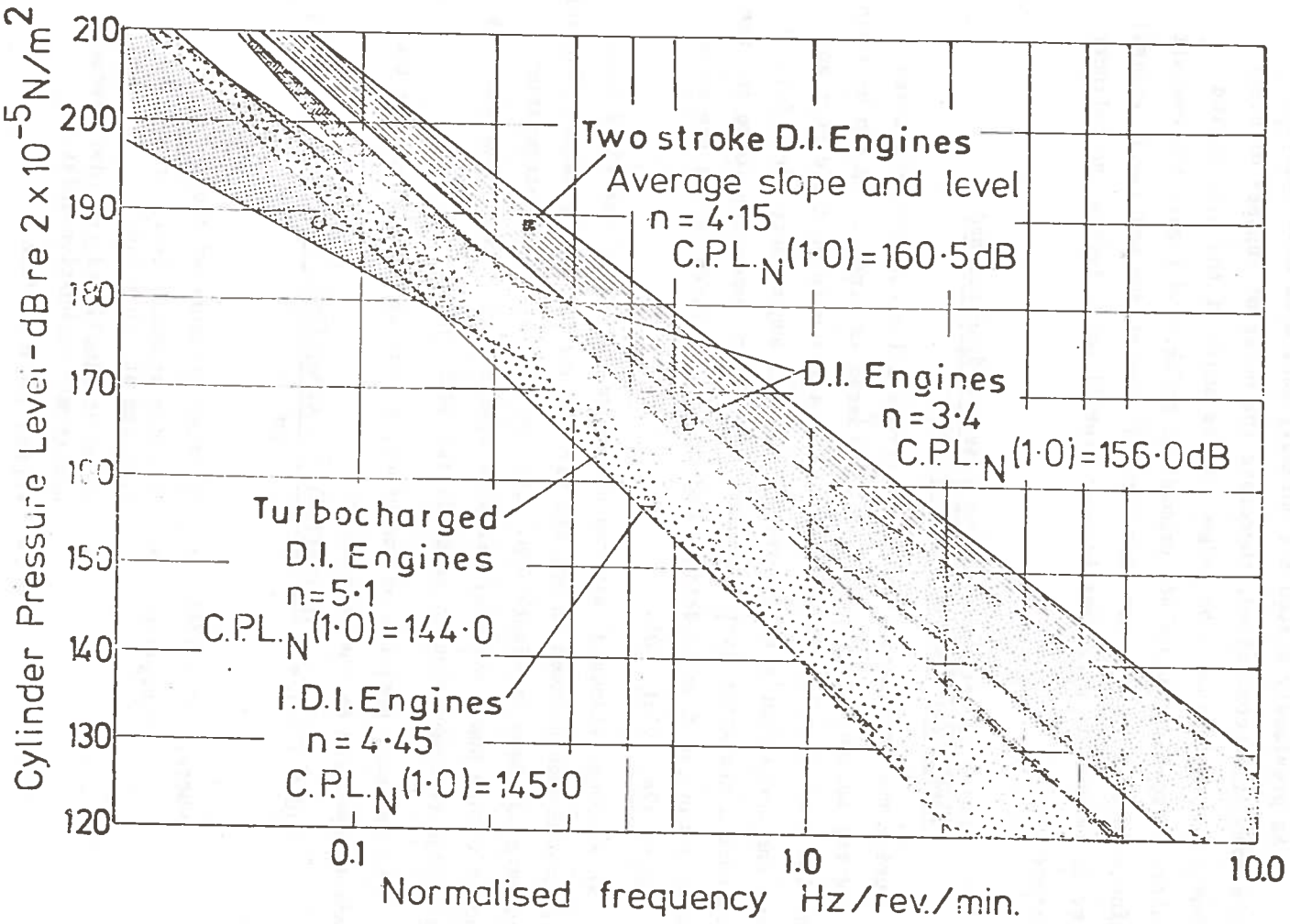

FIGURE 46. FULL LOAD NORMALISED CYLINDER PRESSURE SPECTRA GROUPED ACCORDING TO THE CLASS OF COMBUSTION

As previously stated the normally aspirated D.I. engine is mainly combustion controlled, therefore the noise of engines of other combustion systems should be judged on the basis of the D.i. engine results. Comparing Figure 46, combustion noise, and Figure 43, overall engine noise, it can be seen that for D.I. two stroke and I.D.I. engines there is reasonable agreement between overall noise levels and cylinder pressure levels.

Relation Between Cylinder Pressure Spectrum and Combustion Induced Engine Noise

During the compression and power stroke all clearances are taken up and the engine structure can be considered as linear. It can be shown that the overall noise is proportional to the square of the direct gas force and consequently to the fourth power of engine bore (Ref. 50). A structure attenuation factor linking the direct combustion force and the engine noise can then be defined and typical measured values are shown in Figure 47a. (Ref. 50).

An average 'standard' structure attenuation can be specified from such measurements taken on engines with abrupt cylinder pressure diagrams and this is shown in Figure 47b. The use of a structure attenuation factor with a known cylinder pressure spectrum will then allow the noise level due to combustion to be predicted (Ref. 51).

The cylinder pressure at frequency, f, can be calculated from the reduced spectrum by the relation -

$$(C.P.)^2(f) = \frac{(C.P._R(1.0))^2 \cdot A\log_{10}(3n) \cdot (N/f)^n}{f^n} \qquad (57)$$

where, $(C.P.)(f)$ = cylinder pressure at frequency fHz

$C.P._R(1.0)$ = cylinder pressure level of reduced spectrum at $f/N = 1.0$

n = slope of simplified cylinder pressure spectrum - combustion index

N = engine speed rev/min

In a similar manner the structure attenuation at frequency, f, for the standard attenuation curve can be specified in two parts by :

$$S = \frac{A\log_{10}(S_{1000/10})\ A\log_{10}(3q)}{f^q} \qquad (58)$$

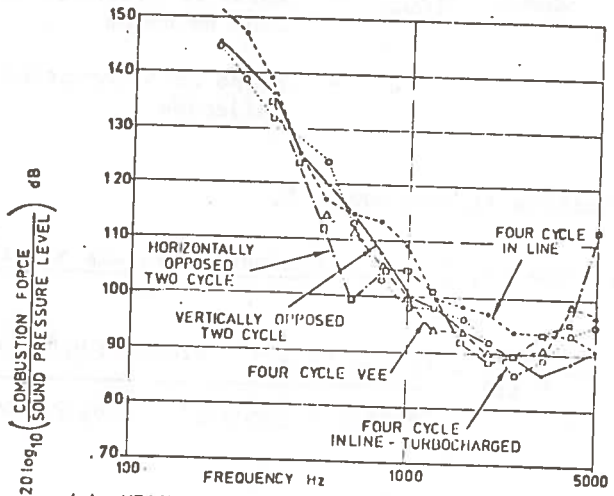

(a) MEASURED STRUCTURE ATTENUATION FACTOR FOR VARIOUS ENGINE CONFIGURATIONS

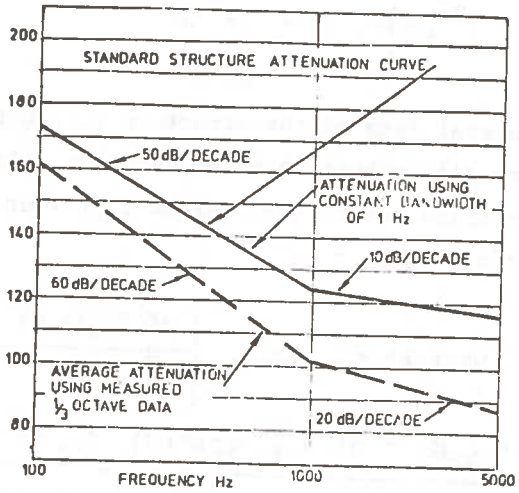

(b) STANDARD STRUCTURE ATTENUATION FACTOR ASSOCIATED WITH A BORE SIZE OF 100 mm

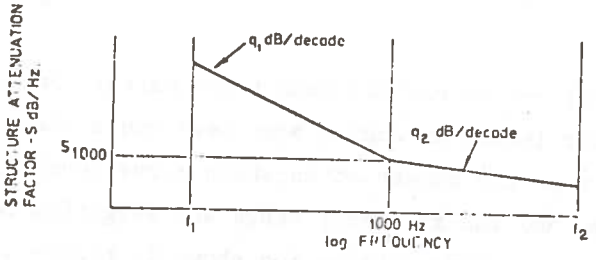

(c) GENERAL FORM OF STRUCTURE ATTENUATION FACTOR

FIGURE 47. STRUCTURE ATTENUATION FACTOR

where, S_{1000} = value of attenuation at 1000 Hz dB/Hz

q = slope of attenuation curve dB/decade

by definition at frequency, f,

$$(\text{Sound Pressure, P})^2_{(f)} = \frac{(\text{cylinder pressure x bore}^2)^2}{S} \qquad (59)$$

$$\text{Therefore } p^2_{(f)} = \frac{(C.P._R\ (1.0))^2\ \ A\log_{10}(3n).(\frac{N}{f})^n\ .\ B^4}{A\log_{10}(S_{1000/10})\ .\ A\log_{10}\ 3q}\ f^{q-n} \qquad (60)$$

The overall sound pressure level is given by

$$p^2\ (\text{overall}) = \int_{f1}^{f2} p^2\ df \qquad (61)$$

Using the general form of the structure attenuation factor shown in Figure 48 the overall combustion noise level is calculated from a measured or computed simplified and reduced cylinder pressure spectrum at an engine speed of N rev/min becomes -

$$(S.P.L.)_{Overall} = 20\log_{10}\left[\frac{(C.P._R(1.0)^2\ .\ A\log_{10}(3n)\ .\ B^4\ .\ N^n}{P_{ref.}\qquad A\log_{10}(S_{1000/10})}\right.\ x$$

$$\left.\left[\frac{[1000^{(q1\ -\ n+1)} - f_1^{(q1-n+1)}]}{(q_1 - n+1)\ A\log_{10}(3q_1)} + \frac{[f_2^{(q2-n+1)} - 1000^{(q2-n+1)}]}{(q_2 - n+1)\ A\log_{10}(3q_2)}\right]\right] dl \qquad (62)$$

Equation (62) can be divided into three parts. One specifying the cylinder pressure level, an engine bore term and a shape factor which is purely dependent on the chosen attenuation curve levels and slopes, the combustion index and the frequency range and weighting networks chosen. For the standard structure attenuation shown in Figure 47 and both the A and Linear weighting networks the value of the shape factor as a function of combustion index is shown in Figure 48.

The predicted noise will vary as the fourth power of bore for direct combustion noise whereas (Figure 43) the measured noise levels of diesel engines vary as the fifth power of bore. This implies that the structure attenuation factor is not constant but varies directly with bore size.

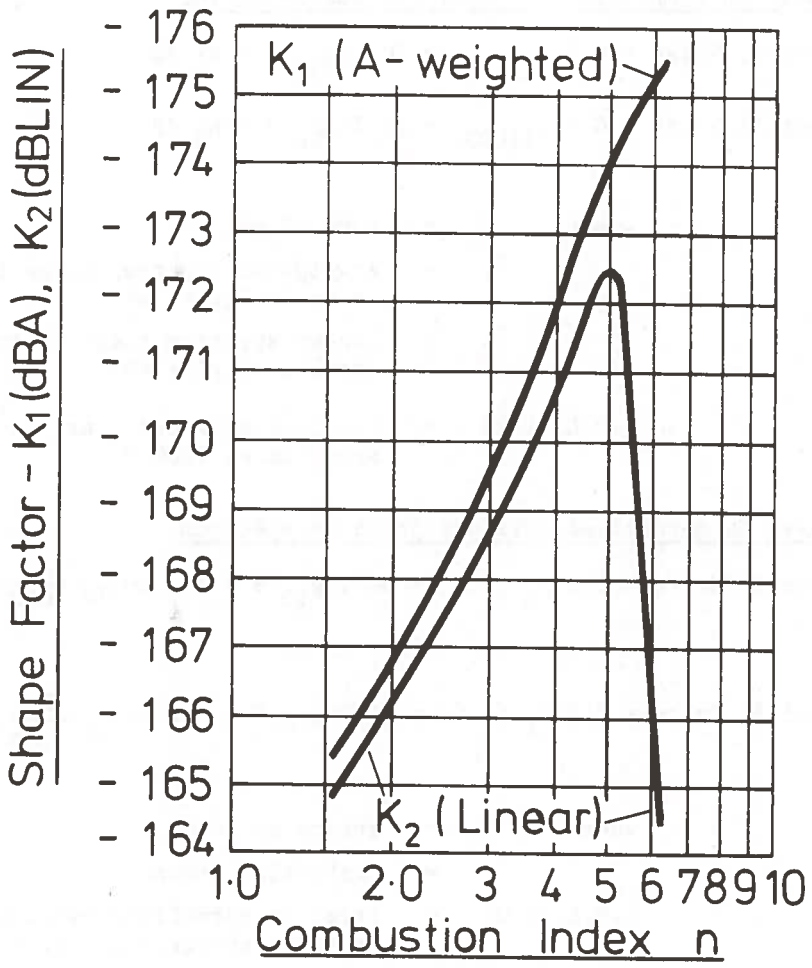

FIGURE 48. SPECTRUM SHAPE FACTORS. K_1 AND K_2

A model for the prediction of combustion induced noise based on measured or estimated simplified cylinder pressure spectra, the engine bore and a structural attenuation factor which varies directly with nore and has the value shown in Figure 47 for a bore size of 100 mm can be put forward. The overall level of direct combustion induced noise at 1 metre is given by the following relations :

Based on simplified cylinder pressure spectrum

$$\text{Overall Noise} = C.P.L_{(1000)} + 50 \log_{10} B - K_1 \text{ dBA} \quad (63)$$

$$\text{and Overall Noise} = C.P.L_{(1000)} + 50 \log_{10} B - K_2 \text{ dB(LIN)} \quad (64)$$

where, B = bore in mm

K_1 = A weighted spectrum shape factor shown in Figure 49

K_2 = Linear spectrum shape factor shown in Figure 49

$C.P.L_N(1.0)$ = Level of cylinder pressure spectrum at 1000 Hz

Based on normalised cylinder pressure spectrum

$$\text{Overall Noise} = C.P.L_N\,(1.0) + 50 \log_{10} B + 10n \log_{10} \frac{N}{1000} - K_1 \text{ dBA} \quad (65)$$

$$\text{and Overall Noise} = C.P.L_N\,(1.0) + 50 \log_{10} B + 10n \log_{10} \frac{N}{1000} - K_2 \text{ dB(LIN)} \quad (66)$$

where, N = engine speed N

n = combustion index

$C.P.L_N(1.0)$ = level of normalised cylinder pressure spectrum at value 1.0

These relations, because they include the absolute level as well as slope of the cylinder pressure spectrum, can be used to predict the level of combustion induced noise in diesel engines of each combustion class at any speed or load. A more exact computation can be obtained by using the exact cylinder pressure spectrum values, as calculated according to the I.S.V.R. Combustion Model, and an exact structure attenuation factor which, at present, can only be obtained experimentally.

A combustion model, described above, enables the prediction of combustion induced noise of the engine based on fundamental principles of thermodynamics and structural attenuation to be carried out. Using this model overall noise of all engines can be predicted. Figure 49 illustrates the relative combustion induced noise levels of engines in the groups shown in Figure 43 against engine size, using the average normalised spectra of Figure 46 for each group.

The model clearly shows that the combustion induced noise of turbocharged engines should be considerably lower than D.I. engines. As the overall noise of the turbocharged engine is relatively higher than would be expected resulting from combustion induced noise alone, it suggests relatively high levels of mechanical exciting force in turbocharged engines.

6. PREDICTION OF COMBUSTION INDUCED NOISE IN DIESEL ENGINES

Modelling of Combustion Noise in Diesel Engines

Knowledge of the cylinder pressure spectrum enables the combustion noise level of diesel engines to be predicted. Over the last ten years the computation of the harmonic cylinder pressure spectrum from a cylinder pressure time history has become possible and therefore a combustion model which can accurately predict the initiation of combustion as well as later burning allows the computation of combustion induced noise. (References 51, 52). Such a model has been developed by Ogegbo and is primarily based on a physical representation of fuel preparation and combustion initiation. This I.S.V.R. model is a two zone model based on modified single droplet and simplified jet theories. It assumes that the physical processes such as atomisation, vaporisation and mixing rates control diesel combustion, and is fully described in Chapter 4 of this report and reference 53.

Figure 50a shows a typical comparison between measured and predicted cylinder pressure development and spectra for a shallow bowl D.I. engine. Figure 50b shows the error in cylinder pressure spectrum prediction, in one-third octave bands as a function of frequency and engine speed for two combustion models, firstly model 1 (a modification of Austen and Lyn's approach relating the injection rate and the rate of burning) and secondly the I.S.V.R. model in which the physical processes leading

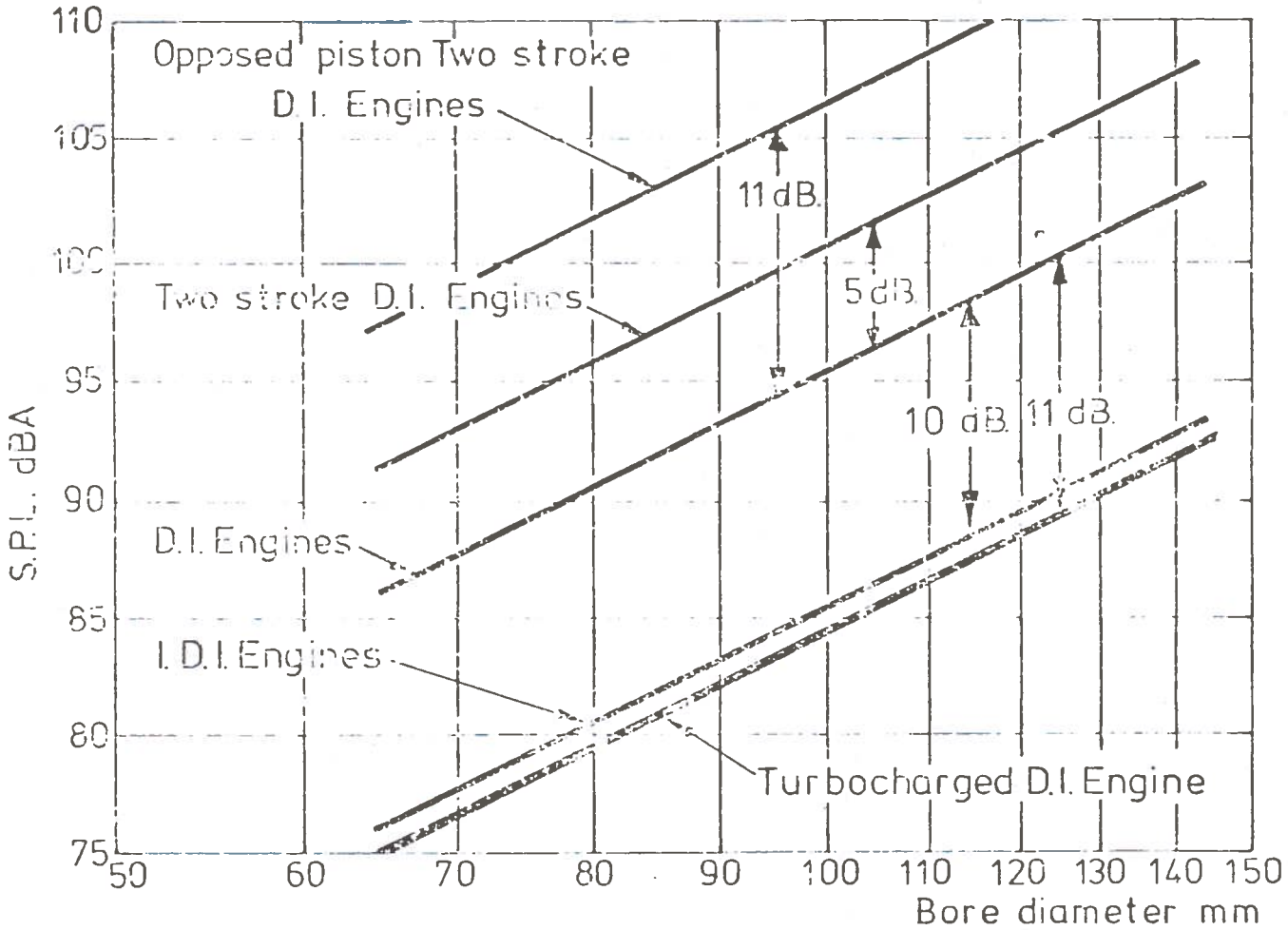

FIGURE 49. PREDICTED DIESEL COMBUSTION NOISE LEVELS AT 2000 REV/MIN

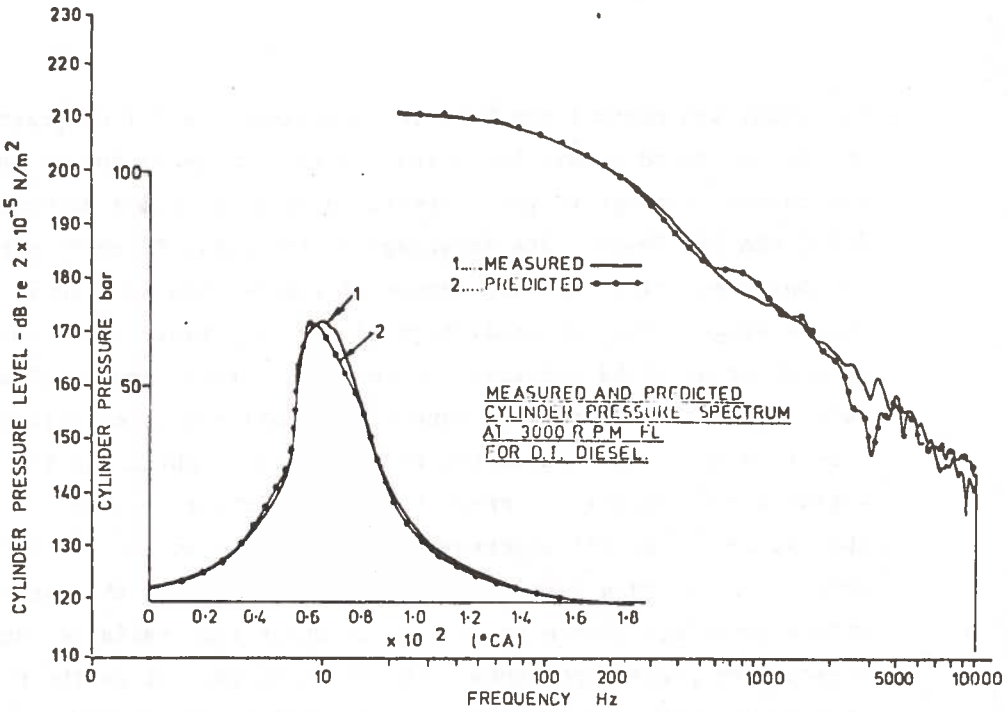

(a) COMPARISON OF PREDICTED AND MEASURED CYLINDER PRESSURE DEVELOPMENT AND SPECTRUM USING I.S.V.R. COMBUSTION MODEL.

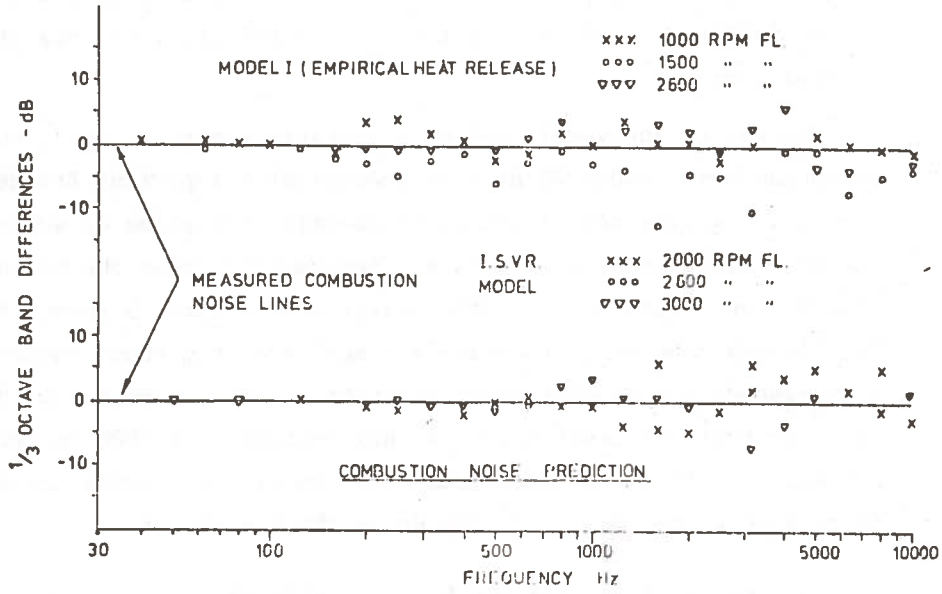

(b) COMPARISON OF PREDICTED AND MEASURED 1/3 OCTAVE BAND CYLINDER PRESSURE SPECTRUM LEVELS

FIGURE 50. PREDICTION OF CYLINDER PRESSURE SPECTRUM LEVELS FROM COMBUSTION MODELS

to combustion control the heat release rates. A ± 7 dB scatter in the higher one-third octave bands results in both cases but in summing over the frequency range to give overall level predictions accuracies of ± 2.5 dBA are found. The advantage of the I.S.V.R. model over model 1 is that predictions for new ranges of engines can be made at the design stage. For the prediction of the resultant noise caused directly by combustion it is necessary to know the detail structural and acoustic response of the engine structure to excitation at each cylinder. Unfortunately this information is difficult to obtain in the built up engine and impossible to predict with sufficient accuracy to warrant the use of the detail spectrum shape predicted by the I.S.V.R. combustion model. In any case even such predictions involving the use of one-third octave bands are liable to so high an error that reliance cannot, at present, be placed upon them. Therefore at this stage the model is used to predict overall level changes, using the standard structure attenuation factor given in Chapter 5, directly from the summed cylinder pressure spectrum input. Alternatively some broad generalisations can be obtained from a mixture of theoretical and practical results in the following manner.

The use of an overall cylinder pressure spectrum level, summed over the frequency range 700-3000 Hz (the acoustically important frequency range for diesel engine noise) either by electric filtering or summation of the spectrum components, precludes any information about the slope and 1000 Hz level without which the analysis of Chapter 5 cannot be applied. In this case the concept of an 'average' spectrum shape factor of -170.5 dB (corresponding to a combustion index of n = 3.3) together with an overall cylinder pressure level (700-3000 Hz) instead of a 1000 Hz level is attractive. It can be shown that for simplified spectra the overall level is related to the level at 1000 Hz by the formula :

$$\text{C.P.L. (overall)} = \text{C.P.L.}_{1000} + 31 \text{ dB} \qquad (67)$$

to an accuracy of ± 1.5 dB for n = 2 to 5.

From the foregoing and equation (7) of Chapter 5 the 'average' predicted overall 'A' weighted combustion induced noise of a diesel engine measured 1 m from the surface is :

Overall Noise, dBA = $C.P.L._{1000} + 50 \log_{10} B - 170.5$

Bore in m.m.

$C.P.L._{1000}$ in dB = 2×10^{-5} N/m^2

and therefore in terms of the overall cylinder pressure level :

Overall noise, dBA = $C.P.L._{overall} + 50 \log_{10} B - 201.5$ (68)

where $C.P.L._{overall} = 20 \log_{10} \left(\sum_{f=700}^{f=3000} \frac{p(f)}{2 \times 10^{-5} N/m^2} \right)$

and p(f) = pressure amplitude at frequency f Hz

In Chapter 1 the relationship between the cylinder pressure spectrum level and the initial peak rate of heat release was observed. Also it is well established in the literature that the rate of pressure rise is strongly related to the magnitude of combustion induced noise.

For the general case of a non-symmetrical triangular waveform it can be shown that the level of the harmonic spectrum at 1000 Hz, b_n^2, is proportional to the square of the rise rate of the waveform and the fourth power of the repetition frequency (speed) or $b_n^2 \propto (RPR)^2 (N)^4$

where RPR = rise rate units /°C.A.

N = equivalent waveform speed rev/min

Thus if the waveform is considered to represent a cylinder pressure diagram the cylinder pressure level at 1000 Hz, $C.P.L_{1000}$, is given by -

$C.P.L._{100} \propto 20 \log_{10} RPR + 40 \log_{10} N$ (69)

with RPR = Rate of pressure rise psi/°C.A.

N = Engine speed psi/°C.A.

Since the overall cylinder pressure level is directly related to the level at 1000 Hz then the form of equation (69) provides a suitable basis on which to plot the results of actual engine measurements. A set of results, taken from a direct injection diesel engine in both its normally aspirated and turbocharged forms is shown in Figure 51. A general trend is found but with a fair degree of scatter. This is because the actual frequency spectrum does not only depend on the rate of pressure rise but also depends on peak pressure and the acceleration of the pressure rise as well as the 'width' of the pressure diagram. Despite this the relation between rate of pressure rise, engine speed and overall cylinder pressure level is clear for this engine and is ;

$$C.P.L._{overall} = 20 \log_{10} RPR + 38.9 \log_{10} N + 28 \text{ dB} \qquad (70)$$

where the speed index 3.89, represents the average measured value

Thus the overall combustion induced noise of an engine with similar combustion characteristics to this direct injection engine can be given in terms of the engine bore, speed and rate of pressure rise by substituting equation 70 in equation (68). Then :

Overall combustion induced noise at 1 m,

$$dBA = 20 \log_{10} RPR + 38.9 \log_{10} N + 50 \log_{10} B - 173.5 \text{ dB}$$

B = Bore in m.m.
RPR = Rate of pressure rise psi/^{o}C.A.
N = Engine speed rev/min

(71)

This relationship is illustrated in Figure 52 for a range of bore sizes and two engine speeds. The effect of variation of rate of pressure rise, within the practical limits of 30 to 150 psi/^{o}C.A. is to vary the noise level by some 14 dBA at constant speed and some 30 dBA together with a speed increase from 1000 to 2500 rev/min. This large variation in predicted noise is in general agreement with the measured results of Figure 43 although it is based on the data from only one engine.

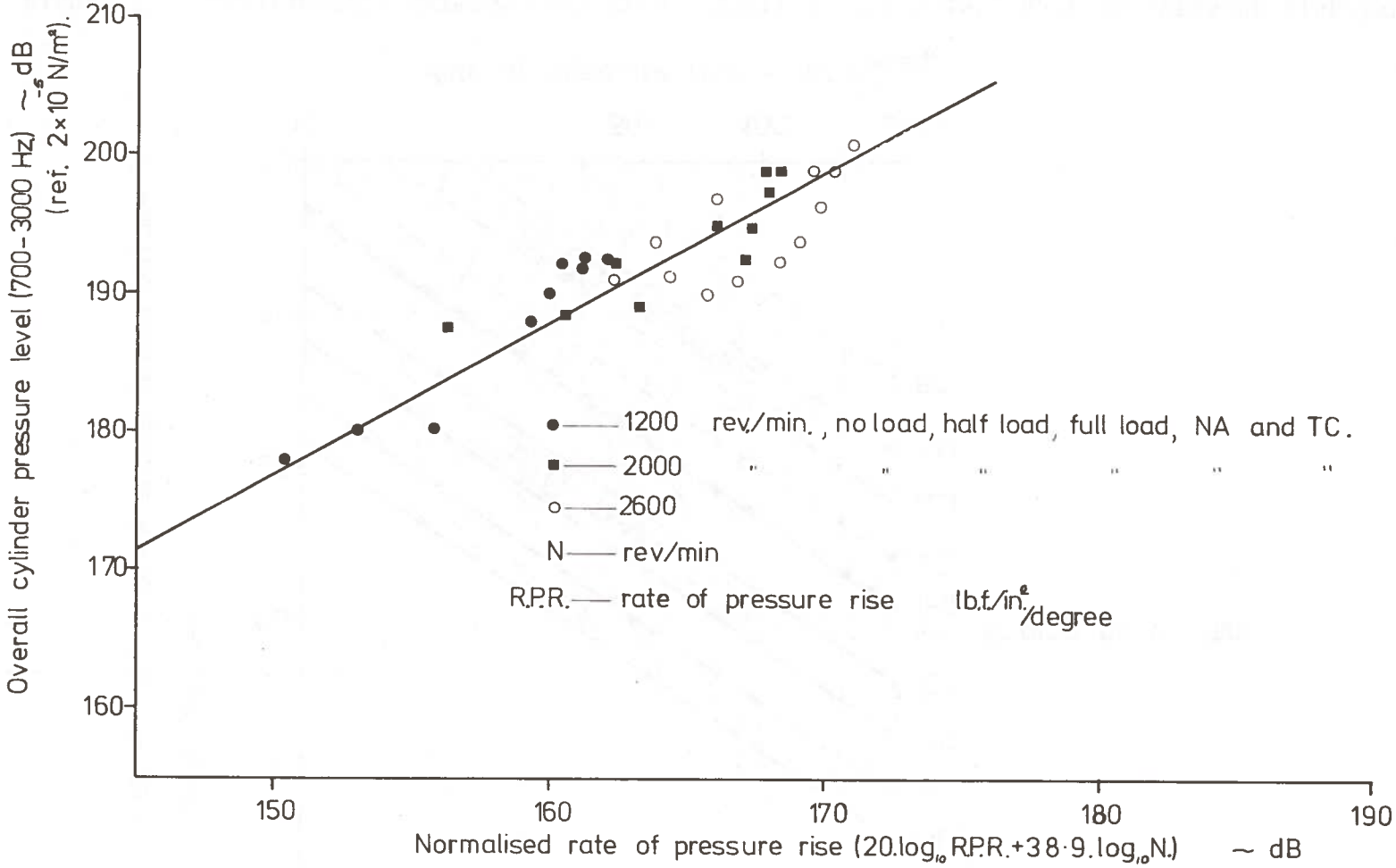

FIGURE 51. RELATIONSHIP BETWEEN OVERALL CYLINDER PRESSURE LEVEL, RATE OF PRESSURE RISE AND ENGINE SPEED FOR A D.I. ENGINE.

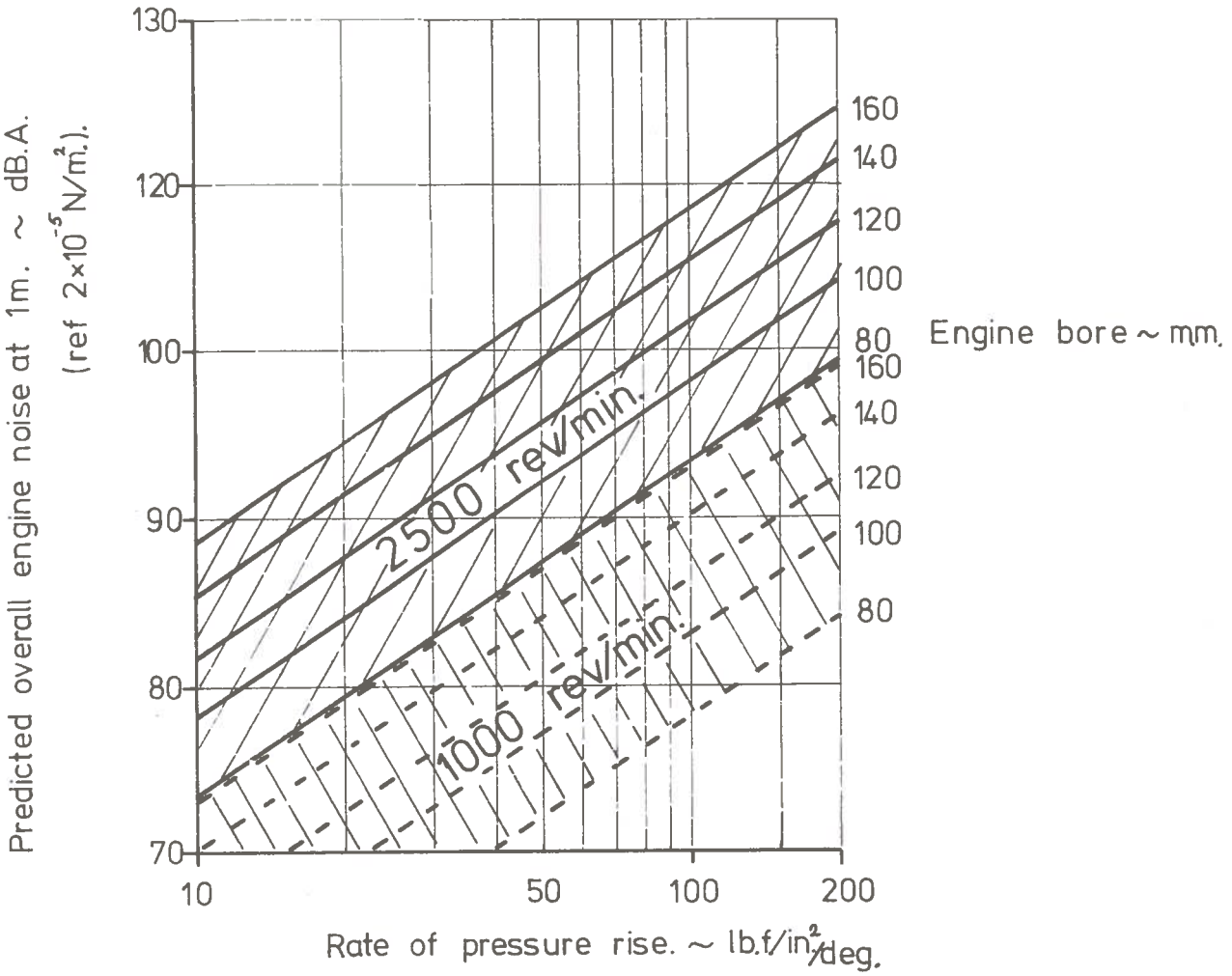

FIGURE 52. RELATIONSHIP BETWEEN PREDICTED OVERALL ENGINE NOISE, RATE OF PRESSURE RISE AND ENGINE SPEED FOR D.I. ENGINE

If it is required to produce an engine with a particular noise level then the relation (71) can be used to indicate the likely maximum rate of pressure rise which could be used with a given engine bore and speed. This relationship is shown in Figure 53 for a noise level of 100 dBA at 1 m. and indicates that the allowable maximum rate of pressure rise reduces rapidly as the engine bore size is increased. A similar trend with increasing engine speed is shown. Since there is a relationship between the rate of pressure rise and the initial peak of the heat release rate then the relation between overall noise and rate of pressure rise can be rewritten to contain the heat release rate peak instead of rate of pressure rise. Thus the conclusions regarding rate of pressure rise can be applied directly to the initial peak of heat release rate, using the average relation

$$RPR = 1.633\ IPHR + 4 \qquad (72)$$

IPHR = Initial peak of heat release rate curve Btu/lb/^{o}R

RPR = Rate of pressure rise psi/^{o}C.A.

illustrated in Figure 54 and hence the overall combustion induced noise at 1 m can be expressed as :

$$dBA = 20 \log_{10}(1.633\ IPHR + 4) + 38.9 \log_{10} N + 50 \log_{10} B - 173.5\ dB \qquad (73)$$

It must be remembered, of course, that these relationships are based on the measured results from one direct injection diesel engine.

These general results can be useful during the initial design studies for new engines but once the design has been firmed then more detailed studies using the I.S.V.R. combustion model can be undertaken. The results of such a study for engine A are summarised in Figure 55 in terms of the predicted overall cylinder pressure level. This, of course, for a given engine can be directly converted into a combustion induced engine noise level by equation (68). However changes in noise level (in dB) are the same as changes in overall cylinder pressure level for a given engine and so the effects shown in Figure 55 can be read directly

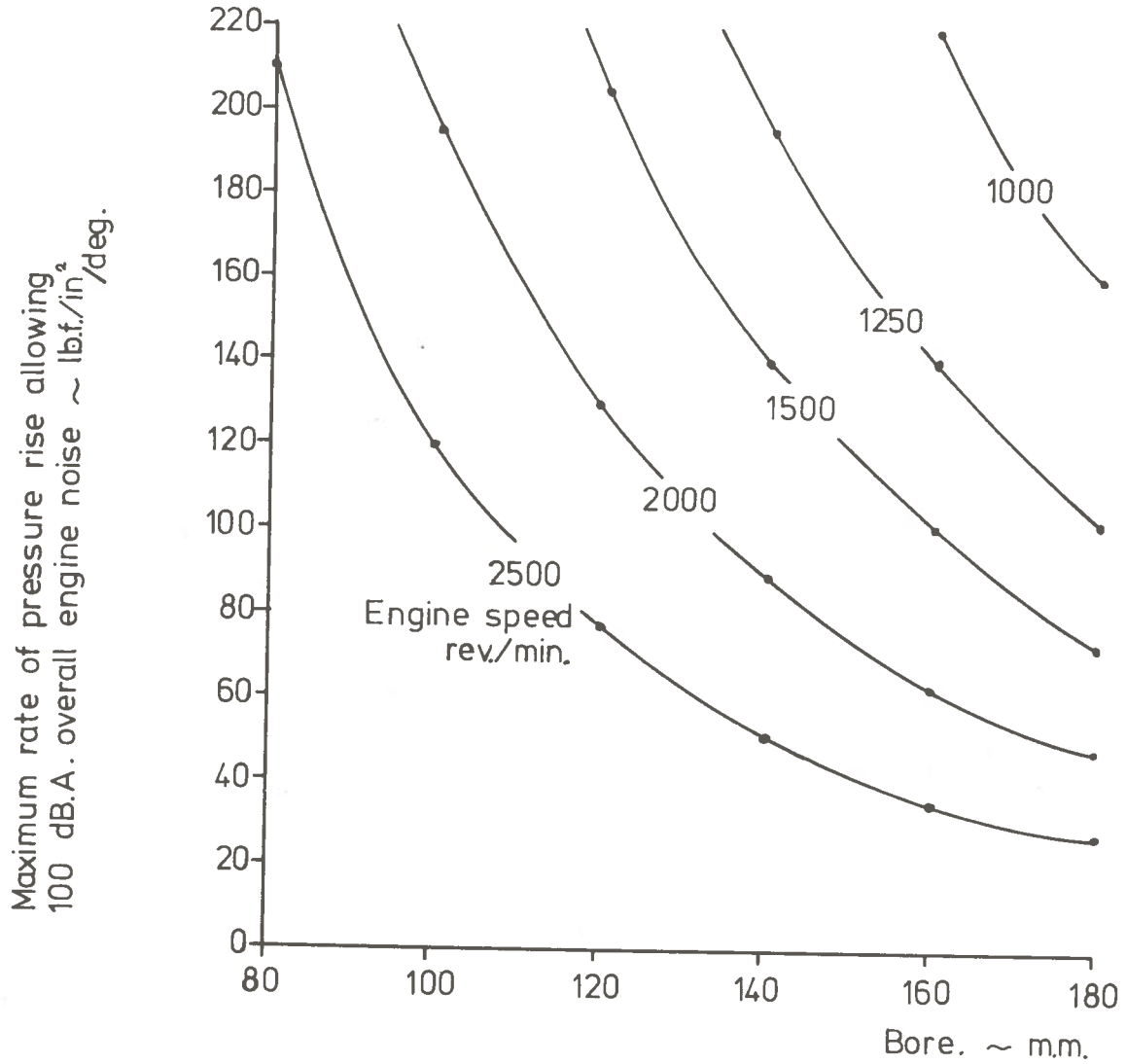

FIGURE 53. ALLOWABLE RATE OF PRESSURE RISE FOR 100 dB.A. NOISE LEVEL D.I. DIESEL

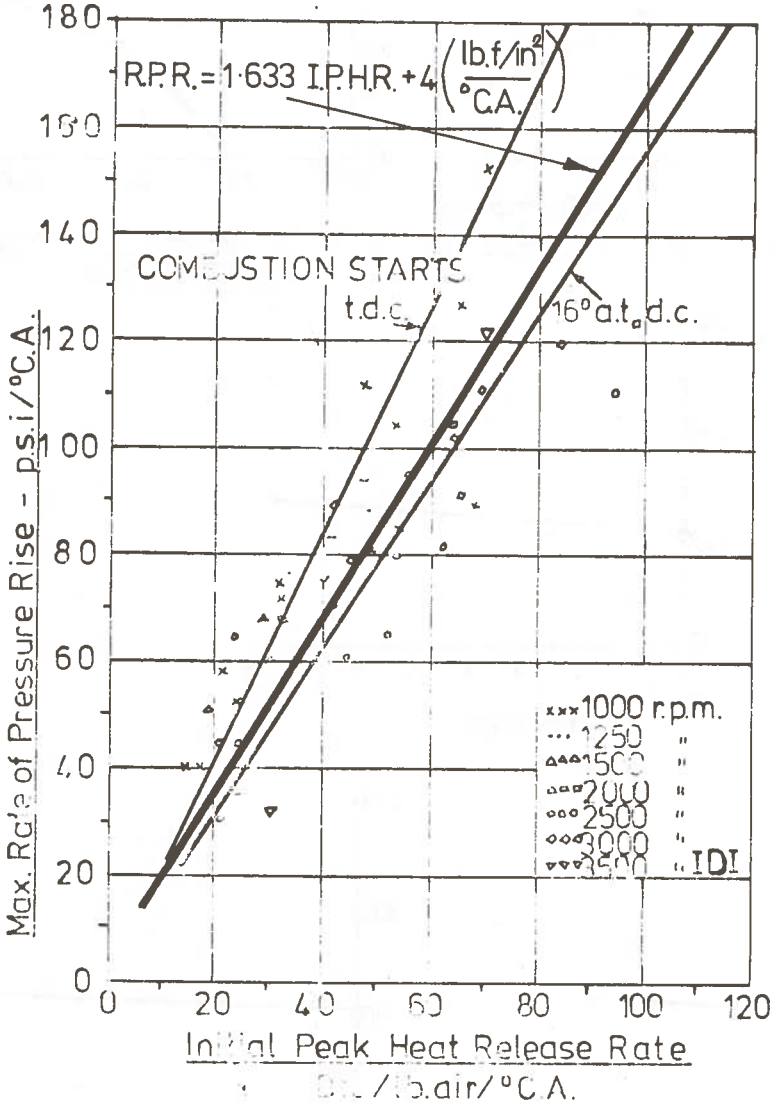

FIGURE 54. AVERAGE RELATIONSHIP BETWEEN RATE OF PRESSURE RISE AND INITIAL PEAK HEAT RELEASE RATE

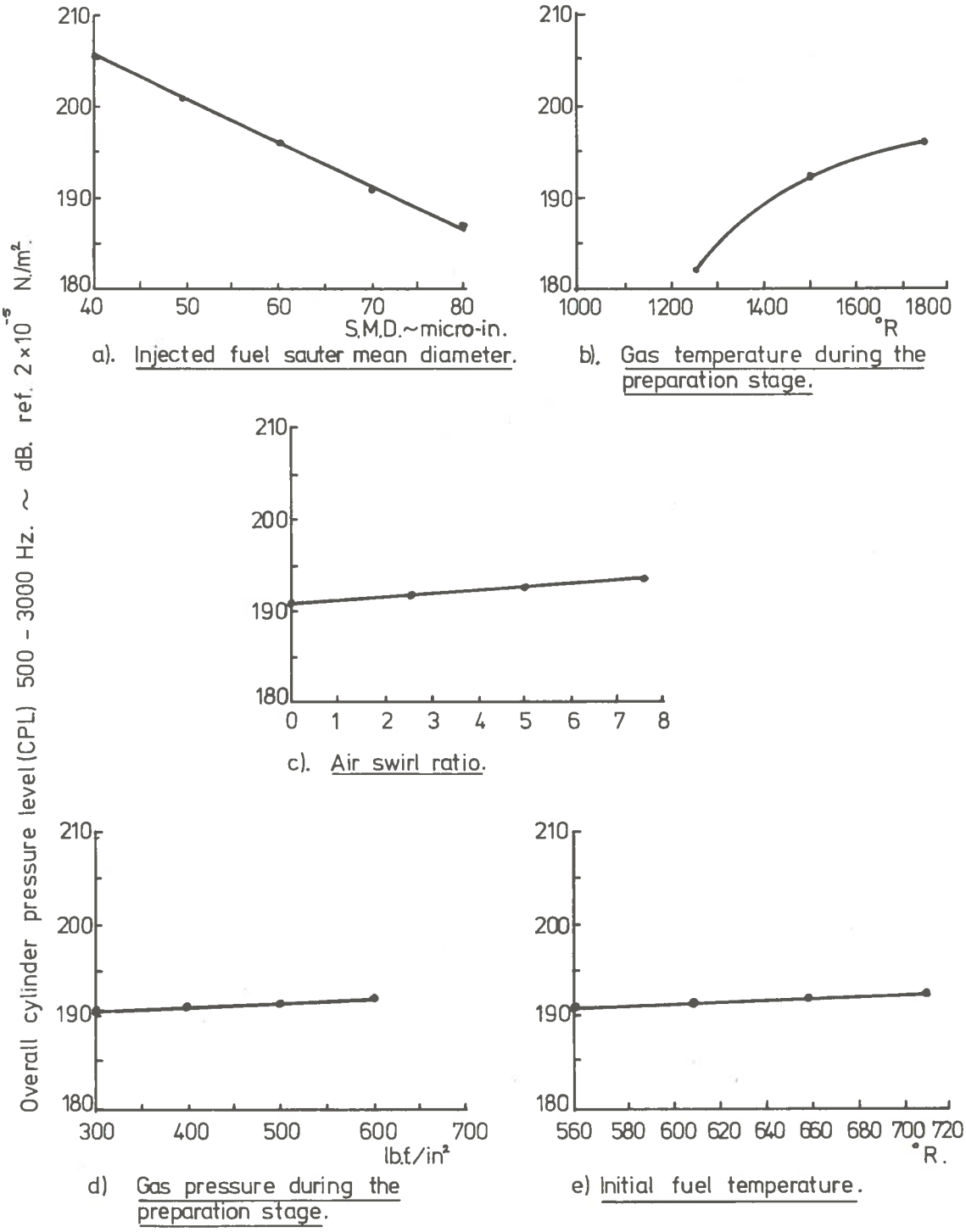

FIGURE 55. PREDICTED EFFECT OF CHANGING DESIGN PARAMETERS ON OVERALL C.P.L.~ENGINE 'A' 1000 REV./MIN.

as noise level changes. For this engine the effect of swirl, initial fuel temperature and air swirl ratio are small (2-3 dB) but the fuel spray droplet size and gas temperature during preparation have large effects (15-20 dB). The droplet size affects the amount of fuel prepared during the delay period. Although individually the air swirl ratio has small effect in practice the fuel Sauter Mean Diameter which can be used is strongly related to the air swirl ratio by the combustion chamber design and number of spray holes.

7. CONCLUSIONS

The concept of heat release in diesel engines is extremely useful when studying the effect of combustion on diesel noise. In particular there is a strong relationship between the initial peak rate of heat release and the level of combustion induced noise, the noise increasing as the peak increases. Since the maximum rate of pressure rise is also related to the initial peak heat release rate then there is found to be a general relationship between it and the level of combustion noise. It is found that, for a given engine noise level (due to combustion), there is a maximum rate of pressure rise associated with a particular bore size and engine speed and that this maximum rate reduces rapidly as the bore size increases.

In modelling the diesel combustion it is found that few models are aimed at the prediction of the premixed burning stage in detail and therefore the I.S.V.R. combustion model is put forward to fill this gap. This model is a two zone model based on modified single droplet and simplified jet theories and it assumes that the physical processes such as atomisation, vaporisation and mixing control diesel combustion. Using this model it is possible to predict the cylinder pressure spectrum. In one-third octave bands an accuracy of $\pm$ 7 dB is found at high frequency but the overall level can be predicted to within $\pm$ 2.5 dB.

Thus at present the predicted overall level is used to investigate the effect of design parameters on engine noise. Design parameters which are predicted as the main controlling features of combustion, from a noise point of view, are the average fuel spray droplet size and the temperature of the cylinder contents during the delay period. It is quite clear that the use of rapid rates of fuel injection, as proposed for reduced gaseous emissions, is detrimental to the design of low noise diesel engines.

8. REFERENCES

1. W.T. LYN. 'Calculations of the effect of rate of heat release on the shape of cylinder pressure diagram and cycle efficiency. Proc. Inst. Mech. Engrs (A.D.) No.1, 1960-61.

2. WIEBE I., "Halbempirische Formel fur die Verbrennungsgeschwindigkeit" 1956 (Moscow, Verlag der Akademic der Wiss. der UdSSR).

3. AUSTEN A.E.W. and LYN W.T. 'Relation between fuel injection and heat release in a direct injection engine and the nature of the combustion processes'. Proc. Auto. Div. Inst. Mech 1960-61, (No 1) 34.

4. SHIPINSKI ET AL. 'A spray droplet model for diesel combustion, Paper 2. Inst. Mech. Engrs 'Symposium on Diesel Engine Combustion' 7-9 April 1970.

5. WHITEHOUSE, N.D. and WAY, R.J.B. 'A simple method for the calculation of heat release rates in diesel engines based on the fuel injection rate'. SAE 710134, p.11-15, 1971.

6. NAGAS, F. and IKEGAMI, M. 'An analysis of combustion knock in diesel engine'. Inst. Mech. Engrs 'Symposium on Diesel Engine Combustion' 7-9 April 1970.

7. PICKEN. 'Diesel combustion'. Ph.D thesis 1970, Ruston Polytechnic.

8. GRIGG H.C. and SYED M.H. 'The problem of predicting rate of heat release in diesel engines' Proc.Inst.Mech.Eng. London, Vol.168, 1954.

9. SAREEN B.K. 'Relationship between fuel injection and heat release in a quiescent chamber diesel engine'. Ph D Thesis 1972. The University of Manchester Institute of Science and Technology, Dept of Mech Eng.

10. LICHTY, L.C. 'Combustion engine processes'. McGraw-Hill, Series in Mechanical Engineering, 1967.

11. TANASAWA, Y, TOYODA, S. 'On the atomising characteristics of injector for diesel engines'. Tech.Reports, Tohoku, University Sundai, Japan. Vol.XX 1 (121)1961.

12. TANASAWA, Y. 'The atomisation of liquid fuels for combustion'. J.Inst. Fuel Vol.22, No.124, Feb 1949, p.150 (London).

13. KNIGHT, B.E. 'Communication on the performance of a type of swirl atomiser'. Proc.Inst.Mech.Eng. London, 1955, p.104.

14. SPIERS, H.M. 'Technical data on fuels'. The British National Committee World Power Conference, 1962.

15. WAKIL et al. 'A theoretical investigation of the heating-up period of injected fuel droplets vaporising in air'. Proc.Inst.Mech.Engrs. 1962.

16. NAGAO, F. et al. 'An analysis of combustion knock in diesel engine'. Bulletin of J.S.M.E. Vol.10, No.39, 1967.

17. HENEIN, N.A. 'M.I.R.A. Abstract - Combustion and emission formation in fuel sprays injected in swirling air'. SAE Paper 710220, January 1971.

18. WILLIAMS, F.A. 'Combustion Theory'. Addison-Wesley Publ.Co.Inc. 1965.

19. PRIEM, R.J. HEIDMANN, M.F. 'Propellant vaporisation as a design criterion for rocket engine combustion chambers'. NACA Tech.Report R-67, 1962.

20. WAKIL, El.M. et al. 'Graphs of reduced variables for computing histories of vaporising fuel drops and drop histories under pressure'. NACA 4338, 1958.

21. INGEBO, R.D. 'Vaporisation rates and heat transfer coefficients for pure liquid drops'. NACA TN 2368, 1951.

22. WAKIL, El.M.M, CHEN, C.S. 'Experimental and theoretical studies of burning drops of hydrocarbon mixtures'. Paper 10, Ref.28.

23. WAKIL, M.M. et al. 'Fuel vaporisation and ignition lag in diese combustion'. SAE Transactions, Vol.64, 1956.

24. WILLIAM, F.A. J.Chem. Physics, 33, 133 (1960).

25. SHIN-I PAI. 'Fluid dynamics of jets'. D.Van Nostrand Company Inc., London, July 1954.

26. GODSAVE, G.A.E. 'Studies of the combustion of drops in a fuel spray - the burning of single drops of fuel'.

27. HOFFMANN, T.W., GAUVIN, W.C. 'Evaporation in a high-temperature environment'. - II. Calculation of the evaporative load distribution. The Canadian Journal of Chemical Engineering, June 1962.

28. JACKSON, P.P. 'Combustion in diesel engine'. Ph.D. thesis, University of Birmingham, 1965.

29. PENNER, S.S. 'Introduction to the study of chemical reactions in flow systems'. Butterworths Scientific Publ. London, 1955.

30. HERBERT, M.V. 'A theoretical analysis of reaction rate controlled systems - Part I'. Combustion Researches and Reviews, p.76, 1957. Pergamon Press.

31. LYN, W.T. VALDMANIS, E. 'Effects of physical factors on ignition delay'. Inst.Mech.Eng. London, 1966.

32. HENEIN, N.A. JAY, A.B. 'Ignition delay in diesel engines'. SAE Transaction 670007, 1967.

33. YU, T.C. UYEHARA, O.A. 'Physical and chemical ignition delay in an operating diesel engine, using the hot-motored technique'. SAE Trans. Vol.64, 1956.

34. Symposium on Diesel Engine Combustion, Institution of Mechanical Engineers, April 1970.

35. SMALL, J. 'Vagaries of internal combustion'. Engineer, London, Vol.164, pp 642-668, 1937

36. TAO, K.C. et al. 'Gas temperatures during compression in motored and fired diesel engines'. SAE Trans. Voo.70, p.136-145, 1962.

37. SITKEI, G. 'Uber den diesel motorischen Zundverzug'. M.T.Z. Jahrg. 24, Heft 6, Juni 1963.

38. SPALDING, D.B. 'The combustion of liquid fuels'. International Symposium on Combustion, 1956.

39. EICHELBERG, G. 'Some new investigations on old combustion engine problems'. Engineering, London, Vol.148, p.603, 1939.

40. ANNAND, W.J.D. 'Heat transfer in the cylinder of reciprocating internal combustion engines'. Proc.Inst.Mech.Eng, London, Vol.177, No.16, 1963.

41. BOLT, J.A. and HENEIN, N. 'The effect of some engine variables on ignition delay and other combustion phenomena in a diesel engine'½ Ref. 34, Paper 13.

42. SAMI, H. and OGASAWARA, M. 'A field study on the behaviour of a fuel droplet injected into the combustion chamber of a diesel engine SAE 670468, 1957.

43. GREEVES, G. 'A combustion study of a supercharged high speed two-stroke diesel engine'. Ph.D thesis, Queen's University of Belfast, Faculty of Applied Science and Technology, December 1969.

44. LYN, W.T. 'The study of burning rate and nature of combustion in diesel engines'. 4th International Symposium on Combustion, New York, 1962.

45. WHITEHOUSE, N.D. and WAY, R.J.B. 'Rate of heat release in diesel engines and its correlation with fuel injection data'. Ref.28, Paper. 1.

46. KNIGHT, B.E. 'Similarity consideration in assessing diesel engine fuel spray requirements'. Symposium - Diesel Engines - Breathing and Combustion. Proc.Inst.Mech.Eng. 1965-66, p.180 (Pt.3N) 10.

47. DICKSEE, C.B. 'High speed compression-ignition engine'. Blackie and Son Ltd., 1946, p.378.

48. GRIGG, H.C. and SYED, M.H. 'The problem of predicting rate of heat release in diesel engines'. Proc.Inst.Mech.Eng, London. Vol.168, p.265, 1954.

49. AUSTEN A.E.W. and PRIEDE T. 'Origins of diesel engine noise' Inst Mech Engrs - Symposium on 'Engine Noise and Noise Suppression'. London October 1958.

50. ANDERTON D. and BAKER J. 'Influence of operating cycle on noise of diesel engines'. SAE Trans 730241, 1973.

51. ANDERTON D. 'Combustion as a source of diesel engine noise'. Ph D Thesis, University of Southampton, England, 1974.

52. PRIEDE T, GROVER E.C. and ANDERTON D., 'Combustion Induced noise in diesel engines' Diesel Engine Users Association, London, Publication 317 March 1968.

53. OGEBO A.M., 'Automotive diesel engine combustion and noise'. Ph D Thesis, University of Southampton, 1973.

APPENDIX A.1.

Physical Properties of Diesel Fuel

As indicated earlier in the report an attempt was made to obtain estimates of all required properties of fuel, fuel vapour and cylinder gas in terms of appropriate variables or curves being fitted to graphical forms of data where necessary.

The pressure P, temperature T and fuel/air ratio, F, dependence of these physical properties are shown in brackets.

Density of the Fuel

DenL (TL) = 0.037441 - 0.00001360 TL (lb/cu.in)

= Density of the fuel in the liquid state as a function of fuel temperature, TL (Ref.14, page 270).

Mean Density of Cylinder Gas

Denm (F,P,Tm) = 0.001565 x P/Tm (lb/cu.in)

= Density of the cylinder gas as a function of cylinder temperature, Tm, pressure, P and fuel/air ratio (refs. 19 and 14, page 43).

Mean Viscosity of the Cylinder Gas

$$\text{Vism (Tm)} = \frac{0.358 \times 10^{-7} \times \text{Tm}^{1.5}}{(0.556\ \text{Tm} + 124)} \qquad \text{(lb/in.sec)}$$

= Viscosity of the cylinder gas (refs. 6 and 14, page 158)

VisL (TL) and Visv (TL) are the viscosities of the fuel in the liquid state (from ref. 14, page 43) and in the vapour (estimated from ref.14, page 56) respectively.

Mean Specific Heat of the Cylinder Gas

Acpm (F, Tm) = 0.2400 + 0.0000127 Tm (Btu/lb deg.F)

= Specific heat of the cylinder gas (ref. 14).

Specific Heat of Liquid Fuel

AcpL (TL) = 0.1980 + 0.0000492 TL (Btu/lb deg.F)

= specific heat of the fuel in the liquid state (ref. 14, page 184)

Specific Heat of Fuel Vapour

AcpV (TL) = 0.2235 + 0.000246 TL (Btu/lb deg.F)

= specific heat of the fuel in the vapour state (ref.14, page 184)

Mean Thermal Conductivity of the Cylinder Gas

Aktm (F, Tm) = 2.325×10^{-6} x Acpm (Btu/in sec deg.F)

= thermal conductivity of the cylinder gas (ref. 14, page 224)

AktL (TL) and AktV (TL) are the thermal conductivities of the fuel in the liquid state and vapour state respectively (ref.14, page 224 and AktV (TL) $\approx$ Visv (TL) x AcpV (TL)

Vapour Pressure of Fuel

AppL (TL) = 1.05×10^{6}/Exp.(9880/TL) (lbf/sq.in)

= vapour pressure of the fuel in the liquid state (reference 6 and reference 14, page 285)

Latent Heat of Vaporisation

AlatL (TL) = $4.20\ |1340.0 - TL|^{0.50}$ (Btu/lb)

= latent heat of vaporisation of fuel.

The only data available for this function was the linear expression proposed in ref. 14 page 273, for fuel temperatures up to 400°F. For the remainder of the temperature range, i.e. 400°F - 880°F (880°F - critical temperature for the compound dodecane, $C_{12}H_{26}$), a parabola suggested by ref.(43), i.e. $|AlatL^2 = \text{constant} \times (Tcritical - TL)|$ shown above, was fitted such that :

(a) it passes through AlatL (400°F) as given by ref. (14)

(b) AlatL (Tcritical) = 0

(c) $\left.\frac{d(TL)}{d(AlatL)}\right|_{AlatL=0} = 0$ (critical point)

Mean Diffusion Coefficient of Cylinder Gas

$$AD_{vm}\ (Tm) = 0.508 \times Vism \times Tm \qquad \text{(sq.in/sec)}$$

= mean diffusion coefficient of cylinder gas (reference 14)

According to ref.(20), NR_e, NP_r and NS_c which are the droplet Reynolds, Prandtl and Schmidt number should be evaluated on the basis of mean gas vapour envelope properties, taken at temperature, Tm, as follows:

Mean Molecular Weight

$$\bar{M} = (1 - AppL(TL)/2P_T)\ Ma + (AppL\ (TL)/2P_T)\ Mf$$

Mean Density

$$Denm = \frac{P_T\ \bar{M}}{R\ Tm}$$

Mean Viscosity

$$Vism = (1 - AppL(TL)/2P_T)\ Visa + (AppL(TL)/2P_T)\ Visf$$

Mean Thermal Conductivity

$$Aktm = (1 - AppL\ (TL)/2P_T)Akta + (AppL(TL)/2P_T)\ Aktf$$

Mean Specific Heat

$$Acpm = (1 - AppL(TL)/2P_T)(\frac{Ma}{\bar{M}})\ Acpa + (\frac{AppL(TL)}{2P_T})(\frac{Mf}{\bar{M}})\ Acpf$$

where

Ma and Mf = molecular weight of air and fuel respectively

P_T = total pressure.

R = universal gas constant

Because $P_T >> AppL(TL)$ in most cases and since an exact molecular weight of diesel fuel is unknown, it was decided not to evaluate NR_e, NP_r and NS_c as suggested by Ref.(20) but in terms of cylinder average properties as previously defined. Thus :

Schmidt Number, NS_c

$$NS_c = Vism\ (Tm)/Denm(F,P,Tm) \times \frac{1}{ADvm\ (Tm)}$$

Prandtl Number, NP_r

$$NP_r = \frac{Acpm\ (F,Tm)}{Aktm\ (F,Tm)} \times Vism\ (Tm)$$

Reynolds Number, NR_e

$$NR_e = \frac{D\ drop \times U\ drop \times Denm\ (F,P,Tm)}{Vism\ (Tm)}$$

Additional Fuel Data

For Dodecane, $C_{12}H_{26}$, which is assumed to be the principal ingredient of diesel fuel, has the following properties:

Mean molecular weight	=	170
Carbon content	=	84.71%
Hydrogen content	=	15.29%
$T_{critical}$ (thermodynamic critical temperature)	=	$880^{\circ}F = 1340^{\circ}R$ (ref. 14, p.285)
$P_{critical}$ (thermodynamic critical pressure)	=	320 lbf/sq.in abs. (ref.14, p.285)
Stoichiometric oxygen required (for complete burning of 1 lb of Dodecane)	=	3.4512598 lbs
Stoichiometric air required	=	14.940519 lbs

APPENDIX A.2

Droplet Size - Distribution

According to Stirling's Theorem a probability curve or an error curve is represented by this equation:

$$y = K_c \, \text{Exp} \, (-h^2x^2) \qquad (A.2.1)$$

A graphical representation of equation (A.2.1) is shown in Figure A.2.0.

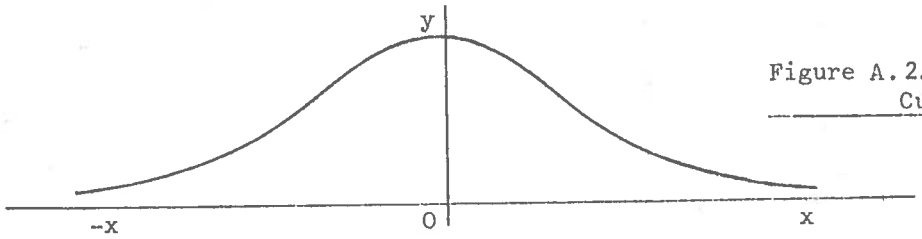

Figure A.2.0: Probability Curve

Equation (A.2.1) is only meaningful if an error is defined as the deviation of each measurement from the arithmetic mean. The value of y is mainly influenced by the absolute measure or the modulus of precision, h. The greater the magnitude of h, the less will be the magnitude of the deviation of individual measurements from the arithmetic mean of the whole set.

Let x_o, x_1, x_2, ... x be a series of errors in ascending order of magnitude from x_o to x. Let the differences between the successive values of x be equal. If x is an error, the probability of committing an error between x_o and x is the sum of the separate probabilities (the sum of equations A.2.1). In other words :

$$P = K_c \, \text{Exp} \, \left| \left(-h^2x_o^2 \right) + \left(-h^2x_1^2 \right) + \ldots . \right|$$

$$= K_c \sum_{x_o}^{x} \text{Exp} \, (-h^2x^2) \qquad (A.2.2)$$

Re-writing equation (A.2.2) and allowing dx to denote the successive integrals between any two limits x_o and x, thus

$$P = \frac{K_c}{dx} \int_{x_o}^{x} \text{Exp}(-h^2x^2) \, dx \qquad (A.2.3)$$

In general, equation (A.2.3) becomes:

$$P = \frac{K_c}{dx} \int_{-\infty}^{+\infty} \text{Exp}(-h^2x^2)\, dx \qquad (A.2.4)$$

From the above equation, it is certain now that all the errors are included between the limits $\pm\infty$ and since certainty is represented by unity, then:

$$P = 1 = \frac{K_c}{dx} \int_{-\infty}^{+\infty} \text{Exp}(-h^2x^2)\, dx = \frac{K_c}{dx} \frac{\sqrt{\pi}}{h} \qquad (A.2.5)$$

$$\text{or} \quad K_c = \frac{h}{\sqrt{\pi}}\, dx$$

Substituting for K_c in equation (A. .1), then the same relation is expressed in another form, namely

$$P = y = \frac{h}{\sqrt{\pi}} \text{Exp}\,(-h^2x^2)\, dx \qquad (A.2.6)$$

In fact, equation (A.2.6) or (A.2.1) is known as Gaussian Law of Errors and dx represents the interval for any special case, between the successive values of x; while x is the size of the error.

N.B. P or y (as already defined) is the probability of errors of observation between the magnitudes x and x+dx. By this is meant the ratio :

$$\frac{\text{Number of errors between x and x+dx}}{\text{Total number of errors}} = P = y.$$

Application of Gaussian Law of Errors to Diesel Spray

The actual diesel spray consists of small and large droplets and in fact the experiments described in ref.(11) have shown that the diameter of the largest droplets is twice the mean diameter of the whole spray. In view of this, nine droplet sizes as suggested by Whitehouse et al have been considered. The mass of the total fuel in proportion to each droplet has been assumed to follow a Gaussian distribution (or Gaussian Law of Errors), with a standard deviation of 0.4 times the mean diameter. Equation (A.2.6) could then be modified as follows:

$$F(D_o) = \frac{h}{\sqrt{\pi}} \left|\text{Exp}\{-h^2 (D_o - D_{AV})^2\}\right| dD_o \qquad (A.2.7)$$

where D_o and D_{AV} are the initial diameter of the droplet size and the mean average diameter of the whole spray respectively and $F(D_o)$ is the mass of each droplet size of diameter between D_o and D_o+dD_o injected.

Processing equation (A.2.7) further, then

$$\int_{-\infty}^{\infty} F(D_o) = \int_{\infty}^{\infty} \frac{h}{\sqrt{\pi}} \left|\text{Exp}\{-h^2(D_o-D_{AV})^2\}\right| \, dD_o = 1 \qquad (A.2.8)$$

or

$$\int_{-\infty}^{\infty} \left|\text{Exp}\{-h^2(D_o-D_{AV})^2\}\right| \, dD_o = \sqrt{\pi}/h \qquad (A.2.9)$$

The expressions on the left and on the right above are functions of h only. Differentiating both sides with respect to h, then:

$$\int_{-\infty}^{\infty} -2h\,(D_o-D_{AV})^2 \left|\text{Exp}\{-h^2(D_o-D_{AV})^2\}\right| dD_o = \sqrt{\pi}/h^2 \qquad (A.2.10)$$

Taking N as the total mass of droplets, and since $h/\sqrt{\pi}\ \text{Exp}\{-h^2(D_o-D_{AV})^2\}\, dD_o$ is the proportion that falls in the range D_o+dD_o, then $\frac{Nh}{\sqrt{\pi}} \left|\text{Exp}\{-h^2(D_o-D_{AV})^2\}\right| dD_o$ will be the actual mass that falls in this range. Multiply this by $(D_o-D_{AV})^2$ and sum this over the whole range $-\infty$ to $+\infty$; this will give the sum of the squares of the deviations from the mean, $(\text{zigma})^2$. Dividing this sum by N it follows that :

$$\begin{aligned}(\text{zigma})^2 &= \frac{1}{N}\int_{-\infty}^{\infty} \frac{Nh}{\sqrt{\pi}} (D_o-D_{AV})^2 \left|\text{Exp}\{-h^2(D_o-D_{AV})^2\}\right| dD_o \\ &= \frac{h}{\sqrt{\pi}} \int_{-\infty}^{\infty} (D_o-D_{AV})^2 \left|\text{Exp}\{-h^2(D_o-D_{AV})^2\}\right| dD_o\end{aligned} \qquad (A.2.11)$$

With the aid of equation (A.2.10)

$$(\text{zigma})^2 = \underline{\underline{1/2h^2}} \qquad (A.2.12)$$

Therefore, equation (A.2.7) becomes

$$F(D_o) = \frac{N}{\text{zigma} \times \sqrt{2\pi}} \left|\text{Exp}\{-0.5(D_o-D_{AV})^2\}/\text{zigma}^2\right| dDO \qquad (A.2.13)$$

N is the total mass of the droplets (expressed as 100%); dD_o is the class interval or width (i.e. $f(D_{AV})$) and zigma is the standard deviation. With zigma $\approx 0.4 \times D_{AV}$, equation (A.2.13) reduces to :

$$F(D_o) \approx 100 \left|\text{Exp}\{-3.125\,(D_o-D_{AV})^2\}/D_{AV}^2\right| dD_o \qquad (A.2.14)$$

N.B. dD_o in equation (A.2.14) is dimensionless, e.g. 0.2 or 0.3 because $0.4\ D_{AV}$ has been substituted for the value of zigma.

With the above equation, the distribution and mass of each droplet size are as follows (see ref. 5 also):

Table A.2.0 Droplet Mass Distribution

Droplet size No.	1	2	3	4	5	6	7	8	9
Droplet size diameter D_o	$0.1D_{AV}$	$0.4D_{AV}$	$0.6D_{AV}$	$0.8d_{AV}$	$1.0D_{AV}$	$1.2D_{AV}$	$1.4D_{AV}$	$1.6D_{AV}$	$1.9D_{AV}$
% Mass at diameter D_o	3.20	6.60	12.30	17.80	20.20	17.80	12.30	6.60	3.20

The atomisation curves for sprays from a single-hole orifice of diameter 0.02in (0.508mm), injected at different pressures in reference (47) are shown in Figure A.2.1. In order to obtain these results, the spray particles were collected on a smoked glass screen and certain zones were examined under the microscope and the size of the globules measured and the numbers counted. These experiments showed that with pressures above 2280 psi the largest percentage of fuel by volume consisted of particles having a group mean diameter of 0.002in (%51 microns), the actual quantity rising from just under 20 per cent at a pressure of 2280 psi to 25 per cent at pressures of 4160 and 5700 psi. Furthermore, as the injection pressure is increased from a low value, the spray tends to become finer and more uniform until a certain injection pressure is attained, beyond which the influence of pressure is less significant.

Comparing the results in Table (A.2.0) with those in Figure (A.2.1) it will be noted that the assumed distribution lies between sprays injected at 2280 and 4160 psi respectively. Thus, the assumed distribution is likely to be valid for most high speed automotive engines because their injection pressures are generally within the above quoted range, although a multi-hole injector of smaller diameters, e.g. about 0.32mm, is used in most cases. Finally, by compensating for the conditions in the cylinder, for instance, the cylinder temperature, density, etc., though their magnitudes are not stated in references (47, 19), it is firmly believed that the assumed droplet size distribution is within practical limit.

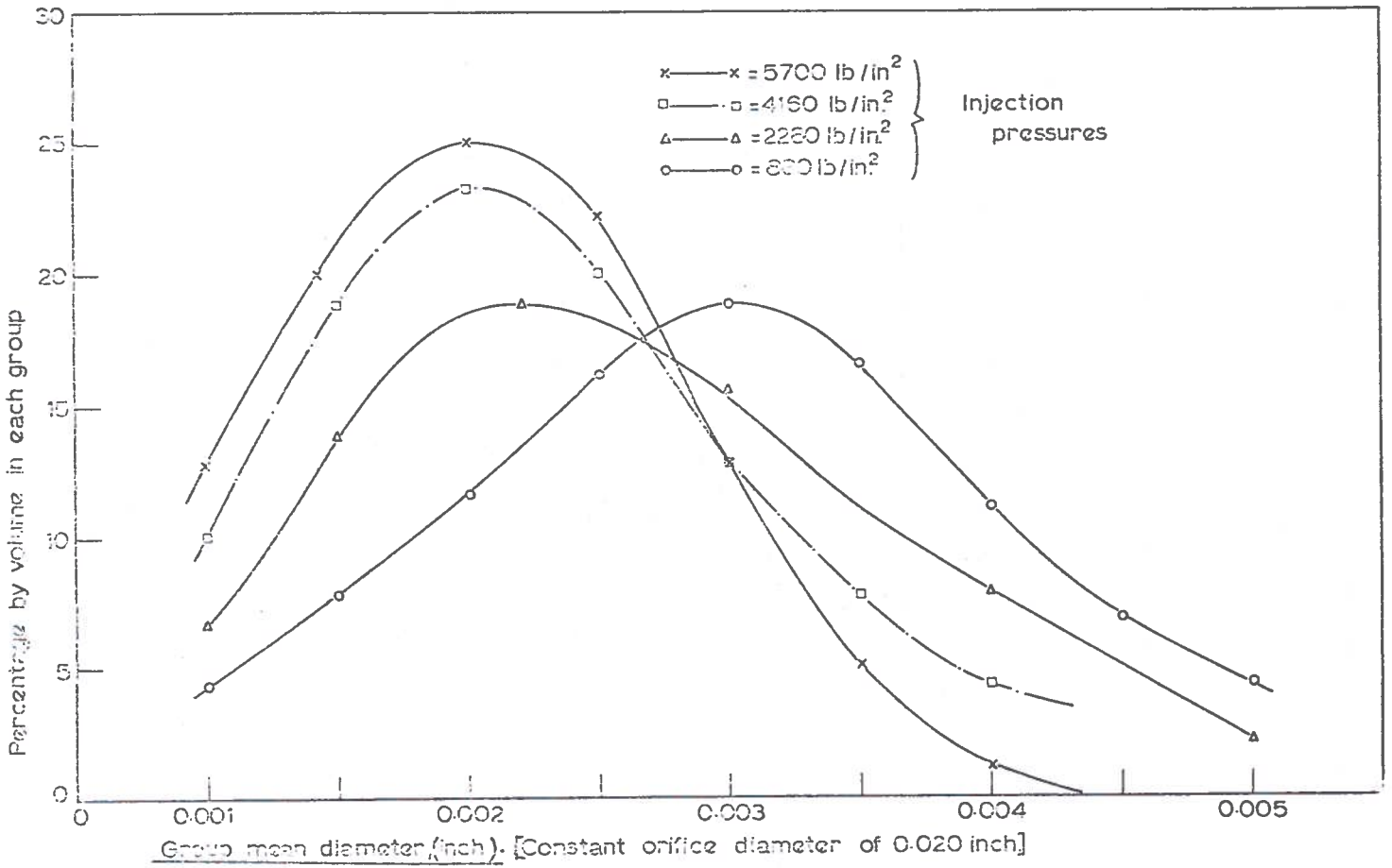

FIGURE A.2.1. DISTRIBUTION OF THE PARTICLE SIZES (ref. 6)

APPENDIX A.3

Calculation of the Total Fuel Injected

With measurements of injector interface (or fuel-line) pressures, needle lift and hence injection period, an instantaneous fuel flow rate, $\frac{dQ_{inj}}{d\theta}$ can be calculated on a step-by-step basis. Its summation over the injection period gives the total fuel injected per cycle.

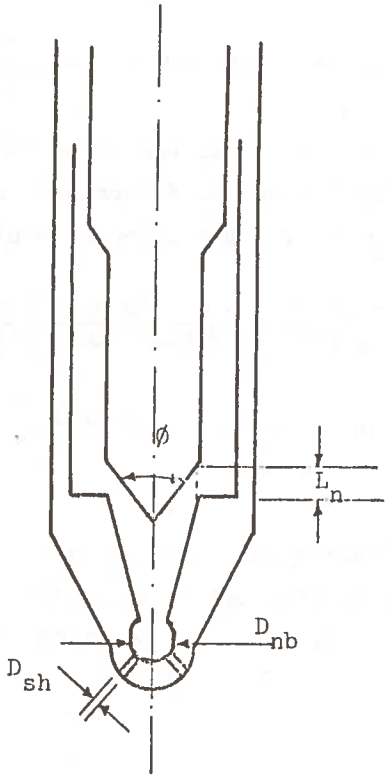

FIGURE A.3.0. A DIESEL INJECTOR

Therefore:

$$\frac{dQ_{inj}}{d\theta} = A_e \times C_{dis} \sqrt{2g(P_{inj}-P_g)\ DenfL} \qquad (A.3.0)$$

where

C_{dis} = discharge coefficient

g = acceleration gravity $\approx$ 980 mm/sec^2

$d\theta$ = degree crank angle

D_{sh} = diameter of the discharge orifice

P_{inj} = fuel pressure at $d\theta$

p_g = cylinder pressure at corresponding $d\theta$

DenfL = density of fuel

D_{nb} = diameter of needle seat bore

L_n = needle lift

ϕ = needle angle

A_e = total effective areas of the discharge orifices

Neglecting the effect of temperature on DenfL and assuming its average to be 0.825 gm/cm^3, after simplification, equation (A.5.0) reduces to

$$\frac{dQ_{inj}}{d\theta} = 4.03 \times A_e \times \sqrt{(P_{inj}-P_g)} \times C_{dis} \quad \left|\frac{mm^3}{msec}\right| \qquad (A.3.1)$$

L_n, L_{sh} , D_{nb} are expressed in (mm) respectively and P_{inj} and P_g in (psi).

Given the engine speed, the total fuel injected per cycle in terms of mm^3 or Btu/lb.Air can be determined from equation (A.3.1). Also the discharge coefficient for the injector could be calculated as follows:

$$C_{dis} = \frac{\text{Total actual mass flow rate (estimated from S.F.C)}}{\text{Total theoretical mass flow rate}} \qquad (A.3.2)$$

Where S.F.C. is the specific fuel consumption.

N.B. The following values were used in Tables (A.3.0 and A.3.1

(a) fuel calorific value = 19,500 Btu/lb (higher calorific value)

(b) mass of air = 0.003230 lb.

TABLE A.3.0 : INSTANTANEOUS FUEL INJECTED (ENGINE H)
AT 1200 rpm FL

$$\frac{dQ_{inj}}{d\theta} = 22.4 \times C_{dis} \times L_n \times (P_{inj}-P_g)^{0.5} \qquad (A.3.3)$$

No.	°CA ATDC/BTDC	Needle lift, L_n (in)	Cylinder Pressure, P_g (lbf/in2)	Fuel Pres., P_{inj} (lbf/in^2)	$\Delta p^{0.5} = (P_{inj}-P_g)^{0.5}$	$\frac{dQ_{inj}}{d\theta}$ (mm2)	Fuel Input (Btu/lb Air/°CA)
1	30.10	0.00054	230.00	0093.00	-	-	-
2	29.10	0.00054	241.00	0093.00	-	-	-
3	28.10	0.00054	252.00	0097.00	-	-	-
4	27.00	0.00054	262.00	0360.00	9.900	0.11950C_{dis}	0.9120
5	26.00	0.00054	272.00	0528.00	16.000	0.19340 "	1.4770
6	25.00	0.00054	284.00	0700.00	20.400	0.23600 "	1.8800
7	24.10	0.00054	296.00	0976.00	26.060	0.31500 "	2.4040
8	22.90	0.00054	307.00	0816.00	22.600	0.27300 "	2.0830
9	22.00	0.00054	321.00	0911.00	24.300	0.29400 "	2.2400
10	21.00	0.00103	333.00	1171.00	29.000	0.67000 "	5.1140
11	20.00	0.00297	349.00	1582.00	35.170	2.34000 "	17.8500
12	19.00	0.00502	359.00	1825.00	38.300	4.30000 "	32.8000
13	18.00	0.00571	373.00	1410.00	32.200	4.11500 "	31.4000
14	17.10	0.00617	387.00	1290.00	30.4000	4.20000 "	32.0500
15	16.00	0.00836	399.00	0880.00	21.930	4.10000 "	31.3000
16	15.00	0.00897	415.00	1211.00	28.200	5.65500 "	43.2500
17	14.00	0.00897	427.00	1359.00	30.600	6.14000 "	46.8000
18	13.00	0.00897	438.00	1889.00	38.100	7.65000 "	58.4000
19	12.00	0.00900	454.00	1910.00	38.150	7.68000 "	58.6000
20	10.90	0.00900	489.00	2396.00	43.700	8.81700 "	67.4000
21	10.00	0.00900	513.00	1845.00	36.600	7.38000 "	56.4000
22	09.00	0.00900	544.00	2069.00	39.040	7.86000 "	60.1000
23	08.00	0.00893	579.00	2181.00	40.000	8.00000 "	61.1000
24	07.00	0.00893	617.00	2312.00	41.200	8.23000 "	62.7500
25	05.90	0.00893	643.00	2368.00	41.550	8.32000 "	63.5000
26	05.00	0.00893	684.00	1945.00	35.600	7.12500 "	54.4000
27	04.00	0.00894	717.00	1506.00	28.040	5.61500 "	42.8000
28	03.00	0.00894	762.00	0988.00	15.010	3.00000 "	22.9000
29	02.00	0.00888	787.00	0568.00	-	-	-
30	01.00	0.00870	818.00	0365.00	-	-	-
31	00.00	0.00754	833.00	0317.00	-	-	-
32	01.10	0.00411	859.00	0126.00	-	-	-
33	01.90	0.00054	883.00	0345.00	-	-	-
34	02.90	0.00036	895.00	0353.00	-	-	-
				Total fuel calculated =		104.00 C_{dis}	794.00 (Btu/lb.Air)
						72.80mm^3	

$C_{dis} \approx 0.7$

TABLE A.3.1 : INSTANTANEOUS FUEL INJECTED (ENGINE H) AT 1800 rpm FL

$$\frac{dQ_{inj}}{d\theta} = 14.93 \times C_{dis} \times L_n \times (P_{inj}-P_g)^{0.5} \qquad (A.3.4)$$

No.	°CA BTDC/ATDC	Needle Lift, L_n (in)	Cylinder Pressure, P_g (lbf/in^2)	Fuel Pres., P_{inj} (lbf/in2)	$\Delta p^{0.5} = (P_{inj}-P_g)^{0.5}$	$\frac{dQ_{inj}}{d\theta}$ (mm3)	Fuel Input (Btu/lb Air/°CA)
1	30.10	0.000450	217.00	112.00	-	-	-
2	29.10	0.000350	229.00	132.00	-	-	-
3	28.10	0.000450	237.00	322.00	9.220	$0.0620C_{dis}$	0.4725
4	27.00	0.000450	246.00	636.00	19.800	0.1330 "	1.0140
5	26.00	0.000450	257.00	790.00	23.100	0.1550 "	1.1800
6	25.10	0.000450	266.00	1074.00	28.400	0.1910 "	1.4550
7	24.00	0.000450	280.00	1422.00	33.800	0.2270 "	1.7300
8	23.00	0.000450	291.00	1482.00	34.600	0.2320 "	1.7700
9	22.00	0.000810	304.00	1700.00	37.400	0.4520 "	3.4500
10	21.00	0.002310	319.00	2002.00	41.000	1.4160 "	10.8000
11	19.90	0.005270	333.00	2050.00	41.500	3.2660 "	23.0600
12	19.00	0.008220	346.00	2116.00	42.000	5.1540 "	39.3500
13	18.00	0.009010	358.00	1874.00	38.900	5.2250 "	39.8000
14	17.00	0.008940	372.00	1622.00	35.400	4.7200 "	36.0000
15	15.90	0.009010	385.00	1374.00	31.400	4.2250 "	32.2000
16	15.00	0.009010	398.00	2050.00	40.650	5.4750 "	41.7500
17	13.90	0.008970	412.00	1912.00	38.800	5.2000 "	39.6500
18	13.00	0.008980	423.00	2492.00	45.550	6.1100 "	46.6000
19	12.00	0.008980	435.00	3484.00	55.100	7.4000 "	56.4000
20	10.80	0.008980	450.00	4116.00	60.600	8.15000 "	62.1660
21	10.00	0.008980	474.00	3686.00	57.600	7.75000 "	59.0000
22	09.10	0.008980	506.00	3850.00	57.800	7.76000 "	59.1800
23	08.00	0.009000	550.00	3654.00	55.600	7.46000 "	57.0000
24	07.00	0.009010	585.00	2550.00	44.400	5.98000 "	45.6000
25	05.90	0.008940	647.00	2292.00	40.600	5.40000 "	41.1600
26	05.00	0.008990	712.00	1790.00	32.800	4.40000 "	33.6000
27	04.00	0.008950	715.00	1500.00	28.000	3.74000 "	28.5000
28	03.10	0.008810	772.00	1088.00	17.800	2.34000 "	17.8400
29	02.00	0.008810	798.00	0822.00	04.800	0.63000 "	4.8000
30	01.10	0.008820	829.00	0590.00	-	-	-
31	00.00	0.008210	854.00	0374.00	-	-	-
32	00.90	0.006830	861.00	0066.00	-	-	-
33	02.00	0.004860	864.00	-	-	-	-
34	03.10	0.002200	880.00	-	-	-	-
35	04.00	0.000170	887.00	-	-	-	-
36	05.00	0.000640	895.00	-	-	-	-
					Total fuel calculated =	$103.2530C_{dis}$	786.0000tu/lb Air)
						$72.2771mm^3$	

$C_{dis} \approx 0.70$

APPENDIX A.4

Local Oxygen-supply Factor

The local oxygen-supply factor, F_{loc} at each step (crank angle degree) can be calculated from equations (A.4.1) and (A.4.4). For instance:

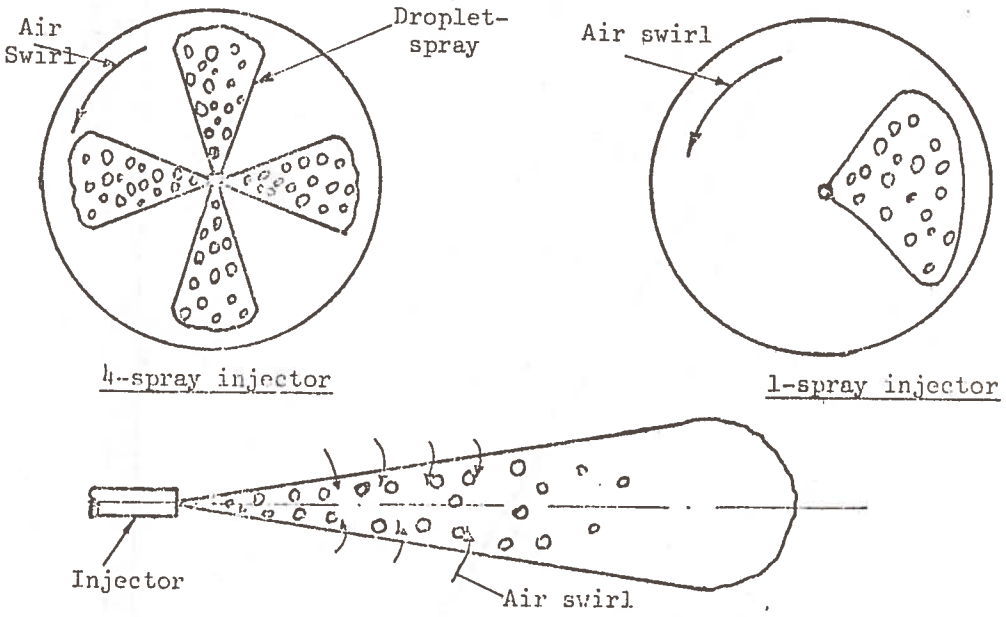

FIGURE A.4.0: A DEVELOPED SPRAY

the total volume of air entrained, assuming momentum continuity (ref. 48) is given by:

$$M_{uti} = Spn\ \pi/3\ X^3 \tan^2\zeta \qquad (A.4.1)$$

where

ζ = half cone angle and is given by $\tan^2\zeta = 0.75 \times 10^{-3}\ n$ (see equation 50)

X = distance penetrated by spray tip (equation 48)

S_{pn} = number of sprays (holes)

For a typical modern diesel engine, the following data are within design limits :

(a) fuel injection pressure, P_{inj} = 3500 psi

(b) fuel injection nozzle diameter, d_h = 0.320 mm

(c) average cylinder pressure, P_g = 500 psi

(d) average engine bore (for high speed diesel) = 4.5in (i.e. r_b = 2.25in)

(e) average cylinder temperature, T_g = 1494°R.

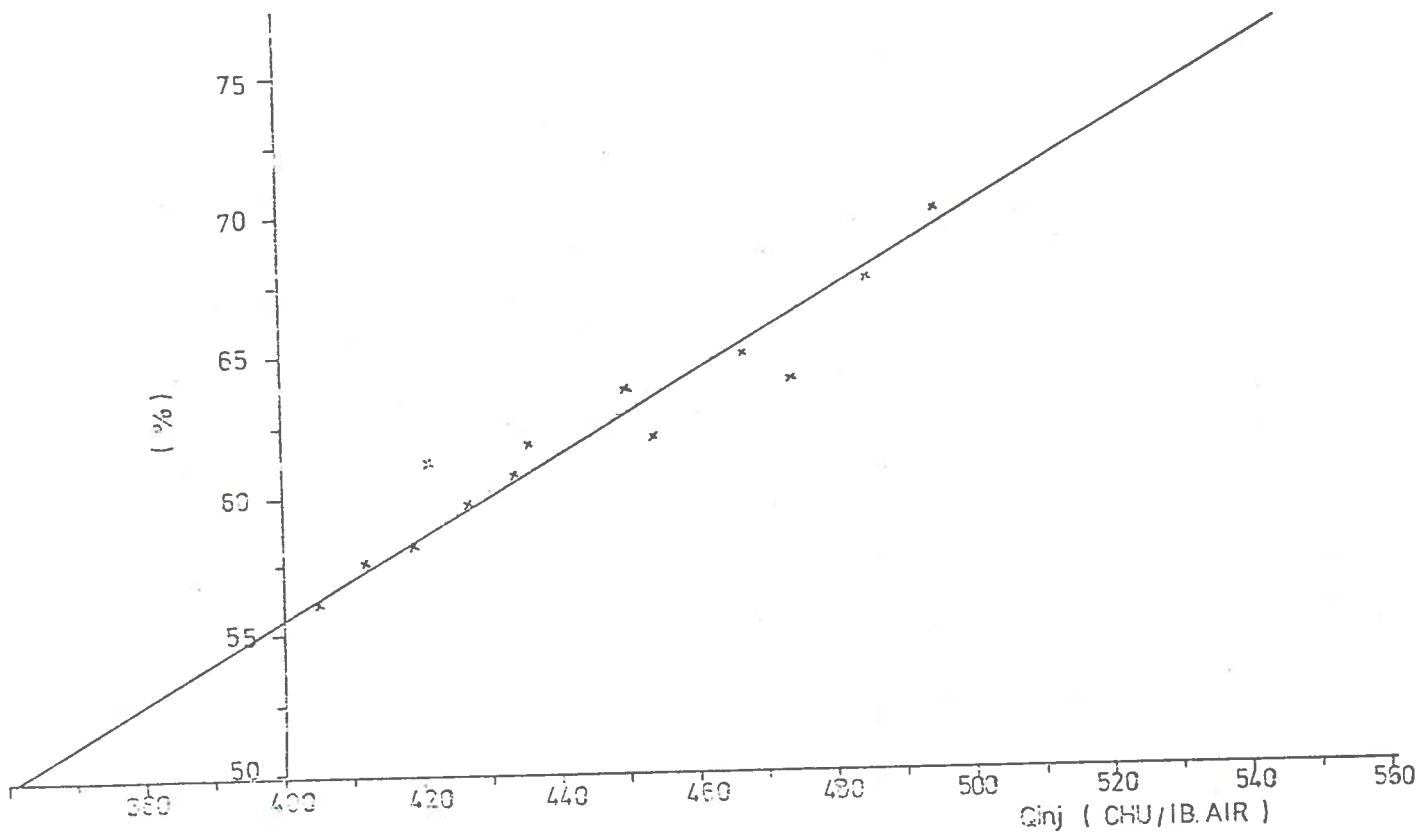

FIGURE A.4.1 AIR UTILISATION (From Ref. 25)

(f) swept volume = 60 cu.in

(g) air utilisation = 60%

(h) volumetric efficiency = 80%

(i) volume of air available for combustion (based on the above values),
M_{oav} = 28.80 cu.in (i.e. 60 x 60% x 80%)

(j) density ratio, n (based on P_g = 500 psi and T_g = 1494°R)
= 12.20

(k) S_{pn} = 4 (in general)

With the aid of equation (48) and after substituting the above values, together with the necessary algebra, X reduces to :

(a) $X = 78t^{0.5}$ for d_n = 0.320mm (A.4.2)

and

(b) $X = 91.5t^{0.5}$ for d_n = 0.45mm (typical of a single-hole injector) (A.4.3)

where t is in seconds and X in inches.

The corresponding values of X are tabulated in Table A.4.0 Finally, F_{loc} is determined from equation (A.4.4) below for a 4-spray hole injector having a hole diameter of 0.320 mm. That is

$$F_{loc} = \frac{M_{oav} - M_{uti}}{M_{oav}} \qquad (A.4.4)$$

Figure A.4.2 and Table A.4.0 show the variation of Floc with time.

It is to be noted that the volume of the instantaneous entrained local air based on spray cones and Schweitzer's equation is in general underestimated and must be modified to account for the air movement in the cylinder, which continuously brings more air into contact with the fuel droplet spray and thus enlarges their surface areas. As a result, a variable multiplying factor was introduced as shown in Figure A.4.2. A curve based on a multiplying factor of 1.5 gives an air entrainment that is consistent with heat release curve and hence used in the heat release model.

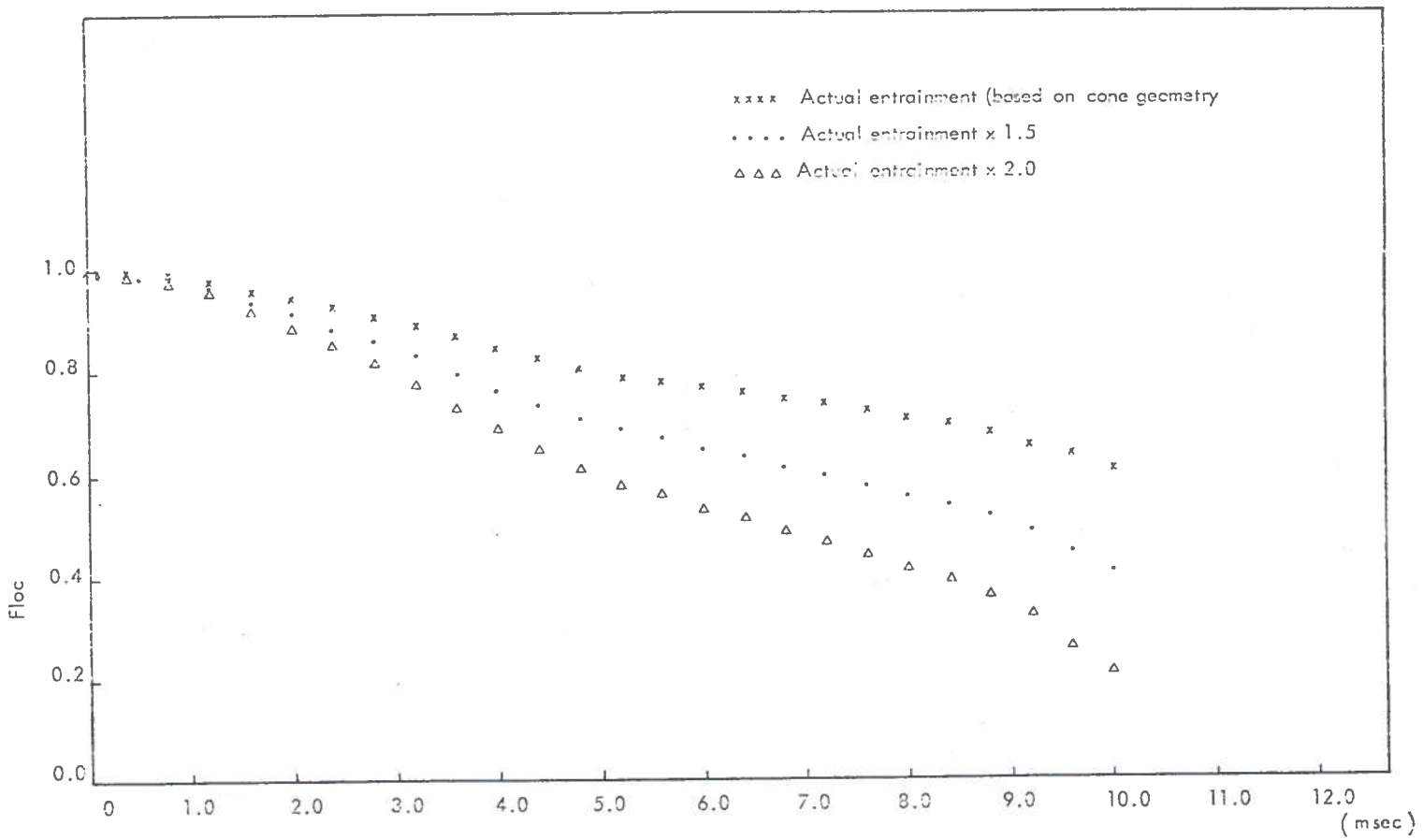

FIGURE A.4.2. NORMALISED LOCAL AIR AVAILABLE DURING THE COMBUSTION PROCESS

TABLE A.4.0: INSTANTANEOUS VOLUME OF AIR ENTRAINED

1	2	3	4	5	6	7	8
Time, t(secs)	$X = 78t^{0.5}$ X(inches)	$X = 91.5t^{0.5}$ X(inches)	M_{uti} based on Col.2 (cu.in)	Actual M_{uti} (with truncation considered)	Actual M_{uti} x 1.5 (cu.in)	Actual M_{uti} x 2.0 (cu.in)	Air Avail. (ie $M_{oaV} - M_{uti}$) based on Col.5
0.0000	0.000	0.000	0.0000	0.0000	0.0000	0.0000	28.8000
0.0001	0.780	0.915	0.0182	0.0182	0.0273	0.0364	28.7818
0.0004	1.560	1.830	0.1450	0.1450	0.2180	0.2900	28.6550
0.0008	2.200	2.580	0.4050	0.4050	0.6075	0.8100	28.3950
0.0012	2.700	3.160	0.7200	0.7200	1.0800	1.4400	28.0800
0.0016	3.120	3.660	1.1650	1.1650	1.7500	2.3300	27.6350
0.0020	3.480	4.080	1.6100	1.6100	2.4150	3.2200	27.1900
0.0024	3.820	4.475	2.1400	2.1400	3.2150	4.2800	26.6600
0.0028	4.120	4.840	2.6800	2.6800	4.0200	5.3600	26.1200
0.0032	4.400	5.160	3.2600	3.2600	4.9000	6.5200	25.5400
0.0036	4.680	5.490	3.9000	3.9000	5.8500	7.8000	24.9000
End of Injection. Spray continues as an expanding truncated conc							
0.0040	4.915	5.760	4.5000	4.4818	6.7400	8.9636	24.3182
0.0044	5.160	6.055	5.2700	5.1250	7.7000	10.2500	23.6750
0.0048	5.400	6.330	6.0400	5.6350	8.4500	11.2700	23.1650
0.0052	5.615	6.600	6.8000	6.0800	9.1400	12.1600	22.7200
0.0056	5.830	6.850	7.5000	6.3350	9.5000	12.6700	22.4650
0.0060	6.040	7.100	8.4000	6.7900	10.2000	13.5800	22.0100
0.0064	6.240	7.320	9.2000	7.0600	10.6000	14.1200	21.7400
0.0068	6.415	7.540	10.1000	7.4600	11.2000	14.9200	21.3400
0.0072	6.600	7.750	11.0000	7.7400	11.6000	15.4800	21.0600
0.0076	6.790	7.950	12.0000	8.1000	12.1500	16.2000	20.7000
0.0080	6.960	8.175	13.0000	8.5182	12.8000	17.0364	20.2818
0.0084	7.140	8.360	14.0000	8.8750	13.3000	17.7500	19.9350
0.0088	7.300	8.560	14.9000	9.2650	13.9000	18.5300	19.5350
0.0092	7.460	8.750	15.9000	9.8200	14.7300	19.6400	18.9800
0.0096	7.625	8.950	17.0000	10.6650	16.0000	21.3300	18.1350
0.0100	7.800	9.150	18.2000	11.4100	17.1000	22.8200	17.3900

TABLE A.4.0 (CONTINUED)

	9	10	11	12	13
Time, t(secs)	Air Avail. based on Col. 6	Air Avail. based on Col.7	F_{loc} based on Col. 8	F_{loc} based on Col. 9	F_{loc} based on Col. 10
0.0000	28.8000	28.8000	1.0000	1.0000	1.0000
0.0001	28.7727	28.7636	0.9998	0.9997	0.99965
0.0004	28.5820	28.5100	0.9950	0.9900	0.9890
0.0008	28.1925	27.9900	0.9850	0.9770	0.9700
0.0012	27.7200	27.3600	0.9750	0.9620	0.9500
0.0016	27.0500	26.4700	0.9557	0.9360	0.9190
0.0020	26.3850	25.5800	0.9430	0.9150	0.8875
0.0024	25.5850	24.5200	0.9250	0.8870	0.8500
0.0028	24.7800	23.4400	0.9060	0.8600	0.8140
0.0032	23.9000	22.2800	0.8860	0.8300	0.7730
0.0036	22.9500	21.0000	0.8650	0.7970	0.7290
End of Injection. Spray continues as an expanding truncated cone					
0.0040	22.0600	19.8364	0.8440	0.7655	0.6880
0.0044	21.1000	18.5500	0.8220	0.7320	0.6440
0.0048	20.3500	17.5300	0.8030	0.7060	0.6080
0.0052	19.6600	16.6400	0.7880	0.6820	0.5775
0.0056	19.3000	16.1300	0.7800	0.6700	0.5600
0.0060	18.6000	15.2200	0.7640	0.6450	0.5280
0.0064	18.2000	14.6800	0.7540	0.6320	0.5100
0.0068	17.6000	13.8800	0.7415	0.6100	0.4820
0.0072	17.2000	13.3200	0.7315	0.5965	0.4620
0.0076	16.6500	12.6000	0.7180	0.5775	0.4370
0.0080	16.0000	11.7636	0.7040	0.5550	0.4080
0.0084	15.5000	11.0500	0.6920	0.5380	0.3840
0.0088	14.9000	10.2700	0.6780	0.5165	0.3564
0.0092	14.0700	9.1600	0.6585	0.4880	0.3180
0.0096	12.8000	7.4700	0.6300	0.4440	0.2593
0.0100	11.7000	5.9800	0.6030	0.4055	0.2080

APPENDIX A.5

Technical Data of the Other Test Engines

No.	Engine Type	No. of cyl's	Stroke	Bore	Total swept vol. per cyl	Total clearance per cylinder	Compression Ratio (nom.)	Connecting Rod Length	Engine Speed	Power	Combustion chamber type	No. of sprays & dia. of spray hole
			(in)	(in)	(cu.in)	(cu.in)	-	(in)	(rev/min)	(bhp)		(mm)
A	AEC A801 4-stroke	8	4.50	5.31	100.00	6.667	16:1		1000.0 1500.0 2000.0 2600.0	89.00 235.00	Direct-Injection Toroidal	5 0.320mm
B	BMC-154 4-stroke	4	4.0	3.5	38.555	2.084	19.5:1		1000.0 1000.0	Max. 66.00 at 3500rpm	Indirect Injection	
C	Perkins 4-stroke	4							1000.0		Direct-Injection Toroidal	
D	Cummins V-8-4-stroke	8	3.50	4.625	58.80	3.460	18:1	6.00	1000.0 1500.0 2000.0 3000.0		Direct-Injection Flat-Toroidal	4
E	K60 Rolls-Royce Opposed Piston 2-stroke	6	2 x 3.60	3.4375	66.820	4.495	16:1	6.50	1000.0 1500.0 2000.0 2400.0	82.40 132.50 160.00 165.00	Direct-Injection	
F	MAN M-system 8.27 litres 4-stroke	6	5.50	4.40	84.00	5.250	17:1		1000.0 2000.0	Max. 100.0	Direct-Injection	

No.	Engine Type	No. of cyl's	Stroke	Bore	Total swept vol. per cylber	Total clear-ance cyl	Compres-sion Ratio (nom.)	Connec-ting Rod Length	Engine Speed	Power	Combus-tion chamber type	No. of sprays & dia. of spray hole
			(in)	(in)	(cu.in)	(cu.in)		(in)	(rev/ min)	(bhp)		(mm)
G	Leyland 500 4-stroke	6	4.92	4.65	83.333	5.208	17:1		1000.0 1500.0 2000.0 2600.0	58.20 143.20	Direct-injection Spheroidal	4 0.355mm
H	Leyland 8.61 4-stroke	6	5.50	4.50	87.45	6.031	15.5:1	11.50	800.0 1000.0 1200.0 1800.0	40.00 53.00 62.50 85.00	Direct-injection	1 0.450mm
I	Perkins 6.354 4-stroke	6	5.00	3.875	59.00	3.933	16:1	8.624	1000.0 2000.0 2500.0 2300.0		Direct-Injection Toroidal	
J	L.60								1500.0 2100.0			
K	AEC 801 Petrol 4-stroke	8	4.50	5.310	100.00	6.667	16:1		1000.0 2600.0		Direct-injection toroidal	
L	Perkins V8-510 4-stroke	8	4.50	4.250	63.837	4.120	16.5:1		1000.0 2000.0 2800.0		Direct-injection Toroidal	
M	TS.3								1000.0 1500.0 2000.0 2400.0			
N	FD6 VII								2400.0			

(a) for details of engine O see Chapter 5, section 5.2.1.1
(b) " " " " P " " " ", section 5.2.1.2.

APPENDIX A.6

An Estimate of both the Physical and Chemical Ignition Delay Periods

The aim of this exercise is partly to compare the ignition delay periods calculated using Wolfer's and Tsao's empirical formulae (i.e. equations 66 and 67 respectively) with experimental data. Results are shown in Table A.6.0 below and Figure 42.

TABLE A.6.0 CALCULATED AND MEASURED IGNITION DELAY PERIOD

For Engine I

Engine Speed (rpm)	Av.Cylinder Pressure (p.s.i)	Av.Cylinder Temperature (^{o}R)	Experimen'l Delay Period(^{o}CA)	Wolfer's (^{o}CA)	Tsao's (^{o}CA)	Lyn's Analysis (^{o}CA)
2800	565.0	1440.0	13.3340	13.800	-19.80	13.440
2500	565.0	1440.0	12.500	12.100	- 9.100	13.100
2000	470.0	1320.0	13.930	14.500	6.500	12.000
1000	520.0	1300.0	7.500	7.830	15.750	7.500

For Engine H

Engine Speed (rpm)	Av.Cylinder Pressure (p.s.i)	Av.Cylinder Temperature (^{o}R)	Experimen'l Delay Period(^{o}CA)	Wolfer's (^{o}CA)	Tsao's (^{o}CA)	Lyn's Analysis (^{o}CA)
1800	423.00	1365.00	11.250	11.200	9.500	11.960
1200	427.00	1410.00	9.250	6.100	13.900	10.500
1000	427.00	1410.00	9.250	5.100	14.000	9.250
800	-	-	8.750	-	-	7.720

As noted in Table A.6.0 above, Wolfer's equation is more accurate than Tsao's. Perhaps more important, the latter's equation becomes negative at any engine speed above 2000 rpm according to the above analysis. This suggests that Tsao's equation is not widely applicable.

On the other hand, Lyn's experimental observation (ref.31) that as the engine speed is doubled (in the 1000-2000 rpm range), the delay is reduced by approximately 20 per cent (of which half is due to increase in compression temperature and half due to increase in injection pressure) is well in agreement with the experimental data presented above. Hence, the ignition data were calculated from Wolfer's equation and compared with the experimental values (and Lyn's estimates) before final use in the heat release model.

APPENDIX A.7

Report of Inventions

A diligent review of the work performed under this contract has revealed no innovations, discoveries, or inventions at this time. In addition, all methodologies employed are available in the open literature. However, an improvement model is provided for the prediction of combustion induced noise based on physical combustion parameters as a function of pressure rise, speed and bore.